THE UNIVERSITY OF HULL

Development of a New Global Rain Model for Radio Regulation

A Thesis submitted for the Degree of

Doctor of Philosophy in Electronic Engineering

In the University of Hull

by

GERALDINE RANGMOEN RIMVEN

(MSc, University of Bradford, UK)

July 2019

Acknowledgement

Abstract

Signal attenuation due to rain scatter is the dominant fade mechanism on the majority of high-capacity microwave telecommunications links, both terrestrial and Earth-space. These links carry a large proportion of the information that underpins the way modern life functions and is a vital component of national infrastructure. Many studies have established the virtuous cycle that exists between the development of telecommunications infrastructure and economic growth. Therefore, it is important that rain fade models exist for the design and optimisation of telecommunications networks, globally, but especially in developing countries.

A set of internationally recognised and agreed radio propagation models is maintained by the International Telecommunications Union - Radiocommunication Sector (ITU-R) in the form of Recommendations. A fundamental input parameter to many of these models is the point one-minute rain rate exceeded for 0.01% (about 50 minutes) of an average year. Historically, the collection of one-minute rain rates has been rare and so very few regions of the world have measured this important parameter. Where local data are not available, the full distribution of one-minute rain rates, including the 0.01% exceeded rate, can be obtained from Rec. ITU-R P.837-7. The input parameters to this Recommendation are the average monthly temperatures and rain accumulations.

The network of meteorological stations is very sparse in equatorial developing countries. This limits the reliability of monthly rain accumulation statistics. ITU-R models are validated against DBSG3: the database of link and meteorological measurements maintained by ITU-R Study Group 3. However, there is very little data from the Tropics in DBSG3. Therefore, there are legitimate concerns that the ITU-R P.837-7 model may not work accurately in the Tropics.

ii

This thesis uses rain rates derived from the satellite Earth observation Tropical Rain Measuring Mission, TRMM, to estimate point one-minute rain rate distributions in the Tropics. Two distinct uses of these data have been tested. Initially, the measured distributions of TRMM rain rates were used to estimate rain distributions in the Tropics. A method was developed to transform TRMM rain rate distributions to those needed for radio systems, based on UK rain radar data. In many cases, this method performed better than Rec. ITU-R P.837-7, particularly with databases of rain rates not included in DBSG3. To extend the work to global application, TRMM data were used to estimate the monthly rain rate distributions conditional upon monthly temperature and accumulation, as used in Rec. ITU-R P.837-7. These were then used to replace the analytic distributions in the Recommendation. The method worked well on several databases of measurements, but appeared to be biased in temperate regions. The measured TRMM conditional distributions were replaced by curve-fit approximations and a hybrid method was developed that combined the standard Rec. ITU-R P.837-7 prediction with the curve-fit TRMM prediction. This algorithm performed as well as or better than Rec. ITU-R P.837-7 for most test databases and at most time percentages.

The direct use of satellite Earth observation data to produce distributions of point one-minute rain rates is a radical departure from methods used before. This thesis has shown the potential of satellite-based measurements to replace the current methods based on downscaling numerical weather prediction output. In the future when more satellite data are available, spanning the globe, this suggests that direct use of satellite data will become standard.

Table of Contents

List of Figures

viii

List of Tables

Notation

MMDA	mean monthly daily accumulations
MT	mean monthly total precipitation accumulation in mm
R	rain rate in mm/hr
$R_{0.01\%}$	average annual point one-minute rain rate exceeded for 0.01% of a year in mm/hr
R_{1km}	1 km rain rate in mm/hr
R_{5km}	5 km rain rate in mm/hr
T	mean monthly surface temperatures in K
$XCD_{curvefit}$	curve-fit conditional monthly exceedance distributions
XCD_{TRMM}	TRMM conditional rain rate exceedance probability distributions
XCD_{1km}	1 km exceedance distributions
XCD_{837}	Rec837 conditional rain rate exceedance probability distributions
$X(R)$	average annual exceedance distribution of point one-minute rain rates

Glossary of Terms

CERES	Cloud and Earth Radiant Energy Sensor
CMORPH	Climate Prediction Centre morphing method
DBSG3	Database of meteorological and radio system measurements maintained by ITU-R Study Group 3
DSD	Drop Size Distribution
ECMWF	European Centre for Medium-Range Weather Forecasts
GEO	Geosynchronous Earth orbit
GOES	Geostationary Operational Environment
GPM	Global Precipitation Measurement
GPCC	Global Precipitation Climatology Centre
GPCP	Global Precipitation Climatology Project
IR	Infrared
ITOS	Improved TIROS Operational Satellite
ITU-R	International Telecommunication Union – Radiocommunication Sector
LEO	Low Earth orbit
LIS	Lightning Imaging Sensor
MSG	Meteosat Second Generation
MTSAT	Multifunctional Transport Satellite
NCAR	National Centre for Atmospheric Research
NCEP	National Centres for Environmental Prediction
NOAA	National Oceanic and Atmospheric Administration
NRCS	Normalised Radar Cross Section
NWP	Numerical Weather Prediction
PIA	Path Integrated Attenuation
PMW	Passive Microwave
PR	Precipitation Radar
SRT	Surface Reference Technique
TCC	TRMM Composite Climatology

TIROS	Television and Infrared Observing Satellite
TMI	TRMM Microwave Imager
TMPA	TRMM Multisatellite Precipitation Analysis
TRMM	Tropical Rainfall Measuring Mission
VIRS	Visible and InfraRed Scanner
WMO	World Meteorological Organisation

Chapter 1   Introduction

"The data-driven world will be always on, always tracking, always monitoring, always listening, and always watching – because it will be always learning" (IDC, 2018). Data is the life-blood of the present information age and underpins virtually every aspect of human life. Data is gathered and analysed by governments, businesses and researchers, to increase efficiency, in decision-making, to gain more understanding of current events and concepts, and to forecast what could happen in the future. The collection and storage of data is only valuable if it can be accessed quickly and efficiently, and this relies upon telecommunications infrastructure. This infrastructure aims for seamless transfer of data between the source and destination, with high capacity, low latency and high availability. A large proportion of data movements are across microwave telecommunications links. High capacity radio links use cutting-edge hardware and signal processing, but their availability is limited by the incidence of rain. Knowledge of the incidence and characteristics of rain drive the design and optimisation of networks of radio links. This project focuses on methods to predict the characteristics of rain over the large areas of the globe where no suitable measurements exist.

1.1   Radio telecommunications

Telecommunication links are required for the transmission of video, audio, images and other data from one point to another. Links can be between stations on the ground or in space. Internet connectivity has revolutionised the lives of individuals and transformed nations by creating new ways to communicate and socialise, for business activities and provision of public services such as healthcare and education. In developing countries where the physical infrastructure is either absent or inadequate, access to the Internet facilitates growth and development by enabling

information and knowledge sharing, access to global markets, agricultural advancements, human resource development and specialisation, as well as financial innovations through services such as mobile banking. Successive advancements in Information and Communications Technology (ICT), often through emerging wireless technologies has enabled innovations such as the Internet of Things (IoTs) through which a huge number of devices are connected to a global network (Alam et al., 2018).

Satellite communication enables point to multipoint connectivity; hence, it plays a major role in international communications and the establishment of mobile base-stations in remote regions. Space missions provide vital data for science and research. Satellite observations of the Earth enable accurate weather forecasts, timely prediction/detection of natural disasters and consistent measurement of features over large areas.

Of particular interest to this project has been the Tropical Rainfall Measuring Mission (TRMM), the first satellite mission aimed at measuring tropical and subtropical rainfall. Rain data were acquired by microwave radars on the satellite and transmitted to Earth via microwave links. The data was stored in one or more data centres where it was accessed over telecommunications systems to be combined with other data from many other sources by algorithms designed to fuse data to yield the best understanding of tropical rain. The data produced has been used in this project to develop prognostic models of rain in the Tropics to design and optimise future microwave systems in these regions.

1.2   Radio Regulation

The mission of the International Telecommunication Union – Radiocommunication Sector (ITU-R) aims "*to ensure rational, equitable, efficient and economical use of the radio-frequency spectrum by all radiocommunication services, including those using satellite orbits, and to carry out studies and adopt Recommendations on radiocommunication matters*" (ITU-R, 2019).

Within this framework, the role of the ITU-R includes apportionment of the frequency spectrum into bands, assignment of radio frequencies and their registration in order to prevent the harmful interference of radio systems of different countries, thereby improving the use of these frequencies to provide efficient radiocommunication services. This is achieved by acquiring and sharing knowledge on radiocommunication systems and radio wave propagation, and equally importantly, by developing policies and international technical standards (ITU, 2017). These standards, usually referred to as Recommendations, are established to guide the performance and metrics of quality of service. ITU-R Recommendations are recognised internationally as they are voted on by representatives of most countries at regular World Radio Conferences. Interested parties, including national spectrum regulators, can forward the results of studies to the ITU-R through Radiocommunication Study Groups.

The ITU-R relies on the database of meteorological and radio system measurements maintained by ITU-R Study Group 3, DBSG3, to validate the models in Recommendations. The data have been provided by the ITU-R member administrations, often national spectrum regulators, of many countries. However, the database contains no data from Africa, and much of the data are from countries in temperate regions of Europe, Asia and the Americas. Hence, the method provided by the internationally recognised Rec. ITU-R P. 837-7 is expected to be less accurate over the Tropics due to lack of data for conditioning and verification from equatorial countries.

1.3   Rain Distributions

Rain-induced attenuation is a major impairment to the performance and quality of service of communication links, especially wireless line-of-sight communication systems operating above 10 GHz, such as terrestrial and Earth-space communication links. The ITU-R maintains models to predict the rain fade on these links. A fundamental input parameter for these models is the average annual point one-minute rain rate exceeded for 0.01% of a year: $R_{0.01\%}$. An accurate

knowledge of rainfall statistics with one-minute integration times is required to predict rain attenuation, in order to design robust links and to optimise spectrum efficiency. The method for estimating the average annual exceedance distribution of point one-minute rain rates globally, using Rec. ITU-R P.837-7, is based on averaging monthly exceedance distributions conditioned upon mean monthly temperature and precipitation accumulation at the point of interest. The accumulations are measured using rain gauges, which are difficult to site, particularly in urban areas and can provide biased measurements when in the wind shadow of buildings, trees, etc. Measurements of low-probability rain rates with the most common funnel gauges are very sensitive to temporary blockage due to insects or plant matter in the funnel.

1.4   Research aim and objectives

In view of the foregoing observations, this project aims to produce an improved method to predict average annual distributions of point one-minute rain rates that focuses on accuracy in the Tropics. This is important for the design and optimisation of telecommunications systems in equatorial countries. The project will critically evaluate the current ITU-R rain model, particularly with respect to its performance in the Tropics. If the performance can be improved through the integration of TRMM satellite data, then a new model will be proposed. To achieve this, the project will:

1. Review the ITU-R rain and rain fade models;

2. Evaluate current ITU-R method for estimating the average annual exceedance distribution of point one-minute rain rates R: $X(R|x)$, where x is position.

3. Evaluate the contribution that TRMM data can make to the estimation of $X(R)$ in the Tropics;

4. Develop a method for estimating $X(R)$ in the Tropics from TRMM data and evaluate against ground truth data;

5. Extend the method to sites in temperate regions and evaluate its performance.

6. Create a new global Recommendation for the estimation of average annual exceedance distribution of point one-minute rain rates.

1.5   Thesis outline

The motivation and objectives of the project have been introduced in this chapter. Chapter 2 discusses rain fade and the physical characteristics of rain that are relevant for calculating attenuation. It also includes a review of ITU-R rain-induced attenuation prediction models. The precipitation datasets used in this project are presented in Chapter 3. It also reviews precipitation-measuring techniques. Chapter 4 presents the estimation of $X(R)$ using distributions of measured TRMM rain rates in the Tropics. Chapter 5 compares the estimation of global $X(R)$ using conditional distributions of measured TRMM rain rates. Chapter 6 presents a curve fit approximation to conditional distributions of measured TRMM rain rates and evaluates a Rec. ITU-R P.837-type model based on them. Chapter 7 presents a hybrid method for tropical and temperate regions, while conclusions are presented in Chapter 8.

Chapter 2   ITU-R Rain Attenuation Models

2.1   Introduction

The electromagnetic radio spectrum lies between the frequencies 3 KHz to 3 THz, but the range managed for atmospheric telecommunications used by the ITU-R spans 10 KHz to 300 GHz. As the frequency increases, the wavelength decreases, waves experience less angular diffraction from edges and are scattered by smaller objects. The frequencies above 1 GHz are used for high capacity and high availability networks. Due to the relatively short wavelengths, these radio links experience severe screening, refraction, reflection and scintillation. Attenuation due to scattering by raindrops becomes increasingly important for frequencies above 10 GHz until it plateaus around 100 GHz, and it is the dominant dynamic fade mechanism for many links.

Rain fade or rain-induced attenuation is the reduction in received signal strength due to hydrometeor scatter and absorption. Typically, more intense rain causes larger rain fade. The average annual distribution of rain rate may be used to predict the average annual distribution of rain fade for radio links, given knowledge of the link geometry and radio system parameters. The distribution of rain fade is critical in the design of line-of-sight terrestrial and Earth-space microwave links to meet availability constraints. It is also important when calculating the interference between radio systems. Hydrometeors can be fog, clouds, ice crystals, raindrops, snowflakes, hail and a wide range of mixed–phase particles. All falling hydrometeors are called precipitation.

The effects of hydrometeors on communication systems depends on the system frequency and the type of particle present. However, the focus of this work will be on rain. Other types of hydrometeor are often included in propagation models as a correction applied to the estimated fade due to rain. The study of rain-fade requires an understanding of the physical characteristics

of rain as well as the interaction of rain and electromagnetic waves propagating in the communication medium.

This chapter reviews the characteristics of rain that are important in radio engineering. Rain is a collection of particles that needs to be described statistically. A sample of atmosphere will contain a distribution of raindrops of differing sizes. Different sized raindrops have different shapes, fall speeds and scattering properties. Furthermore, the summarising properties of rainfall rate and specific attenuation will vary rapidly in time and space. Radio links have both temporal and spatial extent requiring complex statistical models to describe the effects of rain. The second half of this chapter reviews the ITU-R Recommendations relevant to the prediction of rain fade on radio links.

2.2   Rain characteristics

2.2.1 Rain drop shape

Raindrops, especially small raindrops, are often assumed to be spherical. Photographic measurements of rain drop shape have been carried out using water drops falling at terminal velocity in a wind-tunnel e.g. Pruppacher and Beard(1970) and Nelson and Gokhale (1972) showed that drops with diameters less than 1 mm are almost spherical, while larger drops become oblate spheroids, with the distortion in shape increasing with drop size. Similar results were inferred from dual-polarisation radar data by Gorgucci et al. (2006). The Pruppacher-and-Pitter raindrop model describes the shape of water drops falling at their terminal velocity and is based on a balance of forces due to gravity and air resistance. Raindrops are close to spherical when they are very small (less than a few mm in diameter) due to surface tension. As their size increases, the shape increasingly becomes an oblate spheroid due to circulation of water within the drop

and hydrodynamic pressures on the surface, with the base progressively flattening out to develop into a concave base (Pruppacher & Pitter, 1971).

Rain drop shape has been assumed to be oblate spheroid (Pruppacher & Pitter, 1971; Green, 1975; Beard & Chuang, 1987), however, research has shown that raindrops often have other shapes due to natural oscillations, hence raindrop axis ratios can differ in other ways from the equilibrium shapes (Beard et al., 2010).

2.2.2 Drop Size Distribution

Rainfall events are made up of rain drops of different sizes (diameters). The drop size distribution (DSD) is the variation of the composition of these rain drops. It is defined such that $N(D)dD$ is the number of drops per cubic metre with drop diameters between D and $D + dD$. D is the diameter of an equivolumic sphere, since most drops are not perfect spheres.

Many of the properties of rain, such as rain rate and specific attenuation, can be expressed as moments or integrals over the drop size distribution function $N(D)$.

Historically, the DSD has been measured by observing wet patches on filter paper or dried dough pellets after drops fall into flour (T. Oguchi, 1983). More recently, electro-mechanical disdrometers have automated the recording of drop size distributions and have demonstrated the variability in DSD parameters.

Measured DSD are generally irregular due to the problem of sampling enough raindrops while spanning a volume of uniform rain characteristics. The underlying DSD, from which the measured DSD is a sample, are often assumed to follow analytic shapes. An exponential form for *N(D)*, also known as the Marshall-Palmer distribution (Marshall & Palmer, 1948) , is given by

$$N(D) = N_0 exp(- \wedge D) \tag{2.1}$$

where N_0 is the Marshall-Palmer scale parameter and is approximately 8000 cm⁻¹m⁻³.

The exponent parameter Λ tends to decrease with rain rate R:

$$\Lambda = 4.1R^{-0.21} \tag{2.2}$$

where Λ is in mm^{-1} and R is in mmhr^{-1}.

If the terminal velocity as a function of equivalent drop diameter, $V(D)$ is known, then the rain rate may be expressed as:

$$R = \frac{\pi}{6}\int_0^\infty D^3 V(D)N(D)dD \tag{2.3}$$

As R appears in 2.2, this provides a consistency constraint. For an exponential DSD with standard units, the median drop diameter of the distribution D_0, is given by

$$D_0 = \frac{3.67}{\Lambda} \tag{2.4}$$

The Law-Parson's distribution, an antecedent of the Marshal-Palmer, used empirically measured values of $N(D)$ for different types of rain event and presented average DSD in tables (Laws & Parsons, 1943).

A gamma-type of the distribution has been proposed by Ulbrich (1983):

$$N(D) = N_0 D^\mu exp(-\Lambda D) \tag{2.5}$$

where μ has a positive or negative value and N_0 has units of $m^3 cm^{-1-\mu}$

A normalised model of the gamma distribution was presented by Willis (1984), while Haddad et al. (1997) developed a parametrised model suitable for tropical rainfall.

DSD is known to have variations with respect to time and space, and several studies have been carried out to show that it also varies with geographic locations as well as different rainfall regimes (Islam, T., Rico-Ramirez, Thurai et al., 2012). For instance, Sauvageot et al. (1999)

showed the variations in DSDs between the tropics and mid-latitudes; Bringi et al. (2003) demonstrated the variations in DSDs between stratiform and convective rain types in different climates while Tokay and Short (1996) illustrated the DSD variation in these rain types in tropical climate.

Drop size distributions are population statistical models and the DSD experienced by a radio link will vary in space and time. The Marshall-Palmer distribution has been used for attenuation predictions for frequencies between 30 to 300 GHz and above (Barclay, 2003).

Rain attenuation is a function of the drop size distribution as well as other parameters of the propagating medium such as the raindrop water temperature, raindrop shape, etc. (Lin, 1973).

2.2.3 Polarisation dependence

Typically, as large raindrops are shorter vertically than they are wide, they cause greater attenuation to horizontally polarised waves than vertically. Terrestrial telecommunications links are usually either vertically polarised or use both vertical and horizontal polarisation (or left and right circular polarisation). Raindrops are usually rotationally symmetric around the vertical and so cause no change in the incident linear polarisation. However, the presence of a vertical shear in the horizontal wind velocity can lead to drop canting where the axis is angled away from the vertical. Scattering from canting drops causes cross-polar interference. Cross-polarisation is closely related to attenuation and for design calculations, it is convenient to approximate the relation between them as a deterministic one (Barclay, 2003).

2.2.4 The spatial-temporal structure of rain

Temporal (rainfall rate)

Rainfall rate is an important parameter in determining attenuation on a link and annual rainfall statistics are usually expressed as the rain rate exceeded for a given percentage of an average

year. Average statistics over many years are recommended due to the year-to-year variability in the statistics of rainfall. The high-resolution rainfall statistics required for radio regulation (point one-minute rain rates) are not available for most of the world and least likely to be available for developing countries in the Tropics. These high-resolution rain rate measurements require specialist equipment, which are difficult to site, and a long-term commitment to the collection of data. Their principal use is in radio regulation and spectrum management, whereas most hydrological data are collected for water management and agriculture. In places without the required data, estimates of average annual exceedance distribution of point one-minute rain rates are provided by the prediction method in Rec. ITU-R P.837 (ITU-R, 2015b; ITU-R, 2017b).

Spatial (vertical and horizontal structure)

The height of rain events is an important factor in the attenuation of Earth-space paths, and some terrestrial slant paths, because it determines the path length over which rain causes attenuation. The rain height is often assumed to be 300 m above the level in the atmosphere where the temperature has dropped to 0°C. For convective events, there may be many such heights within a single event. However, for a stratified atmosphere in temperate regions the zero degree isotherm height exists and varies significantly with the seasons. In the Tropics, it is higher and more stable. Rec. ITU-R P.839 provides a digital map of the globe showing mean annual zero degree (0 C) isotherm height above mean sea level for locations that do not have sufficient information (ITU-R, 2015a).

2.2.5 Rain scattering

Rain causes attenuation through absorption and scattering. Scattering occurs when the electromagnetic wave encounters an obstacle or a scattering particle, in this case, a raindrop. Radio waves can be refracted through the drops or diffracted around. Due to the relative size of

raindrops compared to microwave wavelengths, Rayleigh and Mie scattering models are appropriate (Kestwal et al., 2014). Rayleigh scattering is applicable to particles that are small in diameter compared to the wavelength. Mie scattering theory is applicable to spheres of any size, but because of its complexity, is usually only applied when the wavelength is similar to the drop diameter. For the majority of radio links, the dominant rain fade process is the scattering of radio power away from the receive antenna.

Other scattering models and techniques include the T-matrix method and the discrete dipole approximation (DDA) method which are used in hydrometeor scattering analysis. T-matrix tools are able to calculate the scattering properties of rotationally symmetric particles only, while the DDA method has the advantage that it can be applied to arbitrarily shaped (asymmetric) drops, though its numerical accuracy is relatively low, and computational costs are extremely high (Thurai et al., 2014).

Rayleigh scattering

A scattering particle of radius a in an electromagnetic field with wavelength of λ is electrically small if $2\pi a/\lambda \ll 1$. In this case, the phase difference across the diameter are small and Rayleigh scattering predicts that the scattered field is close to that of a dipole. The dipole moment induced by the particle is related to the incident electric field. Scattering is near isotropic perpendicular to the polarisation of the incident wave. These assumptions are often made for rain scatter at radio frequencies.

2.3   ITU-R rain attenuation prediction models

The prediction of rain-induced attenuation is required for the regulation and management of the radio spectrum, along with optimising the performance of both individual, and networks of,

microwave telecommunications links. Rainfall rate statistics are required for the prediction of rain-induced attenuation. There are two methods used for the prediction of rain-induced attenuation: the physical method also known as the theoretical or analytical model, by which the physical processes involved in attenuation are reproduced; and the empirical method which is based on measurement databases at various locations (Kestwal et al., 2014). ITU-R Recommendations are based on a combination of these methods. Predicting distributions of rain attenuation requires data on the distribution of rain rate and assumptions on the DSDs experienced.

The ITU-R has various Recommendations containing internationally agreed models for a range of propagation mechanisms and performance prediction methods for communication systems operating in the radio frequency spectrum. The few that will be considered in this project relate to rain-induced attenuation in both terrestrial line-of-sight and Earth-space links. These are reviewed in the following sections.

2.3.1 Recommendation ITU-R P. 837-7

Rec. ITU-R P.837-7 provides a method for the prediction of average annual rainfall rate R_p, exceeded for a given time percentage p, for any point on Earth. The input parameters to the model are *MT*: the monthly mean total rain accumulation, and T: the monthly mean surface temperature, both at the location of interest. These can be determined from reliable local data or obtained from the digital maps in Rec. ITU-R P.837-7 and Rec. ITU-R. P.1510 respectively (ITU-R, 2017b). The following process is taken from Rec. ITU-R P.837-7 (ITU-R, 2017b). *MT* and T are used to derive the monthly probability of rain P_0 (%) using the expression:

$$P_{0_{ii}} = \frac{\text{MT}_{ii} \times 100}{24 \times N_{ii} \times r_{ii}} \ (\%) \tag{2.6}$$

for each month number ii where $ii = \{01, 02, 03, 04, 05, 06, 07, 08, 09, 10, 11, 12\}$ indexing January through to December.

N_{ii} is the average number of days in the month, with $N_2 = 28.25$, and r_{ii} can be calculated from:

$$\begin{cases} r_{ii} = 0.5874 \cdot e^{0.0883 T_{ii}} \; for \; T_{ii} \geq 0°C \\ r_{ii} = 0.5874 \qquad\qquad for \; T_{ii} \leq 0°C \end{cases} \; \text{(mm/hr)} \tag{2.7}$$

When $P_{0_{ii}} > 70$, it is taken as $P_{0_{ii}} = 70$ and $r = \frac{100}{70} \times \frac{MT_{ii}}{24N_{ii}}$. Note that $\frac{MT}{24N}$ is the mean rain rate in mm/hr for the month. The annual probability of rain $P_{0_{annual}}$ is then given by

$$P_{0_{annual}} = \frac{\sum_{ii=1}^{12} N_{ii} \times P_{0_{ii}}}{365.25} \tag{2.8}$$

For time percentage $p > P_{0_{annual}}$, the rain rate at p, $R_p = 0$ mm/hr. For $p \leq P_{0_{annual}}$, and R_{ref} such that $100 \left| \frac{P(R > R_{ref})}{p} - 1 \right| < 0.001$, calculate the monthly exceedance probabilities using

$$P_{ii}(R > R_{ref}) = P_{0_{ii}} Q \left(\frac{\ln(R_{ref}) + 0.7938 - \ln(r_{ii})}{1.26} \right) \; (\%) \tag{2.9}$$

where
$$Q(x) = \frac{1}{\sqrt{2\pi}} \int_x^\infty e^{\frac{-t^2}{2}} \, dt \tag{2.10}$$

is the standard Normal complementary cumulative distribution function. The annual exceedance probability is then calculated using:

$$P(R > R_{ref}) = \frac{\sum_{ii=1}^{12} N_{ii} P_{ii}(R > R_{ref})}{365.25} \; (\%) \tag{2.11}$$

Alternatively, the monthly complementary cumulative distribution function CCDF of rainfall rate R for the ith month is given by

$$P_{ii}(R) = \frac{P_{0_{ii}}}{2} erfc \left(\frac{\ln(R) + \sigma_{ii}^2/2 - \ln(r_{ii})}{\sqrt{2}\sigma_{ii}} \right) \qquad \text{(Luini et al., 2017)} \tag{2.12}$$

where σ_{ii}, a monthly scale parameter of the log-normal distribution is independent of the reference site and is given a fixed value of 1.26.

2.3.2 Recommendation ITU-R P.838-3

This Recommendation (ITU-R, 2008) provides a power-law linking specific attenuation to rain rate:

$$\gamma_R = kR^\alpha \tag{2.13}$$

where the specific attenuation γ_R is in dB/km, R is the rain rate in mm/hr. The values of k and α are functions of the frequency in GHz as shown below:

$$\log_{10} k = \sum_{j=1}^{4} a_j \, exp \left[- \left(\frac{\log_{10} f - b_j}{c_j} \right)^2 \right] + m_k \log_{10} f + c_k \tag{2.14}$$

$$\alpha = \sum_{j=1}^{5} a_j exp \left[- \left(\frac{\log_{10} f - b_j}{c_j} \right)^2 \right] + m_\alpha \log_{10} f + c_\alpha \tag{2.15}$$

The values for k could either be k_H or k_V for the horizontal and vertical polarisation and α could be α_H or α_V. The values of the constants $\alpha_j, b_j, c_j, m_k, c_k, m_\alpha, c_\alpha$ are listed in tables within the Recommendation. The specific attenuation – rain rate $(\gamma - R)$ power law is an average result due to DSD variation, and the actual specific attenuation for a given rain rate will be a statistical distribution with this mean.

2.3.3 Recommendation ITU-R P.530-17

Rec. ITU-R P.530-17 (ITU-R, 2018b) contains models used for planning terrestrial line-of-sight systems. It summarises the propagation effects that must be considered when designing such links, including techniques for mitigating propagation impairments. From the ITU-R P.530-17 model, the long-term statistics of rain attenuation can be calculated using the following steps:

Step 1: Obtain the rain rate $R_{0.01\%}$ exceeded for 0.01% of the time with an integration time of one-minute. This can be obtained from Rec. ITU-R P.837 for locations without adequate information.

Step 2: Compute the specific attenuation γ_R(dB/km) for the frequency, polarization and 0.01% exceeded rain rate for the location of interest using Rec. ITU-R P.838

Step 3: Compute the effective path length d_{eff} of the link, which is a product of the actual path length d and a distance factor r where an estimate of r is given by:

$$r = \frac{1}{0.477\, d^{0.633} R_{0.01}^{0.073} .\alpha\, f^{0.123} - 10.579(1 - \exp(-0.024\, d))} \tag{2.16}$$

where f (GHz) is the frequency, α is the exponent in the attenuation model in step 2, with the maximum recommended value of r of 2.5, so if the denominator for the equation for (2.18) is less than 0.4, r should be taken as 2.5

Step 4: Estimate the path attenuation exceeded for 0.01% of the time by

$$A_{0.01} = \gamma_R d_{eff} = \gamma_R\, dr \quad \text{dB} \tag{2.17}$$

Step 5: The attenuation exceeded for other percentages of time p in the range 0.001% to 1% is given by:

$$\frac{A_p}{A_{0.01}} = C_1\, p^{-(C_2 + C_3 \log_{10} p)} \tag{2.18}$$

where
$$C_1 = (0.07^{C_0})\left[0.12^{\,(1-C_0)}\right] \tag{2.19}$$

$$C_2 = 0.855 C_0 + 0.546(1 - C_0) \tag{2.20}$$

$$C_3 = 0.139 C_0 + 0.043(1 - C_0) \tag{2.21}$$

and
$$C_0 = \begin{cases} 0.12 + 0.4[\log_{10}(f/10)^{0.8}] & f \geq 10 GHz \\ 0.12 & f < 10 GHz \end{cases} \tag{2.22}$$

Methods for calculating as the distribution for the average annual worst month are also included in the Recommendation.

2.3.4 Recommendation ITU-R P.618-13

The propagation effects considered in the design of Earth-space radio systems are different from those of terrestrial line-of-sight links. Multipath atmospheric propagation can be neglected (except in elevation angles < 4˚). However, high altitude ice particles and variations in atmospheric radio refractive index have to be considered. Rain effects are similar for both Earth-space and terrestrial line-of-sight systems, but there are differences in the effective path length. For Earth-space systems, the effective path length through rain is derived from the height of the rain event; also, the variation in rain rate along the link. For terrestrial line-of-sight links, the length of the link and the horizontal distribution of rain is important (Barclay, 2003). They also differ in the effects of the melting layer. This is the layer of mixed-phase hydrometeors, for a stratified atmosphere around the zero-degree isotherm, where precipitation causes significantly more attenuation than the equivalent rain rate. Horizontal terrestrial links may or may not be in the melting layer while Earth-space links nearly always pass through the melting layer if it is raining at the Earth terminal. These considerations are captured in Rec. ITU-R P.618-13.

The Recommendation provides a systematic method for calculating the long-term rain attenuation statistics on a slant path using the $R_{0.01\%}$ and link parameters

$R_{0.01}$: the point rainfall rate for the desired location for 0.01% of an average year (mm/hr);

h_s: height above mean sea level of the Earth station (km);

θ: elevation angle (degrees);

φ: latitude of the Earth station (degrees);

f: frequency (GHz); and

R_e: effective radius of the Earth (8500km).

The geometry is shown in the figure below:

A: frozen precipitation
B: rain height
C: liquid precipitation
D: Earth-space path
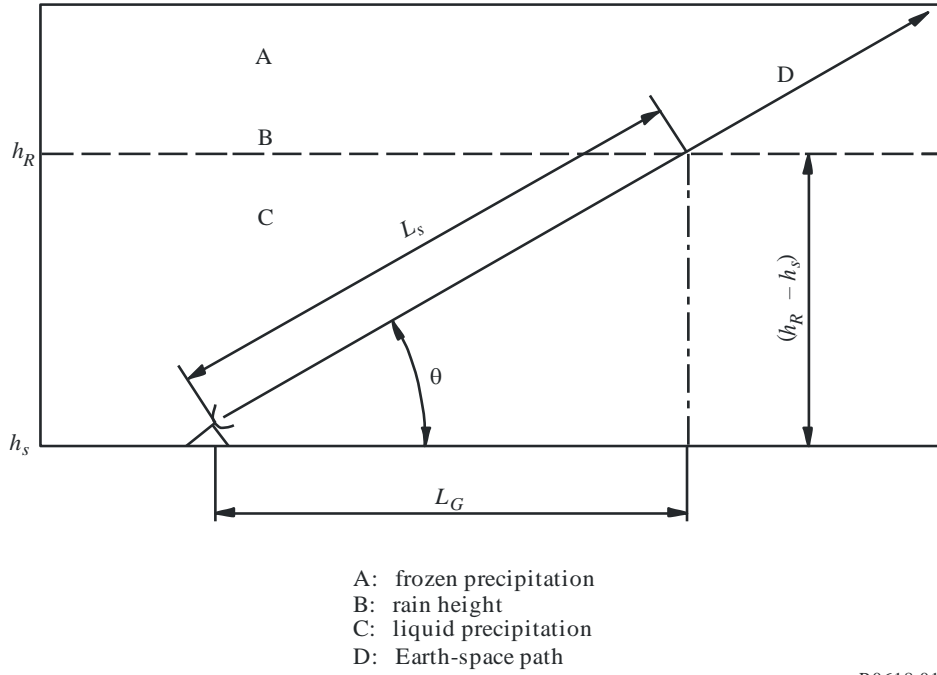
P.0618-01

Figure2.1. Schematic presentation of an Earth-space path showing the input parameters of the attenuation prediction process (ITU-R, 2018d)

The long-term statistics of attenuation due to rain is estimated as follows:

Step 1:Determine the rain height, h_r, as given in Recommendation ITU-R P.839.

Step 2: For $\theta \geq 5°$ compute the slant-path length, L_s, below the rain height:

$$L_S = \frac{(h_R - h_S)}{sin\theta} \quad km \tag{2.23}$$

For $\theta < 5°$,

$$L_S = \frac{2(h_r - h_s)}{\left(sin^2\theta + \frac{2(h_r - h_s)}{R_e}\right)^{1/2} + sin\theta} \tag{2.24}$$

18

If $h_R - h_s$ is less than or equal to zero, the predicted rain attenuation for any time percentage is zero and the following steps are not required.

Step 3: Calculate the horizontal projection, L_G of the slant-path length:

$$L_G = L_s \cos\theta \quad \text{km} \tag{2.25}$$

Step 4: Obtain the rainfall rate, $R_{0.01\%}$, exceeded for 0.01% of an average year (with an integration time of one-minute) from local data sources, or from maps of rainfall rate given in Recommendation ITU-R P.837. If $R_{0.01\%}$ is equal to zero, the predicted rain attenuation is zero for all time percentages and the following steps are not required.

Step 5: Obtain the specific attenuation, γ_R, using the frequency-dependent coefficients given in Recommendation ITU-R P.838 and the rainfall rate, $R_{0.01\%}$ determined from Step 4, by using:

$$\gamma_R = k(R_{0.01\%})^\alpha \quad \text{dB/km} \tag{2.26}$$

Step 6: Calculate the horizontal reduction factor, $r_{0.01}$ for 0.01% of the time:

$$r_{0.01} = \frac{1}{1+0.78\sqrt{\frac{L_G\gamma_R}{f}}-0.38(1-e^{-2L_G})} \tag{2.27}$$

Step 7: Calculate the vertical adjustment factor, $v_{0.01}$ for 0.01% of the time:

$$\zeta = tan^{-1}\left(\frac{h_R-h_s}{L_G r_{0.01}}\right) \quad \text{degrees}$$

For
$$\zeta > 0, L_R = \frac{L_G r_{0.01}}{\cos\theta} \quad \text{km}$$

else,
$$L_R = \frac{h_R-h_s}{\sin\theta} \quad \text{km}$$

If
$$|\varphi| < 36°, \chi = 36 - |\varphi| \quad \text{degrees}$$

else,
$$\chi = 0 \quad \text{degrees}$$

$$v_{0.01} = \frac{1}{1 + \sqrt{\sin\theta}\left(31\left(1 - e^{-(\theta/(1+\chi))}\right)\frac{\sqrt{L_R\gamma_R}}{f^2} - 0.45\right)}$$

Step 8: The effective path length is:

$$L_E = L_R v_{0.01} \quad km \tag{2.28}$$

Step 9: The predicted attenuation exceeded for 0.01% of an average year is:

$$A_{0.01} = \gamma_R L_E \quad dB \tag{2.29}$$

Step 10: The estimated attenuation to be exceeded for other percentages of an average year, in the range 0.001% to 5%, is determined from the attenuation to be exceeded for 0.01% for an average year:

If $\qquad$ p ≥ 1% or | φ | ≥ 36°: $\;\;$ β = 0

If $\qquad$ p < 1% and | φ | < 36° and θ ≥ 25°: $\quad$ β = –0.005(| φ | – 36)

otherwise: $\qquad$ β = –0.005(| φ | – 36) + 1.8 – 4.25 sin θ

$$A_p = A_{0.01}\left(\frac{p}{0.01}\right)^{-(0.655 + 0.033\ln(p) - 0.045\ln(A_{0.01}) - \beta(1-p)\sin\theta)} \quad dB \tag{2.30}$$

2.3.5 Recommendation ITU-R P.452-16

While Recs ITU-R P.530 and P.618 deal with the effects on the wanted signal in relation to system planning, interference between Earth stations and terrestrial stations (operating within the frequency range of about 0.1 GHz to 50 GHz) are addressed in Recommendation ITU-R P.452-16. The methodology for hydrometeor-scatter interference prediction using the transmission loss between two stations (ITU-R, 2018a) is based on the application of the bi-static equation, which

can be written in terms of the power P_r received at a receiving station from scattering by rain of the power P_t transmitted by a transmitting station

$$P_r = P_t \frac{\lambda^2}{(4\pi)^3} \iiint_{all\ space} \frac{G_t G_r \eta A}{r_t^2 r_r^2}\ dV \qquad (2.31)$$

where

λ: wavelength

G_t: gain (linear) of the transmitting antenna

G_r: gain (linear) of the receiving antenna

η: scattering cross-section per unit volume, δV (m^2/m^3)

A: attenuation along the path from transmitter to receiver (in linear terms)

r_t: distance from transmitter to the scattering volume element

r_r: distance from scattering volume element to the receiver (ITU-R, 2016)

The scattering cross-section per unit volume depends upon rain rate and the method to calculate this are found in the Recommendation. To calculate annual interference statistics, the rain rate distribution is needed.

2.4   Chapter Summary

The search for greater capacity forces telecommunications links into ever-higher microwave and millimetre wave frequencies. However, as frequencies increase from 10 to 100 GHz, rain scattering attenuation and interference become increasingly important. Although interactions of individual raindrops and radio waves may be calculated from established physical models, the effects of rain require statistical models due to the complex spatial and temporal variation of rain rate and drop size distributions. The ITU-R provides a range of Recommendations with models

allowing the prediction of rain fade and rain scatter interference on a range of links. Many of these models rely upon knowledge of the average annual distribution of point one-minute rain rates This distribution varies between locations due to local climate and topography. In much of the world, these distributions have not been measured. The rest of the thesis focuses on models for predicting the rain rate distribution, applicable globally.

Chapter 3   Precipitation Datasets

3.1   Introduction

Rain data are useful for monitoring the environment, forecasting the weather, in agriculture, for meteorological and hydrological studies and in aviation. Rainfall rate plays a major role in the performance of radio links, especially those operating above the 10 GHz, and many other parameters can be derived from it. This chapter reviews the current major sources of rain data and introduces some of the databases of meteorological and propagation measurements used in this project.

3.2   Major sources of rain data

The major sources of rain data are discussed in this section along with their quality.

3.2.1   Ground Based Measurements

Rain gauge data

The 5000-year-old Nilometer is often cited as the first rain measurement. This pillar was used to measure the depth of the Nile's annual inundation. Strangeways (2004) describes the measurement of rainfall in India in the 4th Century BC followed by the Jews in Palestine in the 2nd Century BC (Danby, 1933). The use of rain gauges is recorded in China around AD 1247 and the Lee Dynasty in Korea in 1441; rain gauges were not used in Europe until the 17th Century, the first being in Italy by Benedetto Castelli, a Benedictine monk under Galileo's tutelage (Strangeways, 2006a).

A rain gauge is a device that collects rain falling through a horizontal aperture and measures the volume of water collected. The volume measurement may be manual, mechanical or electronic.

23

The basic construction of a manual rain gauge is a funnel with deep sides to minimise loss due to splashing, fitted onto a collection vessel, fixed into the ground. The quantity of water collected by the funnel is estimated using a graduated cylinder. Historical mechanical rain gauges include the float- and balance-type, both of which move a pen across a chart to take records. The most common type of the electronic rain gauge is the tipping-bucket rain gauge, which was first invented by Sir Christopher Wren in the 1600s. His was a single-sided design that worked on the principle that an internal container tipped over when filled with water and then fell back into place, an antecedent to the two-bucket design by Crosslet in1829 (Strangeways, 2006c).

Modern designs of the tipping-bucket system are symmetrical with calibrated buckets. As the rocker holding buckets tips, an attached magnet triggers a reed switch, the number and times of the triggers indicates the intensity and duration of rainfall. This method was improved upon by the UK Meteorological Office design, which included weighing the bucket as well as counting the tips to monitor the increase in the rain volume between tips (Strangeways, 2006c).

Weighing gauges are another modern form of the electronic rain gauge. The volume of water collected is estimated by weighing the collection container, often via a load cell. Capacitance rain gauges use two electrodes in the collection cylinder, acting as a capacitor, to estimate the water volume (Strangeways, 2006c). Volume estimates were historically recorded using moving pens on paper rolls but modern gauges record the estimates digitally.

In the last few decades, optical or laser rain gauges have found wide application. Individual or groups of raindrops are measured by the light they scatter as they fall through a shaped laser beam. These gauges can provide many other measures apart from rain rate, such as optical visibility, hydrometeor shape, phase and fall speed. Unlike funnel gauges, they are robust and require very little maintenance.

Funnel gauges produce measurements with both systematic and random errors, and require considerable maintenance to function reliably. Errors can be instrumental, due to a mismatch between the size of the collector and experienced rain rates, or due to improper installation of the gauge (Tapiador et al., 2012). Errors can also be intrinsic, such as wind effects especially during light rain, and evaporation when rain intervals are intermittent (Strangeways, 2006c). Serious errors can be caused by blockages from dust, pollen, bird faeces and insects. This can lead to rain events being missed entirely or anomalous extreme rain events when the blockage clears. Rain gauges are also very hard to site due to the constraints on the height of nearby objects such as trees and buildings. The World Meteorological Organisation (WMO) (Ranatunga, 2014) suggest stringent standards in the siting and maintenance required by funnel gauges. They are almost impossible to site within urban areas with the added complexity of security to protect the equipment from interference. In spite of these sources of error, rain gauges are universally considered to be gold-standard reference data for precipitation observation, as they physically collect and measure precipitation at a given spot (Tapiador et al., 2012).

Important global datasets have been created using measurements from networks of rain gauges. These include the Global Precipitation Climatology Centre, GPCC (GPCC, 2018) database, derived by the World Meteorological Organisation from 50,650 weather stations distributed globally. The dataset dates back to the last century and gridded products are available over $2.5° \times 2.5°$, $1.0° \times 1.0°$, $0.5° \times 0.5°$ and $0.25° \times 0.25°$ grids. The dataset by the Climate Prediction Centre of the National Oceanic and Atmospheric Administration (NOAA) is the Monthly Analysis of Global Land Precipitation collected from 1948 to the present from 17,000 stations at $0.5° \times 0.5°$ gridded spatial resolution (Michaelides et al., 2009). Almost all of the gauges in these datasets are sited on land, and so rainfall over the sea is not captured. In addition, for gridded products, the gauges are not evenly distributed across the grid cells, and for high-resolution grids, many cells will contain no gauges at all.

Disdrometers

Disdrometers measure the size, and often the fall speed, of raindrops. They are useful for measuring the variation in the drop size distribution (DSD) with time (Michaelides et al., 2009). As described in Section 2.2.2, many rain parameters, such as rain rate and rain attenuation, may be calculated from the DSD. Early manual disdrometers used slates lined with filter paper, bowls of flour or plaster of Paris, to detect the drops of rain (Strangeways, 2006c). The first electronic impact disdrometers, such as the Joss-Waldvogel developed in 1967, used magnetic induction or the piezoelectric sensors developed by John Hopkin's University (Michaelides et al., 2009; Strangeways, 2006c), to measure the momentum of impacting rain drops. More recently, optical disdrometers have dominated the market. The OTT Parsivel and Thies disdrometers operate by measuring scattering from a laser beam, while other two-dimensional video disdrometers measure the silhouette of falling hydrometeors. Disdrometers are able to record drop size distributions, hydrometeor phase, precipitation type and particle fall velocity (Tapiador et al., 2012).

Radars

The term *radar* is a contraction of *ra*dio *d*etection *a*nd *r*anging. Radars operate by radiating energy and detecting the signal reflected from targets. The amplitude and delay of the reflected signal indicate the presence, size and range of the target. Mapping rainfall by the returned power started in the mid-1940s (Tapiador et al., 2012). Radars give an instantaneous volume average estimation of precipitation rather than the point temporal average provided by rain gauges (Kidd & Huffman, 2011). A single radar can image the rain over very large areas as large as 15000 Km^2. A typical meteorological radar consists of a dish antenna transmitting microwave pulses in main beams subtending angles between 1 and 2-degrees depending upon the antenna size. The range and the reflectivity of the precipitation can be calculated from the delay and strength of the

returned signal respectively. The Doppler shift of the returned frequency shows the radial velocity of the target, and the polarisation of the signal indicates the shape and orientation of the hydrometeors. The typical wavelengths used in radars include 3 cm (X band or 10 GHz), 5 cm (C band or 6 GHz), 10 cm (S band or 3 GHz) and 2cm (K_U band or 15 GHz). On the TRMM satellite, a wavelength of 2.2 cm (13.8 GHz)) is used with a phased array rather than a dish.

Rainfall rate R is derived from radar reflectivity using power-law relations:

$$Z = aR^b \tag{3.1}$$

where Z is the radar reflectivity in mm^6m^{-3}, and R is rain rate in $mmhr^{-1}$. The *Z-R* relations are often refined by calibration against rain gauges covered by the radar.

The parameters, *a* and *b*, are determined by the DSD and have a wide range of possible values, the most common being $a = 200$ mm^6m^{-3} and b =1.6. Values of *a* can change depending on the rainfall type and location (Strangeways, 2006b). For instance, for tropical rainfall, the relationship $Z = 250R^{1.2}$ is often used (Fulton et al., 1998).

One of the largest source of error in rain radar estimates comes from variation in DSD. Drop size distribution and *Z-R* relation is affected by rain event type (stratiform, convective, frontal, etc.) and hydrometeor phase. Rain measurements at altitude can be strongly affected by hydrometeor phase in the melting layer (known as the bright band by radar meteorologists). A fundamental problem is that radar measurements are the same whether hydrometeors are falling or not. Where there is convection, the smaller drops will be rising rather than falling. Rain rate is defined by the volume of water that falls through a horizontal area. Radars can estimate the number of drops of different sizes (by assuming the form of DSD) but generally assume that drops fall at their terminal velocity. This assumption is often invalid.

Other errors also affect estimates. Reflectivity estimates at distance rely upon corrections due to reflectivity of the atmosphere closer to the radar. Errors accumulate along the propagation path away from the radar. Anomalous propagation, such as ducting can also yield erroneous results. Ground based radars may be affected by tall objects that obstruct the radar beam (Michaelides et al., 2009). Although range averages are formed almost instantaneously, spatial averages in the direction of scanning rely upon the physical rotation of the antenna and so take a substantially longer period. For radars that scan across a wide arc, there may be an appreciable time delay between data collected in different directions. This limits the time resolution of these systems. Attenuation of the radar signal by rain, interception by the ground, and ground clutter caused when the main radar beam or side lobes encounter ground targets, are also sources of error (Harrison et al., 2000).

3.2.2   Re-analyses data

Reanalysis helps in overcoming the inherent weaknesses of observation data by assimilating them into a physical model. Reanalyses data are the output of numerical weather prediction (NWP) systems after assimilation of all available historic data. Often, the NWP algorithm is unchanged throughout the analysis period so that observed changes in climate are not obscured or created by changes in algorithms. Re-analysis output can only be validated using data from observations not used in the reanalysis. ERA40, with a spatial resolution of about 120 km, and ERA-Interim datasets, both from European Centre for Medium-Range Weather Forecasts (ECMWF), are examples of reanalyses datasets. Others include NCEP-2 with a grid resolution of 210 km and JRA-25, the Japanese 25-year reanalysis with a resolution of 125 km. They are all tri-dimensional (latitude-longitude-time), except ERA-Interim, which includes altitude and so is 4D (Tapiador et al., 2012). The data usage and issues of quality control for ERA 40 and ERA Interim are contained in (ECMWF, 2011).

3.2.3   Satellite data

The first satellite put into orbit was the Russian Sputnik in1957, although it did not record any measurements. The first weather satellite was USA's TIROS1 –Television and Infrared Observing Satellite, in1960 followed by ITOS - Improved TIROS Operational Satellite in 1970. Both of these made use of television cameras to capture images of the Earth. Later the National Oceanic and Atmospheric Administration (NOAA)-2 satellite, included radiometers and a camera sensitive to non-optical frequencies.

Satellite orbits are usually high altitude to achieve geo-stationarity (GEO - geosynchronous earth orbit), or faster, lower orbits (LEO – low earth orbit) that cross the poles or at an angle skewed to the equator. Geostationary orbits require a specific altitude of approximately 36000 km and orbit around the equator, while LEO can be at a range of altitudes above the atmosphere. Meteorological satellites can fly as low as 850 km. Geostationary satellites include the U.S Satellites operated by the Geostationary Operational Environment GOES, the Meteosat Second Generation (MSG) satellites operated by the European Organisation for the Exploitation of Meteorological Satellites (EUMETSAT) 1, the Feng-Yun_2 satellites from China and the Japanese Multifunctional Transport Satellite (MTSAT) series (Kidd & Huffman, 2011). The Russian Meteor, the EUMETSAT's Metop series and the NOAA satellites are examples of polar orbiting satellites, while TRMM and Global Precipitation Measurement (GPM) are skewed LEOs. Geostationary satellites get nearly the same view of the Earth from directly above a point on the equator, but from a very high altitude. LEO satellites are much closer to the Earth, and can view some or all of the Earth over time, but provide measurements at a particular point at irregular times determined by the orbit and rotation of the Earth.

Satellites do not measure precipitation directly but measure incident electromagnetic radiation. Methods for precipitation measurements have evolved from passive visible, infrared (IR)

microwave (PMW) methods, to active and merged IR and MW methods, since the launch of TRMM (Michaelides et al., 2009).

Satellite based infrared-based methods yield consistent rain rate estimates over wide areas with high temporal sampling. Their drawback is that the observations have an indirect relationship with precipitation as only the cloud tops can be observed (Sapiano & Arkin, 2009). They associate cold cloud processes with the heaviest surface rainfall, which may not always be the case. Moreover, the cloud-temperature relationship with rainfall is not stable as it changes with different seasons and with location (Tapiador et al., 2012; Kidd & Huffman, 2011).

Microwave techniques are more direct as microwaves penetrate the cloud and reflect off precipitation (Sapiano & Arkin, 2009). They use microwave and millimetre-wave frequencies that yield large hydrometeor-scatter as wavelengths approach the diameter of raindrops. In PMW methods, the sensors measure a signal that is a blend of emitted radiation from raindrops and emission from land. PMW methods are more effective over water than over land because of the higher emissivity of land. They have poorer resolution than IR methods: $50 \times 50 \text{ km}^2$ over water and $10 \times 10 \text{ km}^2$ over land. They assume that the rainfall structure is homogenous rather than three-dimensional (Michaelides et al., 2009) and they are currently only possible from LEO satellites, limiting the number of daily observations of a particular point (Kidd & Huffman, 2011). Active microwave techniques measure the power that is reflected back from transmitted pulses. TRMM, the first precipitation radar operating in space (Kidd & Huffman, 2011), uses an active microwave technique, giving estimates through radar and radiometric measurements (Tapiador et al., 2012).

Improvements in precipitation measurements have been achieved by the use of merged techniques, which combine the resolution of Visible/IR with the accuracy of PMW, to give products with better estimates and improved spatial and temporal resolution. The TRMM

Multisatellite Precipitation Analysis (TMPA), which provides data every 3 hours on a $0.25° \times 0.25°$ latitude/longitude grid, and the Climate Prediction Centre morphing method (CMORPH) are examples (Tapiador et al., 2012; Michaelides et al., 2009).

The Global Precipitation Climatology Project – GPCP has produced a dataset that combines not only microwave and IR estimates but rain gauge data as well, and has improved from the initial monthly data on $2.5° \times 2.5°$ latitude/longitude grid (1979 upwards) to $1° \times 1°$ daily, since 1997 (Tapiador et al., 2012). Another is the Climate Prediction Centre Merged Analysis of Precipitation (CMAP), which is a combination of satellite IR and re-analyses data from the National Centres for Environmental Prediction (NCEP) and the National Centre for Atmospheric Research (NCAR) (Kidd & Huffman, 2011).

Validation of Satellite precipitation estimates

Precipitation estimates from satellites have the advantages of wide coverage over both land and water bodies, continuous observation regardless of time or season, freedom from effects of terrain, the high cost of in-situ networks, and provision of near-real time information (Gebregiorgis & Hossain, 2015). The high variability and irregular statistics of rainfall requires frequent observations often over large regions. This can be achieved far more cost-effectively through satellites observation than by ground-based gauge networks. Satellites carrying a combination of sensors, which can provide global estimates of precipitation with high accuracy, wider coverage and finer spatial resolution (Huffman et al., 2007). Satellites are not limited by geo-political boundaries and additional information such as lightning and detection of areas experiencing high convection can be observed from satellite sensors (Kidd & Huffman, 2011). Satellite products are widely used for model validation over the ocean and high-resolution

satellite data have the advantage over daily accumulation rain gauges of representing the diurnal cycle of precipitation (Sapiano & Arkin, 2009).

Despite the advantages of satellite data over ground observations, they have issues of inaccuracies that arise from the process of sampling, or from limitations of the sensors. They also show discrepancies when using different temporal scales, for different rain regimes, and over different terrains (Yang et al., 2016) as well as in the algorithms used in converting measured quantities into rainfall parameters (Kidd & Huffman, 2011). Satellite precipitation data are also not used widely because of the lack of skill required to use them (Sorooshian et al., 2011) resulting in poor feedback that could lead to improvement. Because of this, satellite precipitation estimates usually require validation by ground-based measurements, particularly from rain gauges, as they are considered to be the gold standard source of rain rates at specific points.

Several validation studies have been performed in different regions using different datasets. Feidas et al. (2009) compare gauge-corrected and satellite-estimated rainfall accumulations, over the central-eastern Mediterranean region from September 2004 to August 2005. There was a high correlation coefficient of 0.88 between the two estimates during summer, and a poorer performance in the winter.

Joshi et al. (2012) validate TMPA and the GPCP, 1-degree daily accumulation, against rain gauge data obtained from the India Meteorological Department (IMD) in the summer monsoon season of 1998 – 2007 over India. The study showed that the satellites underestimated the average rainfall over the region. Satellite and rain gauge estimates were highly correlated but the root mean square difference was high, suggesting a scale factor difference. Five, high-resolution satellite estimates – PEHRPP, CMORPH, TMPA, NRL, and PERSIANN - were evaluated against rain gauge data spanning 2003 to 2006, from the United States and the Pacific Ocean by (Sapiano & Arkin, 2009). The satellite estimates showed higher correlation to the gauge estimates

in the warm season than in the cold season. Satellite estimates with gauge-correction performed better than those without. This is to be expected where gauges are considered to be ground-truth. However, gauge correction is likely to be of benefit to satellite estimates.

There have been views however, that it is impossible to perfectly match point-temporal measurements from gauges and instantaneous-volume averaged estimates from satellite products (Sapiano & Arkin, 2009; Bowman, 2005). As a result, validation of satellite estimates has been conducted using other means. For instance, the international Precipitation Working Group (IPWG) also initiated an online programme to test the accuracy of satellite estimates against radar and rain gauge measurements (Ebert et al., 2007). This aimed to provide up-to-date information on the quality of estimates.

3.3   Precipitation datasets for Radio Regulation

Precipitation affects radio communication, as rain fade is the dominant cause of outages on fixed-terrestrial and Earth-space microwave (>10 GHz) and millimetre wave links. High-quality input data are required for modelling these precipitation effects. This section reviews the various precipitation datasets that are relevant to this project.

3.3.1   TRMM Precipitation data

The TRMM satellite hosts multiple instruments. These include the Visible and InfraRed Scanner (VIRS), the Cloud and Earth Radiant Energy Sensor (CERES) and the Lightning Imaging Sensor (LIS). The Precipitation Radar (PR) and the TRMM Microwave Imager (TMI) are primarily used for measuring rainfall. The combination of satellite-borne passive (TMI) and active (PR) sensors is complementary and provides critical information on precipitation. While the passive microwave radiometers measure radiances that are a result electromagnetic effects through

precipitation clouds along the path of view of the sensor, the active microwave sensors provide specific height information based upon the time delay of the precipitation-backscattered return power (Kummerow et al., 1998). The spatial and temporal resolutions of rainfall measurements changed after the boosting of the TRMM orbit in August 2001. The satellite was lifted to higher orbit to counter the effect of atmospheric drag; reducing fuel consumption and lengthening the life span of the satellite (DeMoss & Bowman, 2007). TRMM yields various precipitation products, which are either orbital or gridded, and are produced using different algorithms. The outputs of measurement processing are prescribed a level. Level 1 data are "*reconstructed, unprocessed instrument data at full resolution*", while level 2 data are "*derived geophysical parameters at the same resolution and location as those of the Level 1 data*" (NASA, n.d.).

In getting estimates of rain rates from the TRMM PR, one of the methods used in correcting radar signal attenuation is the Surface Reference Technique (SRT). The technique involves using the signal received by the radar from rain-free areas as a reference for obtaining path integrated attenuation (PIA) (Iguchi, T., Kozu, Meneghini, & Okamoto, 2000). The SRT technique assumes that the difference between the measurements of the surface normalized radar cross section (NRCS) within and outside the raining area provides a measure of the PIA. The SRT works better over the ocean than over the land because the land surface is not so much uniform as the ocean surface, therefore the NRCS is expressed as a function of the incidence angle over land, as well as other physical parameters of land such as vegetation index, surface roughness, and soil moisture so as to increase the accuracy of the SRT technique (Okamoto et al., 2010). The PR is able to separate out rain echoes for vertical sample sizes of about 250 m when looking straight down.

TRMM Composite Climatology

TRMM Composite Climatology provides a map of average values of surface precipitation over the tropical area between 36°N and 36°S constructed from multiple precipitation estimates from TRMM, covering a period of 13 years for each month of the year. It has a latitude-longitude resolution of 0.5° and contains information over both land and sea. These include 2A12 product from the TMI, 2A25 from the PR, the TMI-PR combined 2B31 product for the rainfall estimates over the ocean and TMPA 3B43 rainfall estimates over land (NASA, 2012). The TCC (2009) generated initially was based on TRMM version 6 (V6) data spanning a 10-year period from 1998 – 2007, which was updated by (Wang et al., 2014) to use TRMM version 7(V7) and to restrict the input data only to satellite. Other improvements were made in terms of orbit-boost for the PR product, quality control and an increase in the coverage period to a 15-year span of 1998 – 2012. The 3B43 is a "*best-estimate precipitation rate and root-mean-square (RMS) precipitation-error estimates*" composed of the 3-hourly IR estimates - 3B42, SSM/I estimates - 3A46 and the monthly accumulations of the GPCC rain gauge analysis – 3A45 (NASA Goddard Space Flight Center, 2015). The dataset based on the 2A25 algorithm is used for this research and is described here in detail.

The TRMM 2A25 algorithm estimates rainfall rates from vertical profiles of radar reflectivity. Because the radar echo at the PR frequency of 13.8 GHz experiences attenuation, the effective reflectivity Z_e is estimated from the measured reflectivity Z_m and the rainfall rate is derived using the power law given by

$$R = aZ_e^b \qquad (3.2)$$

where *a* and *b* are functions of rain type and heights of the 0 C isotherm and storm top.

The TRMM 2A25 dataset is a level 2 precipitation rate and profile product from the TRMM PR. It is the instantaneous spatial average rainfall rate between the two pre-defined altitudes over a

square region, with a geographic coverage of latitude 38°S - 38°N and longitude 180°W - 180°E. The spatial resolution changed due to an orbit boost on August 2001. The satellite had pre- and post-boost orbital periods of 91.5 and 92.5 minutes, yielding about 16 orbits per day, with spatial resolutions ~4.3 km and ~5.0 km respectively. The data span the interval from December 1997 to April 2015.

The TRMM 2A25 estimates are derived from 1C21, 2A21 and 2A23 data files where 1C21 is the measured reflectivity profile and miscellaneous rainfall height information, 2A21 contains path attenuation and 2A23 provides information on rain-type, bright-band- and freezing-heights (Iguchi, T., Kozu, Meneghini, Awaka et al., 2000).

TRMM 2A25 has evolved from version 3 which was in use when the satellite was launched in 1997 to version 4 which produced the data that were made available to the public in 1998; versions 5 and 6 were released in 1999 and 2004 respectively and the current version 7 was released in 2011. The main reason for the revisions was the disagreement between TMI and PR records, which showed an underestimation by the PR (Iguchi, Toshio, 2011). As with terrestrial radar, PR rainfall estimates are sensitive to local variation in the reflectivity/rainfall (Z/R) relationship, ground clutter and other factors. Retrieval errors are sensitive to both rainfall rate and meteorological regime (Duan et al., 2015). The TRMM PR 2A25 V7 has been used in various studies exploring on weather patterns and climate characteristics (Chan et al., 2004; Islam, M. N. & Uyeda, 2007), precipitation trends (Fu et al., 2016) and comparative analysis of rain rates (Chiu et.al, 2006).

The currently operational Global Precipitation Measurement (GPM) mission launched in February 2014 serves to build on the achievements of TRMM mission, which came to an end in April 2015. In comparison with the TRMM, the GPM measures precipitation to higher latitudes of up to 65°. The core GPM satellite carries the GPM microwave imager (GMI) with channels

similar to those of the TMI with addition of four high frequency millimeter-wave channels (Islam, T., Rico-Ramirez, Han et al., 2012). In contrast to the single frequency of Ku-band in the TRMM, the dual-frequency precipitation radar (DPR) of the GPM consists of Ku and Ka band dual frequency radars. The GPM DPR is more adept at capturing light rain, at a higher frequency of 35.5 GHz (Gao et al., 2017). However, the GPM has been in operation for a relatively short period and studies to understand the technical capabilities of the DPR and the quality of its products are ongoing.

3.3.2 Nimrod

The UK Meteorological Office Nimrod system combines data from a network of fifteen C-band terrestrial radars with satellite data, together with surface reports and Numerical Weather Prediction (NWP) fields. It produces composite rain field images with a 5-minute sample interval and presented on a 1-km spatial Cartesian grid, spanning the UK and parts of Western Europe. These are available from the British Atmospheric Data Centre from April 2004 to the present. Although presented on a uniform grid, the actual spatial averaging is limited by the distance from the nearest radar. The Nimrod system, radar calibration, and the formation of composite rain field data are described in Harrison et al. (2000). Distributions of Nimrod rain rates have been shown to be good estimates of distributions of one-minute rain rates derived from networks of rapid-response rain gauges (Paulson, 2016). Furthermore, Nimrod data can be spatially integrated to compare rain rate distributions over 1 km and 5 km squares, for the same rain fields. From a previous project, rain data from five regions have been analysed, from 2005 to 2014 inclusive. The five regions are 200 km squares and cover southern England (SE), the Midlands (ML), northern England (NE), Southern Scotland (SS) and Northern Scotland (NS).

3.3.3 ITU-R Study Group 3 Dataset (DBSG3)

The database of the ITU-R Study Group 3, DBSG3, contains records of annual exceeded rain rates from 198 global sites collected since 1959. A selection of rain rates exceeded at time percentages from 1% to 0.001% are presented for each site and for a range of measurement intervals. Often, individual years are reported as well as results derived by accumulating data from several consecutive years. The data are provided by the ITU-R member administrations of many countries. For this project the most recent version of the database was used i.e. Version 7 Release 2.

ITU-R models are judged by how well they match the DBSG3 data. However, there are concerns regarding the representativeness of the data, given climate change and the uneven distribution of data sites. The database contains no data from Africa, and much of the data are from countries in temperate regions of Europe, Asia and the Americas. Furthermore, there is no information in the public database of measurement reliability. Rain gauges are difficult to site, particularly in urban areas, and can provide biased measurements when in the wind shadow of buildings, trees etc. Measurements of low probability rain rates are also very sensitive to temporary blockage, due to insects or plant matter in the funnel. Finally, several authors have published evidence of temporal trends in $R_{0.01\%}$ (Paulson, 2016; Paulson et al., 2014a; Tjelta & Mamen, 2014) starting in the 1980's. The non-stationarity of $R_{0.01\%}$ should be considered when comparing estimates measured in different decades.

3.3.4 ERA-Interim

This re-analyses data, provided by the European Centre for Medium Range Weather Forecast (ECMWF) spanning from 1979 till date, is a replacement for the ERA-40 reanalyses data, with

improvements made to cater for the difficulties encountered in presenting ERA-40, especially in data assimilation and secondly, in technical presentation (Dee et al., 2011). Berrisford et al. (2011) have documented the ERA Interim products at ECMWF. By combining initial conditions from an assimilating forecast model with available observations, ERA-Interim is able to predict future observations. This involves the analyses of basic upper-air atmospheric fields, near-surface parameters (2 m temperature and 2 m humidity), soil moisture and temperature, snow, and ocean waves. Dee et al. (2011) have documented these and other improvements made in generating the ERA-Interim. ERA Interim 2 m temperature is used in this project.

3.3.5 Global Precipitation Climatology Centre data

The Global Precipitation Climatology Centre (GPCC) was established in 1989 and provides gridded gauge-analysis products derived from quality-controlled station data (GPCC, 2018). The database comprises data collected predominantly on a monthly basis from several sources, which include the World Meteorological Organisation (WMO) Global Telecommunication System (GTS) network for near-real time analysis as well as non-real time data contributed from about 190 countries (Schneider, Udo et al., 2014). The key errors affecting gridded data are systematic errors from gauges and sampling errors from the density of the rain gauge network. GPCC uses an anomaly interpolation method to reduce sampling error (Becker et al., 2013) and an improved correction method to tackle systematic error (Schneider, Udo et al., 2014). Becker et al. (2013) have given a detailed description and analysis of GPCC products, which include the Climatology (CLIM) V2011, the Full Data Reanalysis (FD) V6, the Monitoring Product (MP) V4, the First Guess Product (FG), and GPCC – Homogenized Precipitation Analysis (HOMPRA) Version 1.0.

The GPCC version 15 dataset used by the Rec. ITU-R P. 837-7 has been derived from a network of 75000 weather stations, with input from more countries and island/atoll regions than previous

versions. Furthermore, additional levels of quality control that have been introduced, resulting in a significant improvement over the previous version 11 (Schneider, U. et al., 2017).

This project uses the GPCC Full Data Monthly Product Version 7.0. rather than the more recent GPCC version 15, which has a higher resolution, because the archives did not contain data for the years covered as at the time this study was carried out.

3.4   Chapter Summary

The measurement of precipitation is useful for various applications, but the measurement of rain parameters is difficult. Rain gauges provide the most direct measurement of point precipitation, but are expensive to operate, hard to site and produce point measurements with both systematic and random errors. Weather radars measure over larger areas while satellites offer the advantage of coverage beyond geo-political boundaries and carry a combination of various sensors to give global estimates of high accuracy, wider coverage and finer resolution. However, radar estimates need to be calibrated against gauges. There are various precipitation datasets, each with its peculiar characteristics, strengths and weaknesses. For application to radio propagation, rain measurements need to have high resolution in both space and time, and wide area coverage. For propagation work, point one-minute rain rates are required. Global databases are typically monthly or daily accumulations, averaged over regions tens or hundreds of kilometres across. The closest datasets, in terms of resolution and coverage, come from TRMM yielding instantaneous rain rates over 5 km squares spanning the Tropics. This project uses these data, combined with gridded global rain gauge data and re-analysis temperatures, to produce a global model of point one-minute rain rates.

Chapter 4   Estimating Rain Rate Distributions in the Tropics Using Distributions of Measured TRMM Rain Rates

4.1   Introduction

This chapter explores the use of TRMM derived surface rain rates to estimate average annual distributions of point one-minute rain rates across the Tropics. TRMM rain rates are spatial averages and so a method is required to transform distributions of TRMM rain rates to the point one-minute rain rates used for radio regulation. This is achieved using UK Nimrod rain radar data and presented in this chapter. The derived transformation is applied to distributions of TRMM rain rates and these are compared to the predictions of ITU-R Recommendations and two databases of site measurements.

During the course of this project, the previous Rec. ITU-R P.837-6 (ITU-R, 2017b; ITU-R, 2015b) was superseded by Rec. ITU-R P.837-7 (ITU-R, 2017b). For this reason, some background into Rec. ITU-R P.837 and related analysis are initially presented.

4.1.1 History of Rec. ITU-R P.837

The first version of Rec ITU-R P.837-1 divided the world into fifteen rain zones labelled A to Q (with no zone O). In 1999, this was superseded by Rec. ITU-R P.837-2, based on work by Salonen and Poiares-Baptista (SPB), (Salonen & Poiares Baptista, 1997a; Poaires Baptista & Salonen, 1998), and the ITU-R Study Group 3 (ITU-R Study Group 3, 2012). The SPB method underpins all versions of the Recommendation up to and including version 6. It assumed that that the average annual one-minute rain rate complementary cumulative probability function (CCPF or exceedance), globally, was well approximated by a double exponential distribution. The SPB method linked the four distribution parameters to three output parameters from

Numerical Weather Prediction (NWP), in this case the ECMWF ERA40: the annual total accumulation, annual convective accumulation and proportion of six-hour intervals containing rain. The SPB method had serious deficiencies, described in Paulson (2016). A fundamental problem was that the NWP outputs were precipitation accumulations over regions much larger than convective rain events, and over intervals that are much longer than their life span. These convective events typically produced the moderate or heavier rain than lead to outage on telecommunications links. A second major problem was that the annual accumulations, used by the SPB method, were very poorly correlated to any parameter of one-minute rain rate distributions. Due to these and other problems, the 0.01% exceeded rain rates derived from the SPB method deviated from measured results in the ITU-R Study Group 3 database by an average of 30% (Paulson et al., 2014b; Blarzino et al., 2009). There were particular concerns about the accuracy of the SPB method in the Tropics, where 0.01% exceeded rain rates were high and there was little validating data in DBSG3.

4.1.2 Rec. ITU-R. P.837-7

The Recommendation, just as its antecedent, also provides an estimate of the local, average annual, distribution of point one-minute rain rates. The input data are monthly average surface (2 m) temperature from Rec. ITU-R P.1510-1 and monthly precipitation accumulation. These inputs are derived from a global rain gauge network and reanalysis data i.e. the Global Precipitation Climatology Centre (GPCC) gridded rain gauge dataset over land, and the European Centre for Medium-Range Weather Forecasts (ECMWF) ERA Interim database over water. These variables are linked to the parameters of a monthly lognormal distribution of rain rates. The Recommendation also provides a method for estimating the distribution of one-minute rain rates rain rates for locations with reliable rainfall data collected using a larger integration time. Rec. ITU-R P.837-7 replaced the previous version in July 2017. In this report, Rec837 refers specifically to this version of the Recommendation.

4.2　Estimating One-Minute Rain Rate Distributions from Distributions of TRMM Rain Rates

The TRMM system supplies estimates of instantaneous rain rates over approximate squares with sides of ~5 km. However, radio regulation requires distributions of point rain rates averaged over one minute. This section presents a method to transform distributions of instantaneous 5 km rain rates to distributions of point one-minute rain rates. A link between instantaneous 1 km rain rates and point one-minute 0.01% exceeded rain rates has been demonstrated in Paulson (2016). This section uses UK Nimrod composite rain rate data to derive the transformation between distributions of 5 km and 1 km rain rates.

4.3　Nimrod 5 km to 1 km Transformation

The UK Meteorological Office Nimrod system has been described in detail in section 3.3.2. In this section, a method is developed to transform exceedance distributions of 5 km rain rates into the equivalent distributions of 1 km rain rates.

The transformation is estimated from distributions of 1 km and 5 km rain rates derived from the same Nimrod composite rain rate fields. Each Nimrod composite rain rate map yields 200×200 rain samples at approximately 1 km resolution, each 5 minutes, for each of the five regions defined in section 3.3.2. When rain rates in 5 by 5 arrays are averaged, they yield an estimate of the rain rate averaged over a 5 km square. Each region, for each composite rain field, yields 196×196 not-independent 5 km rain rates. Over a year there are 365×24×12 maps yielding 4.2 billion 1 km rain rates and 4.0 billion 5 km rain rates. These data allow annual distributions of equivalent 1 km and 5 km rain rates to be compared down to very low exceedance probabilities. The next stage is to devise transformations from 5 km to 1 km distributions. Two methods are

considered: transforming rain rates for the same exceedance probability, and transforming exceedance probabilities for the same rain rate. These are considered in subsequent sections.

a. Same exceedance transformation

Ten years of Nimrod data were analysed from 2005 to 2014 inclusive. 1 km and 5 km daily histograms were calculated from the composite data, which were then aggregated into annual histograms. The annual histograms were converted to 1 km and 5 km annual rain rate exceedances respectively. Figure 4.1 is a plot of 1 km and 5 km annual rain rate exceedances for a region. The 5 km distributions exhibit fewer extreme rain rates than the 1 km distributions.
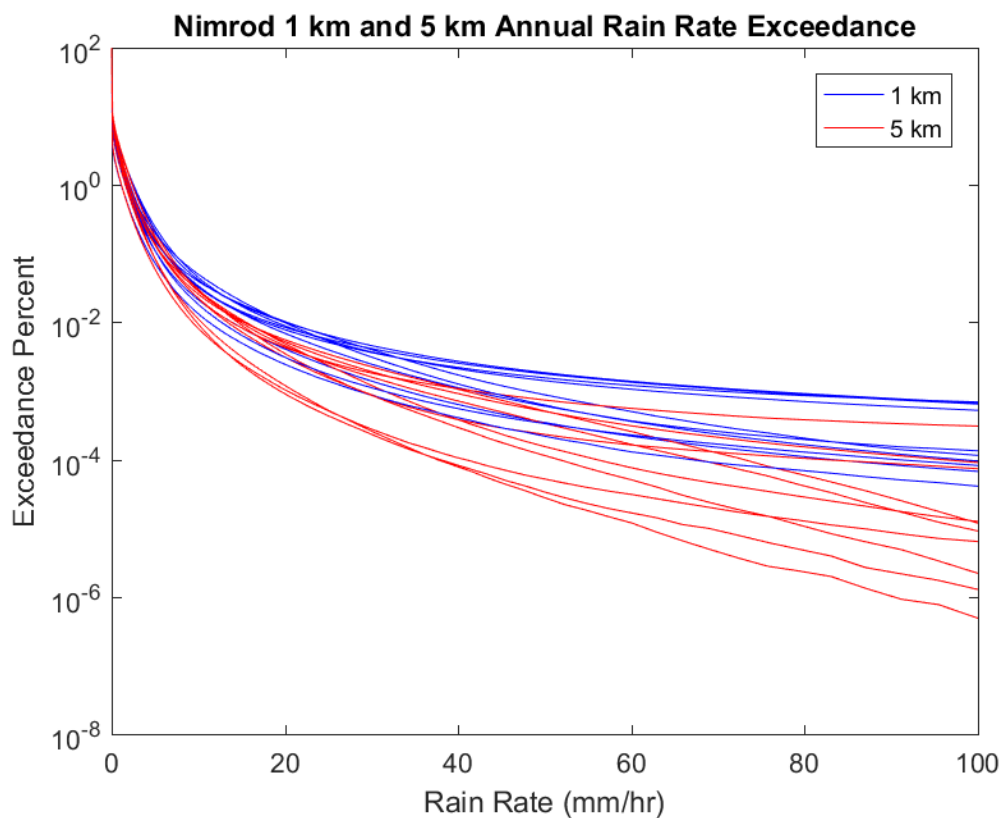
Figure 4.1. Nimrod 1 km and 5 km annual rain rate exceedances

Figure 4.2 shows the 1 km and 5 km exceeded rain rates for the same exceedance probabilities in the Midlands region. The blue lines are for each of the ten individual calendar years, and the red line is the best-fit quadratic to these relationships.
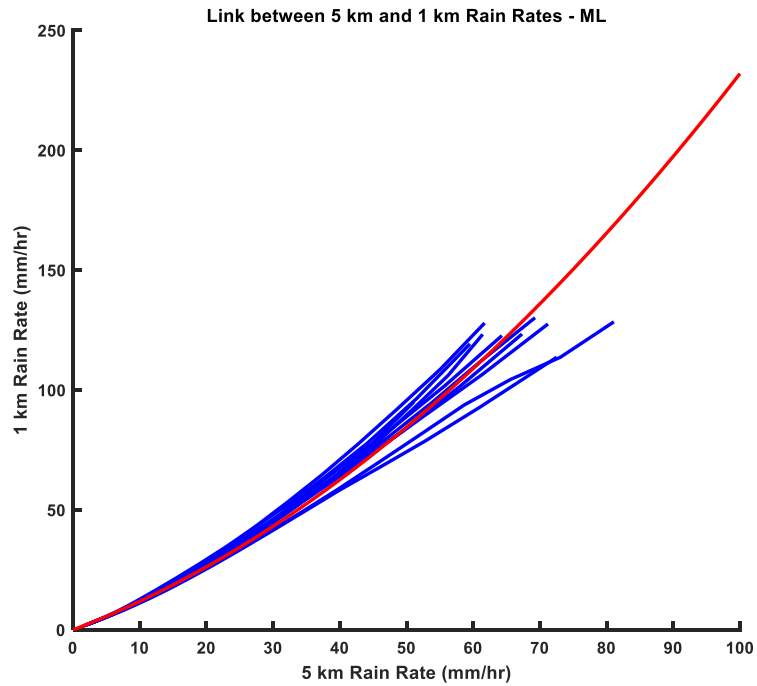
Figure 4.2. Equi-probable 1 km and 5 km rain rate relationships for the ten years in the Midlands region (blue) and the best-fit quadratic (red)

The best-fit quadratic for all ten years in each of the UK regions is shown in Figure 4.3
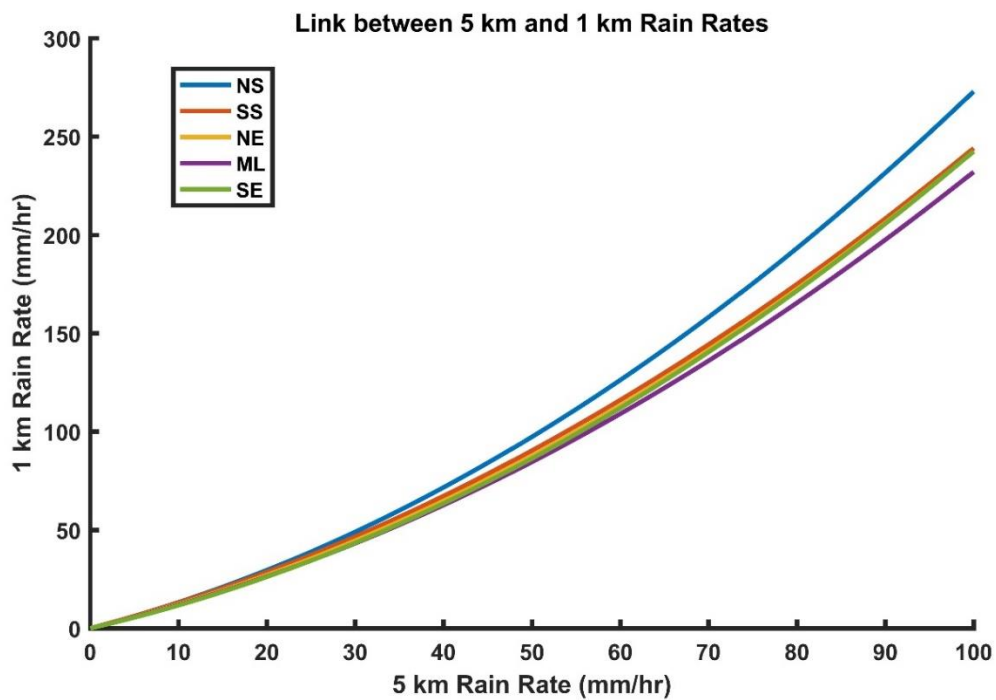
Figure 4.3 Equi-probable 5 km and 1 km rain rate relationships for the five UK regions.

45

From this, a correction factor was determined using the mean quadratic fit, yielding a relationship between 1 km and 5 km rain rates at the same exceedance as

$$R_{1km} = \gamma R_{5km}^2 + \delta R_{5km} \qquad (4.1)$$

where R_{1km} is the 1 km rain rate;

R_{5km} is the 5 km rain rate;

γ and δ are constants with the values 0.0126 and 1.0619 respectively.

The climate across the five UK regions varies from Northern Scotland, dominated by stratiform rain off the Atlantic, to Southern England with a large proportion of heavy convective events originating in continental Europe. Despite this, there is little variation in the equi-probably 1 km - 5 km exceeded rain rate relationships, particularly over the important range up to the typical 0.001% exceeded rain rate of 60 mm/hr. Furthermore, there was no discernible trend in the four southern-most regions. The transformation parameters for the four lower regions (SS, NE, ML and SE) are very similar. The probability of the observed differences in these parameters being just due to chance is high: 0.22. There is no evidence of differences in the transformations for these southern-most regions and so it is reasonable to assume that the transformations would be valid for some latitudes south of the UK into the tropics. This suggests that the average relationship may be applicable to tropical regions. This is clearly speculative, and there would have been more confidence in a transformation based on data from the Tropics, if such data were available.

b. *Same rain rate transformation*

An alternative transformation is between exceedances for the same rain rate. A range of rain rates was selected and the 1 km and 5 km exceedances were determined for those rain rates. Figure 4.4 is a plot of 1 km and 5 km exceedances at the same rain rate.
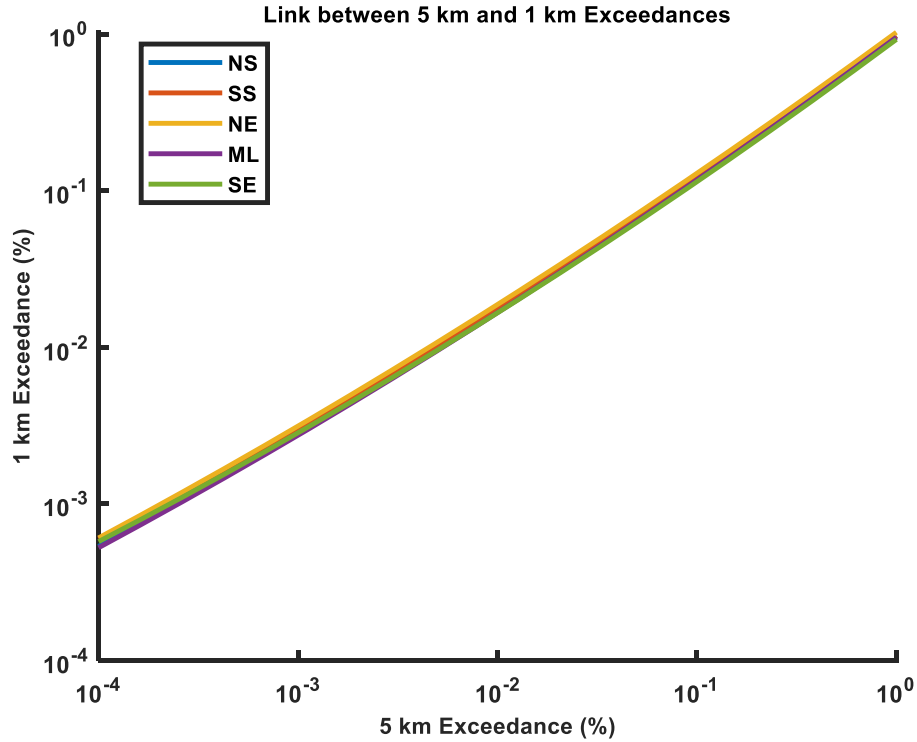
Figure 4.4. Nimrod 1 km and 5 km annual exceedances for the same rain rate

A correction factor using a quadratic fit gave the relationship between the 1 km and 5 km exceedances as

$$X_{1km} = 10^{(\gamma\phi^2 + \delta\phi)} \qquad (4.2)$$

Here
$$\phi = 2 - \log_{10} X_{5km} \qquad (4.3)$$

where X_{1km} is 1 km exceedance, X_{5km} is 5 km exceedance and γ and δ are constants with values 0.0358 and -1.0879 respectively.

The outcome of the two transformations are close to equivalent, showing little variation in the equi-probably 1 km - 5 km exceeded rain rate relationships in spite of the varying climate across the five UK regions. The same-rain rate transformation is more complicated, and so the same-exceedance transformation has been used in the rest of the project. It means that a 5 km rain rate exceedance distribution can be transformed to a 1 km exceedance distribution just by transforming the rain rate scale.

4.3.2 Applying the Transformation to TRMM Distributions

Each orbit of the TRMM satellite yields a 247 km-wide swath of ~5 km rain rate measurements under an orbit that extends 38° north and south of the equator, see Figure 4.5. The satellite orbits just less than 16 times a day and the orbit path shifts around the world giving near universal coverage over the Tropics, but with irregular return times.
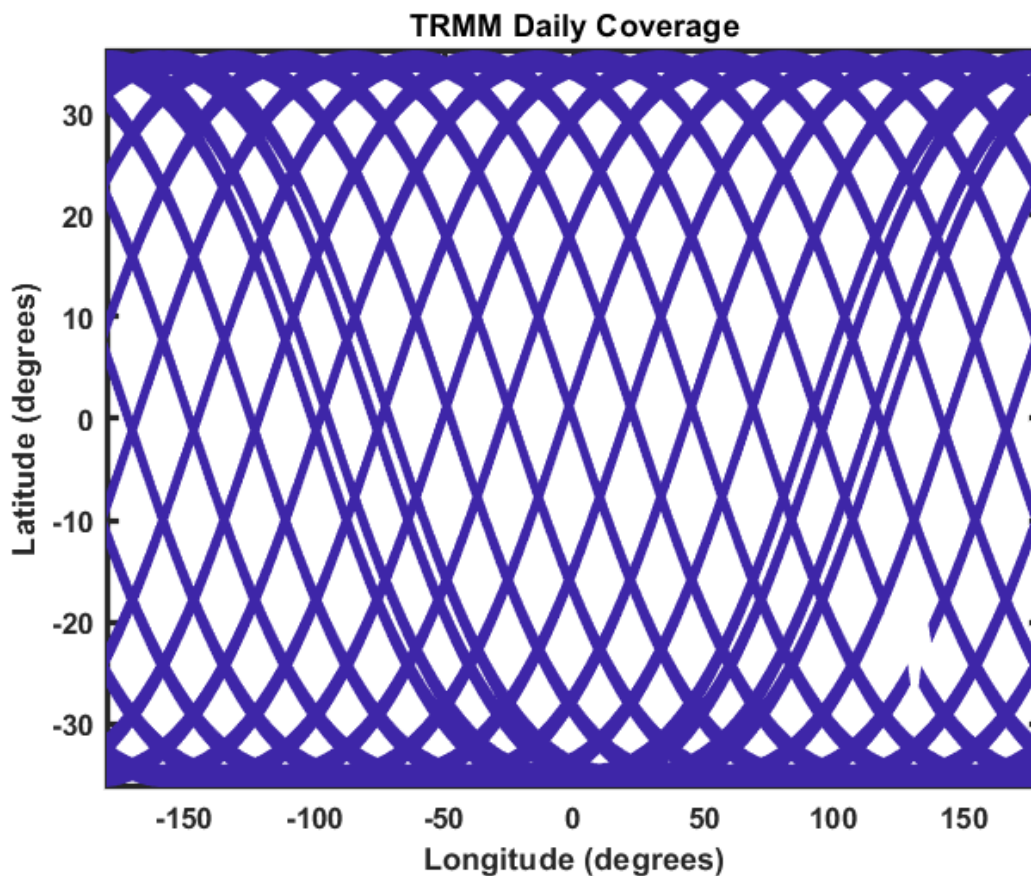
Figure 4.5. Typical coverage captured in one day from the 16 orbits of TRMM satellite

TRMM 2A25 data from 9 years, 2004 to 2012, were downloaded and analysed. Each rain rate measurement was allocated to a single 1° by 1° square by its latitude and longitude. Histograms of measurements were calculated for each 1° square and these were transformed into 5km exceedance distributions. Applying the transformation given by Equation (4.1) to the

5 km rain rate distributions yielded estimates of the instantaneous 1 km distributions, and hence the point-one-minute distribution, for each 1° square in the Tropics. The 0.01% exceeded rain rates can be estimated directly from these distributions. Figure 4.6 shows the 0.01% exceeded rain rate derived from the transformed distributions of TRMM 5 km rain rates. These estimates are compared with Recs. ITU-R P.837-6 and 837-7, and DBSG3 site data, in the next section.
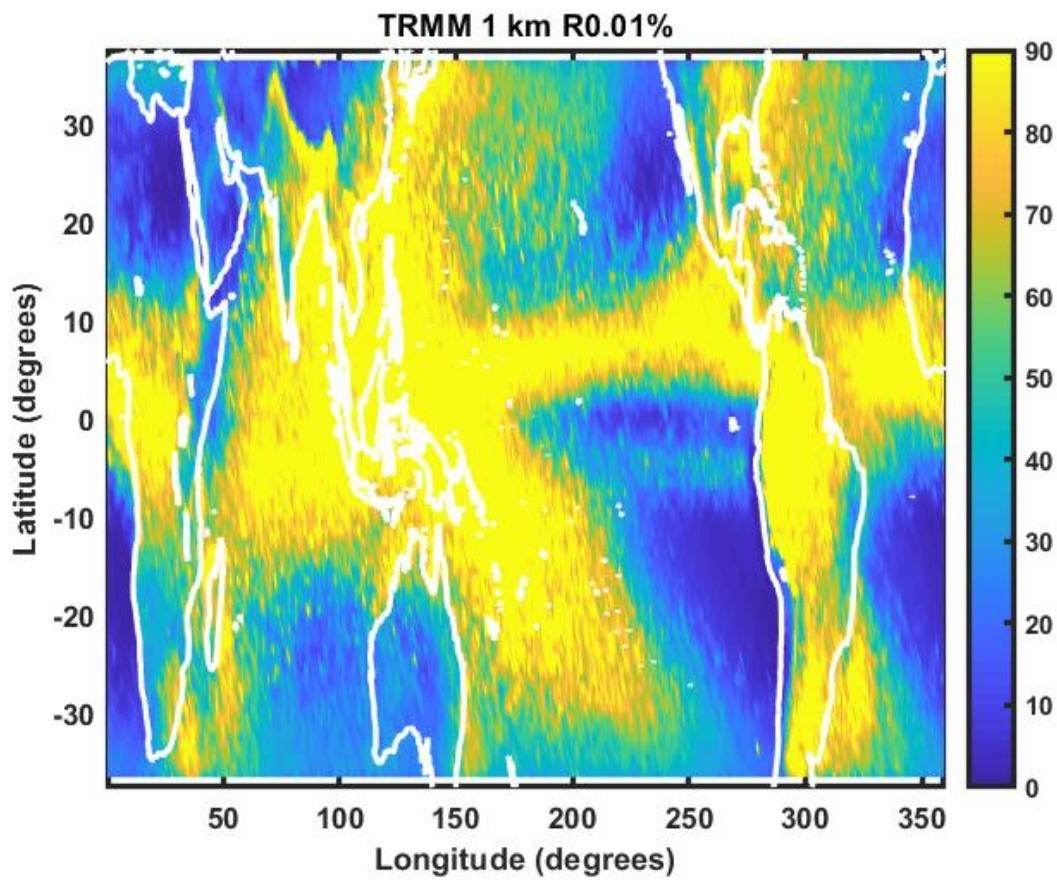
Figure 4.6. 0.01% exceeded rain rate (mm/hr) derived from the transformed TRMM 5 km distributions

4.4   Comparison of point one-minute TRMM estimates to Rec. ITU-R P.837-6 and ITU-R.837-7 predictions and DBSG3

The spatial variation of the $R_{0.01\%}$ derived from TRMM data is similar to those provided by Rec.

ITU-R P.837-6 and Rec. ITU-R P.837-7, as shown in Figure 4.7 a) and b) respectively.
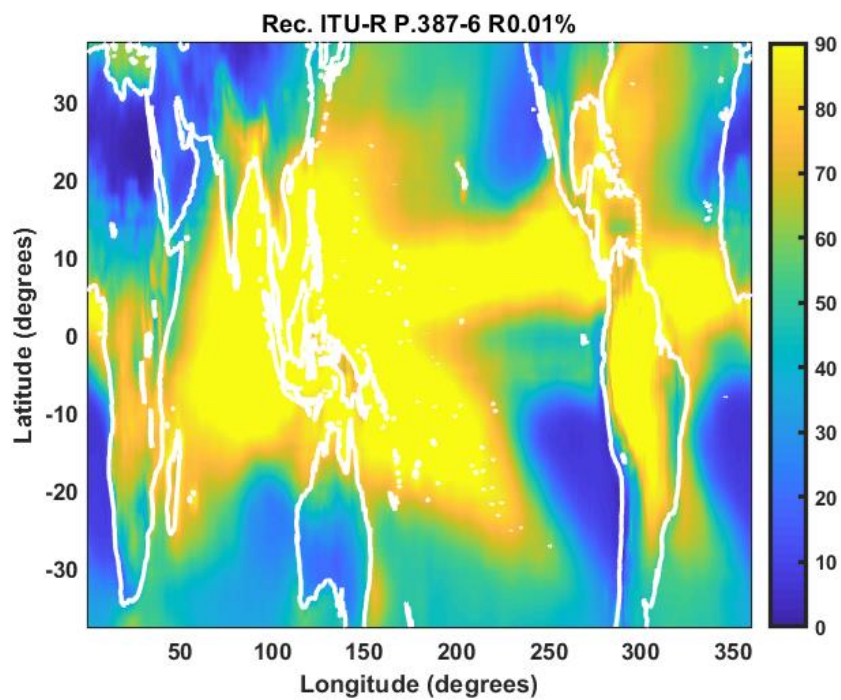
a)
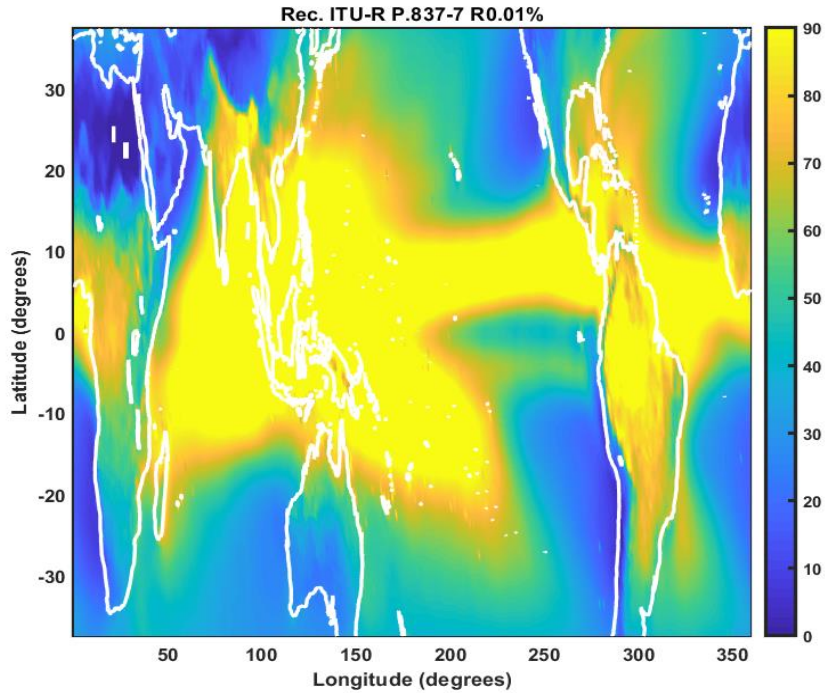
b)

Figure 4.7. 0.01% exceeded rain rate (mm/hr) derived from a) Rec. ITU-R P.837-6 b) Rec. ITU-R P.837-7.

However, there are significant regional differences. For example, regions along the lower coastal regions of West Africa extending to locations in central Africa, coastal areas of Southern Africa as well the island of Madagascar, have been estimated from TRMM distributions to have 0.01% exceeded rain rates between 80 and 90 mm/hr. This is much higher than the Rec. ITU-R P.837-6 values around 20 - 30mm/hr along the coast of Southern Africa and 60 -70mm/hr for the West and central African regions. The TRMM distributions show high rain rates over areas around Argentina in South America. Coordinates of locations over the Pacific and the North Atlantic also show rain rates higher than the Rec. ITU-R P.837-6 predictions. These and other differences are shown in Figure 4.8a), which is a plot of the difference between the TRMM rain rates and Rec. ITU-R P.837-6 prediction.

TRMM 1km Minus P.387-6 R0.01%

a)

TRMM 1km Minus P.837-7 R0.01%
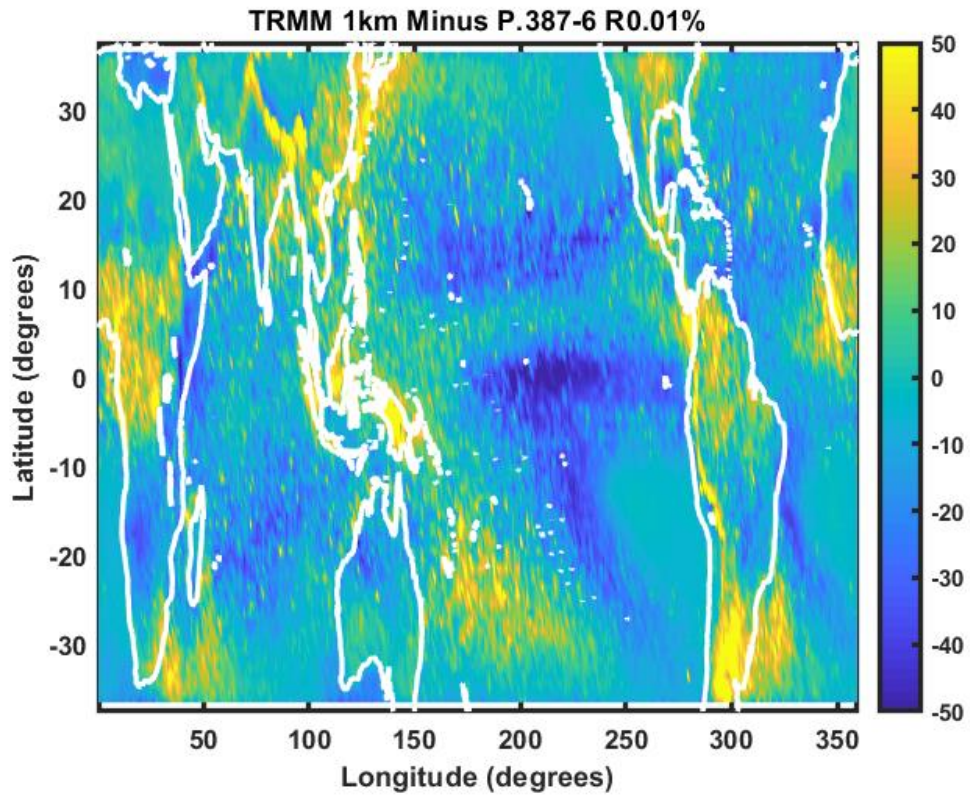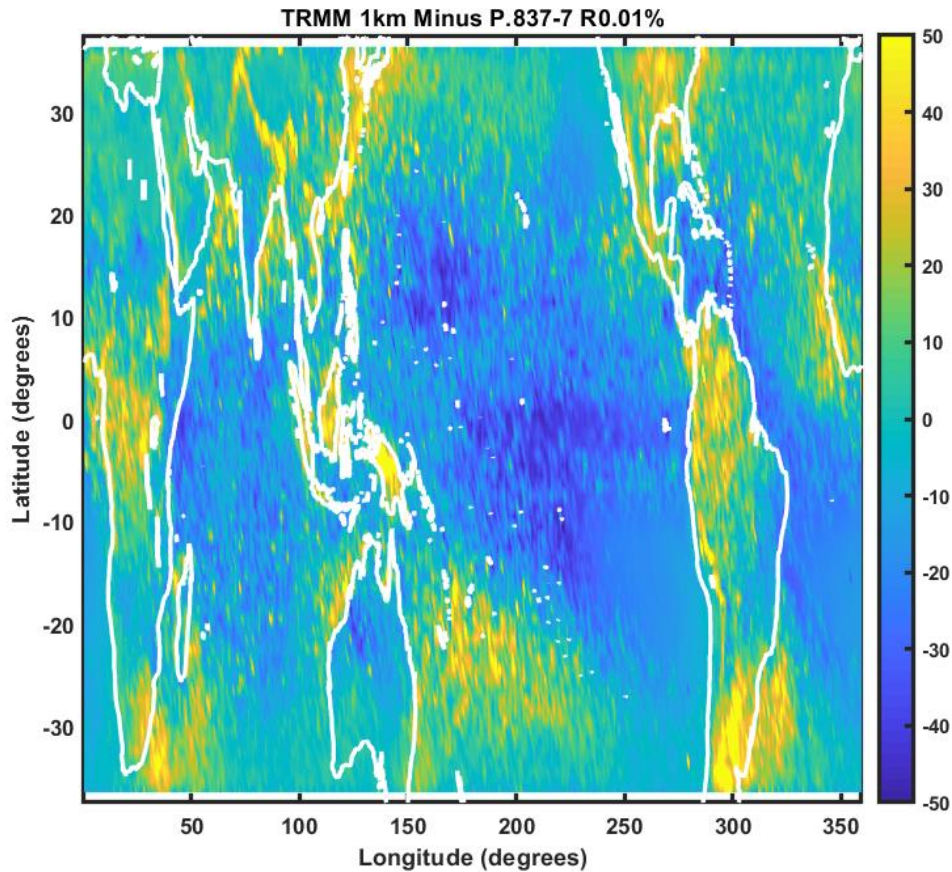
b)

Figure 4.8. Difference between 0.01% exceeded rain rates (mm/hr) derived from transformed TRMM 5 km rain rates and a) Rec. ITU-R P.837-6 b) Rec. ITU-R P.837-7.

Figure 4.8b) is a plot of the difference in 0.01% rain rates exceeded for TRMM and Rec ITU-R P.837-7. The similarities in the plots are as observed when comparing TRMM with ITU-R P.837-6 where rain rates between 80 to 90mm/hr are recorded along the coastal areas of West Africa, in the Northern regions of South America and over the South Atlantic, Pacific and Indian oceans. In this case, however, the TRMM plot has captured rain rates of the same level of 80 to 90 mm/hr in regions of West and Central Africa, the island of Madagascar, southern regions of South America, and some regions of North America, which the Rec ITU-R P.837-7 does not record.

The large negative differences in the northern Pacific are due to the band of heavy rain extending west-to-east being narrower in the TRMM results compared to Rec. ITU-R P.837.

The 0.01% exceeded rain rates derived by this process were also compared with those in the DBSG3 database. Sites with at least four individual years of measurements were selected, yielding 50 sites out of 64 that fall within the TRMM boundary. Selection was performed as the year-to-year variability provided by the four or more years of results allows the standard error in the $R_{0.01\%}$ to be estimated. Figure 4.9 compares the $R_{0.01\%}$ predicted using the TRMM data, Rec. ITU-R P.837-6 and Rec. ITU-R P.837-7 with the average DBSG3 value for each site.
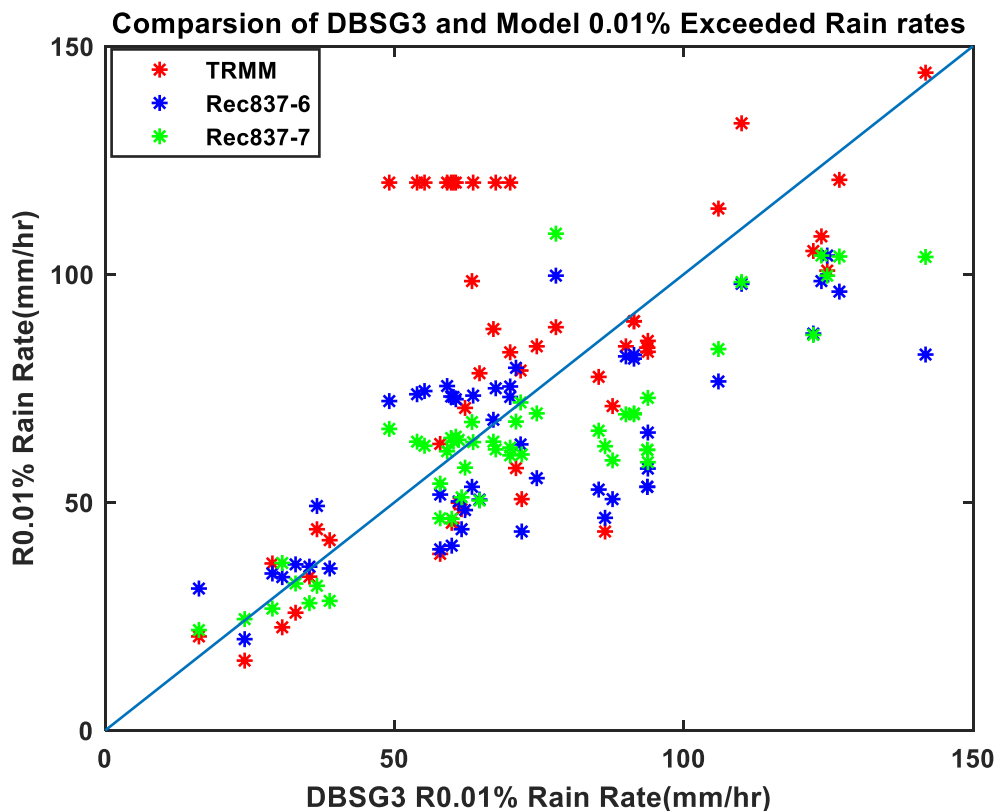
Figure 4.9. Comparison of 0.01% exceeded rain rate from 1 km TRMM distribution, Rec. ITU-R P.837-6 and Rec. ITU-R P.837-7, with DBSG3 data from the Tropics

In comparing Rec837-6 and Rec837-7 values with TRMM, Figure 4.9 shows that the TRMM method yields generally better estimates of DBSG3 values than Recs. ITU-R P.837-6 and ITU-R. P.837-7. The Recs. ITU-R P.837-6 and ITU-R. P.837-7 values show a bias at high rain rates

that the TRMM values do not have. The notable outliers are the group of sites where TRMM estimates $R_{0.01\%}$ to be 120 mm/hr compared to the DBSG3 values around 60 mm/hr. These sites (which include Ayura, Chorillos, Convento down to San Cristobal in Table 4.1) are close together in Colombia, within the Ayura valley and in the wind shadow of the Central Range Mountains. It is likely that the TRMM values are more representative of the region over the 1-degree (100 km) resolution of the rain rate histogram binning. Furthermore, it is likely that ITU-R Recommendations are artificially biased by taking the fit to these sites as a measure of quality of a method.

Table 4.1 lists the estimates from Rec. ITU-R P.837-6 and -7 predictions, those derived from TRMM and the average over at least 4 years of DBSG3 site data.

Table 4.1

Rec. ITU-R P.837 PREDICTION, TRMM 1 KM DISTRIBUTION AND AVERAGE DBSG3 MEASUREMENT FOR POPULATION CENTERS IN TROPICS						
SITE	LAT	LON	DBSG3	TRMM	Rec837-6	Rec837-7
ALMERIA	36.85	-2.38	16.2	20.6	31.1	22.0
CADIZ	36.50	-6.26	36.6	44.1	49.2	31.7
MALAGA	36.67	-4.48	35.3	33.7	35.9	27.9
MELILLA	35.28	-2.92	28.9	36.6	34.4	26.7
TENERIFE NORTE	28.47	-16.32	32.9	25.8	36.4	32.2
DAEJON	36.37	127.36	87.7	71.1	50.7	59.2
TAEGU	35.88	128.62	57.9	62.8	51.7	54.1
PUSAN	35.10	129.03	93.7	83.9	53.4	61.5
CHONGQING	29.58	106.47	72.0	50.7	43.6	60.5
DONGXING	21.53	107.97	141.8	144.2	82.4	103.8
FUZHOU	26.08	119.28	85.3	77.5	52.8	65.7
GUANGZHOU	23.05	113.32	106.0	114.4	76.5	83.6
GUILIN	25.33	110.30	93.8	85.4	57.4	72.9
HAIKOU	20.03	110.47	122.4	105.1	87.0	86.7
HANGZHOU	30.32	120.20	61.1	49.9	50.2	63.7
JINAN	36.68	116.98	61.6	48.5	44.1	51.1
KUNMING	25.02	102.68	59.9	45.5	40.5	46.4
LANZHOU	36.05	103.88	24.1	15.3	20.0	24.4
NANCHANG	28.67	115.97	74.6	84.2	55.3	69.5
NANGJING	32.32	118.80	62.2	70.7	48.3	57.6
WUHAN	30.63	114.07	86.4	43.6	46.6	62.3
XIAN	34.30	108.93	30.6	22.6	33.6	36.7
YICHUN	27.80	114.38	63.4	98.5	53.4	67.6
ZHENGZHOU	34.72	113.65	57.9	38.7	39.7	46.5
PUSAN	35.10	129.03	93.7	83.9	53.4	61.5
BUKIT TIMA	1.30	103.90	124.8	100.8	104.1	99.7
HOUSTON	29.77	-95.73	93.8	83.0	65.3	58.8

JACKSONVILLE	28.34	-80.93	91.4	89.7	81.5	69.5
FLORIDA	28.34	-80.60	91.4	89.7	82.3	69.3
NORMAN	35.21	-97.44	64.7	78.3	50.6	50.4
WHITE	32.54	-106.61	38.8	41.7	35.5	28.4
TAMPA	28.06	-82.42	90.0	84.2	82.0	69.3
AYURA	6.17	-75.57	60.2	120.1	73.1	63.3
CHORRILLOS	6.30	-75.51	60.6	120.1	72.6	64.4
CONVENTO	6.34	-75.52	59.8	120.1	73.2	64.1
CUCARACHO	6.29	-75.61	67.5	120.1	75.0	61.6
GERONA	6.23	-75.56	63.6	120.1	73.4	63.2
GIRARDOTA	6.39	-75.46	49.1	120.1	72.2	66.1
MANANTIALES	6.32	-75.54	53.9	120.1	73.7	63.3
PEDREGAL	6.31	-75.58	55.2	120.1	74.4	62.4
SAN ANTONIO DE PRADO	6.19	-75.66	70.0	120.1	75.4	62.0
SAN CRISTOBAL	6.28	-75.64	59.1	120.1	75.5	61.2
BELEM	-1.45	-48.48	126.9	120.7	96.2	103.9
BRASILIA	-15.48	-47.83	71.0	57.5	79.5	67.7
MANAUS	-3.15	-60.02	110.0	133.1	97.9	98.3
RIO DE JANEIR0	-22.92	-43.95	71.8	78.9	62.7	71.9
STA RITA DO SAPUCAI	-22.25	-45.72	70.0	82.9	73.1	60.3
SAO PAULO	-23.55	-46.63	67.1	88.0	68.1	63.3
PALAU PIG (SAINS)	5.35	100.30	123.8	108.3	98.5	104.1
KWAJALEIN	8.79	167.62	77.9	88.4	99.7	108.9

4.4.1 *t*-test

Using a *t*-test, Table 4.2 shows the probability that the TRMM estimates differ from the DBSG3 values only by chance, with the null hypothesis that the measured DBSG3 and predicted TRMM values come from the same distribution. The test statistic is the difference in the $R_{0.01\%}$ scaled by their standard errors, estimated from year-to-year. With a level of significance of 0.05, only the Ayura valley sites, Melilla and Rio De Janiero, yield significant differences, with all other tested sites having differences with high probabilities. The conclusion is that TRMM provides good estimates in the majority of places. The Ayura valley site rain rates may not be representative of the surrounding region due to topography.

Table 4.2

COMPARISON OF POINT ONE-MINUTE RAIN RATES (mm/hr) FOR 1 km TRMM AND DBSG3						
SITE	DBSG3			TRMM			PROBABILITY OF DIFFERENCE
	Number of Years	STDEV(σ)	MEAN	Number of Years	STDEV(σ)	MEAN	
ALMERIA	20	7.40	15.01	9	8.38	20.38	0.24
CADIZ	5	4.85	36.81	9	22.16	44.04	0.44
MALAGA	10	14.93	32.58	9	10.15	31.67	0.91
MELILLA	18	7.09	25.40	9	8.29	35.61	0.03
TENERIFE NORTE	14	6.38	31.00	9	14.41	26.59	0.50
DAEJON	10	18.07	83.79	9	51.18	78.07	0.81
TAEGU	10	11.15	57.31	9	15.80	59.28	0.82
PUSAN	10	27.94	85.81	9	29.93	80.26	0.77
HOUSTON	8	20.65	92.19	9	25.77	76.76	0.33
JACKSONVILLE	8	18.35	88.80	9	28.35	81.82	0.66
NORMAN	4	4.57	68.64	9	15.63	79.33	0.15
WHITE	5	7.69	39.91	9	11.72	40.03	0.99
TAMPA	4	8.21	95.46	9	26.64	81.05	0.27
AYURA	4	0.45	60.26	9	38.66	130.38	0.00
CHORRILLOS	4	3.83	60.08	9	38.66	130.38	0.00
CONVENTO	4	12.14	57.97	9	38.66	130.38	0.00
CUCARACHO	4	8.72	65.95	9	38.66	130.38	0.00
GERONA	4	9.82	61.48	9	38.66	130.38	0.00
GIRARDOTA	4	8.18	49.86	9	38.66	130.38	0.00
MANANTIALES	4	7.86	54.49	9	38.66	130.38	0.00
PEDREGAL	4	17.69	61.93	9	38.66	130.38	0.00
SAN ANTONIO DE PRADO	4	9.60	69.69	9	38.66	130.38	0.00
SAN CRISTOBAL	4	7.29	60.87	9	38.66	130.38	0.00
BELEM	7	12.31	126.86	9	31.61	121.74	0.74
BRASILIA	4	26.58	71.03	9	20.20	61.86	0.65
MANAUS	7	2.71	109.78	9	39.01	132.94	0.10
RIO DE JANEIRO	11	11.19	58.80	9	27.30	84.10	0.04
KWAJALEIN	7	16.70	63.95	9	24.64	83.16	0.19

4.4.2 Rec. ITU-R P.311 Goodness of Fit

The Rec. ITU-R P.311 provides the procedure for the acquisition, presentation and analysis of data in studies of radio-wave propagation (ITU-R, 2018c). Of importance is the Goodness of Fit (GoF) metric, which measures the distance between pairs of fade exceedance distributions. It is calculated using the logarithm of the ratio of rain rates exceeded at the same time percentage, and results in a statistic that is approximately normally distributed where a value close to zero

indicates a good fit. Although designed for fade distributions, it can be applied to distributions of rain rate. The log-ratio is approximately the relative-error and so allows the comparison of exceedances that span many orders of magnitude.

The estimates of TRMM, Rec. ITU-R P.837-6 and Rec. ITU-R P.837-7 were compared to DBSG3 data for the tropical locations of interest. The GoF for the 0.01% exceeded rain rate for TRMM compared to DBSG3 data was 0.1451 and for Recs. ITU-R P.837-6 and ITU-R. P.837-7 it was 0.0985 and 0.05 respectively. When the Ayura Valley sites are excluded, the GoF for TRMM was seen to improve to a value of 0.0542 and those for Recs. ITU-R P.837-6 and ITU-R P.837-7 were 0.1092 and 0.0582 respectively. In both cases, the ITU-R P.837-7 performs better than the ITU-R P.837-6, but with Ayura excluded, the TRMM method is superior.

4.4.3 Other rain rate exceedances

The annual point one-minute rain rates exceeded in 0.01% of an average year: $R_{0.01\%}$, is a parameter of primary interest as it is an input to models for microwave link fade distributions. However, 0.1% and 0.001% are also considered when analysing rain attenuation on these links. The following plots compare 0.1 and 0.001% exceeded rain rates i.e. $R_{0.1\%}$ and $R_{0.001\%}$, for DBSG3 and model rain rates.
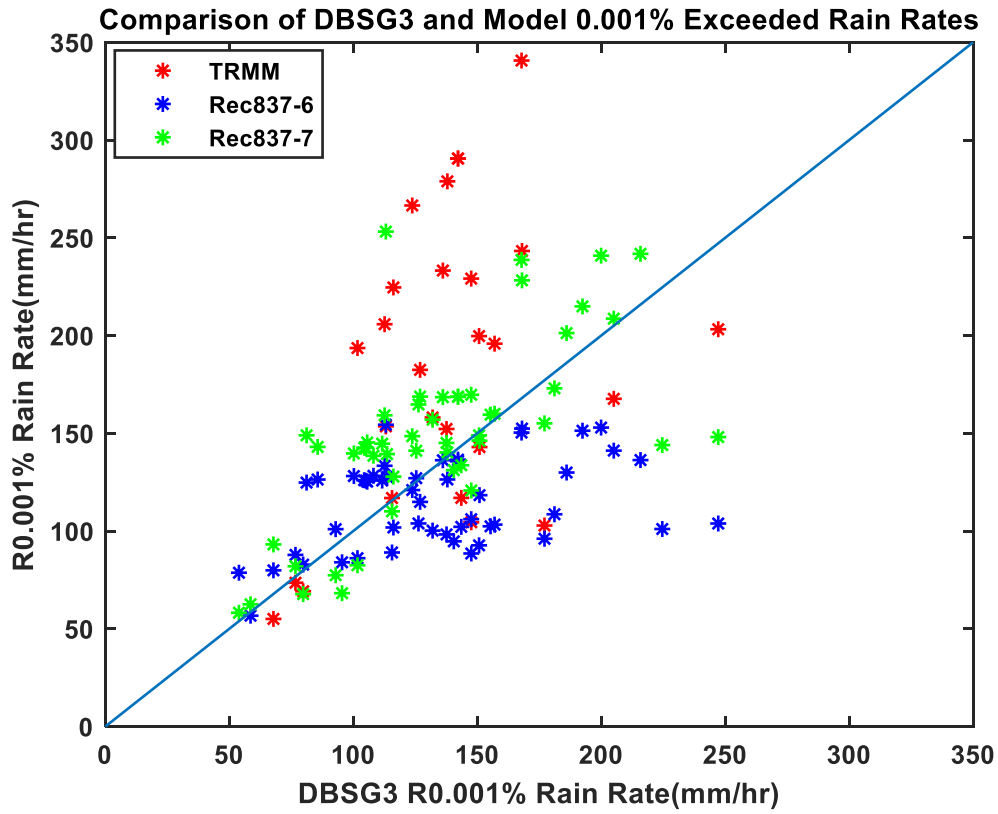
Figure 4.10. Comparison of 0.001% exceeded rain rate (mm/hr) from 1 km TRMM distribution, Rec. ITU-R P.837-6 and Rec. ITU-R P.837-7 predictions, with DBSG3 data from the Tropics
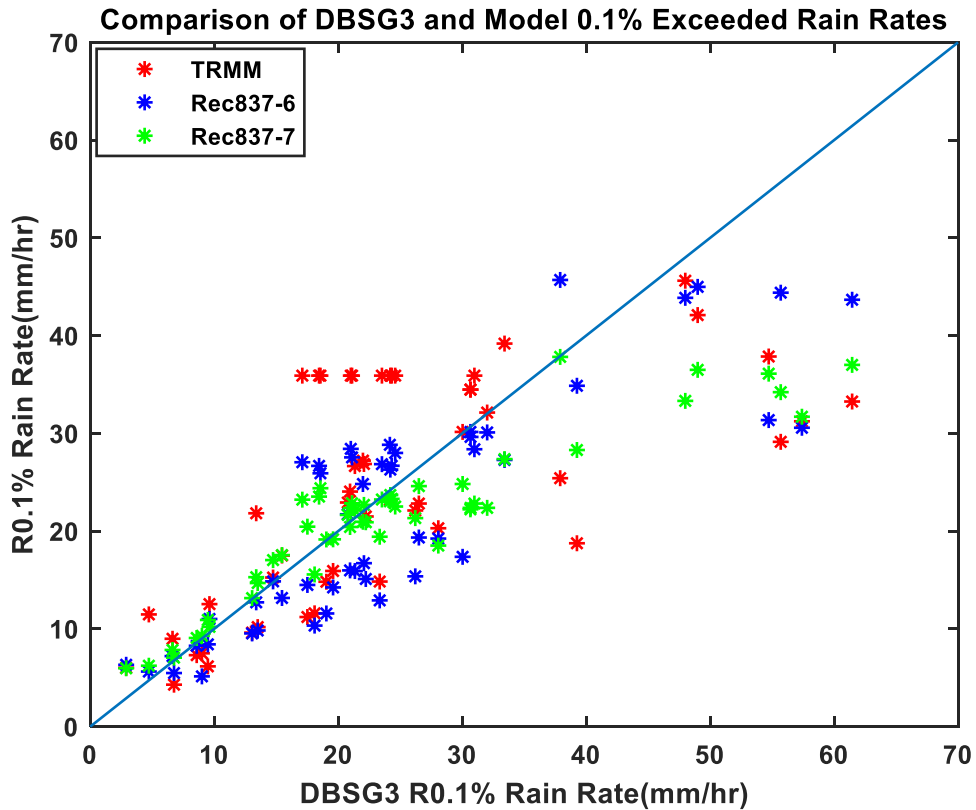
Figure 4.11. Comparison of 0.1% exceeded rain rate (mm/hr) from 1 km TRMM distribution, Rec. ITU-R P.837-6 and Rec. ITU-R P.837-7 predictions, with DBSG3 data from the Tropics

Figure 4.10 shows an overestimation of 0.001% exceedance by TRMM and an underestimation by Rec. ITU-R P.837-6. Rec. ITU-R P.837-7 appears to have the least bias. Considerable spread is expected in 0.001% exceeded values due to the large year-to-year variation in these values. There is also the probability of error in measurements of extreme rain rates over 150 mm/hr. Anomalous values can occur due to temporary gauge blockage or restrictions to the flow rate through the gauge. Figure 4.11 considered the much lower 0.1% exceeded rain rates. All three methods appear to provide equally good estimates below 40 mm/hr. TRMM appears to yield more scatter in estimates while Rec. ITU-R P.837-7 and P.837-6 both appear to underestimate the rain rates above 40 mm/hr.

4.5 Comparing one-minute Rain Rates to Alternative Site Data

A study by Singh & Acharya (2018) contains values of measured 0.01% exceeded rain rates collected from various published works. Fifty-six tropical sites from Africa and Asia, within the boundaries of TRMM data were selected for this study, and are referred to as the S&A sites. The site names are those used by Singh and Acharya.

There are legitimate concerns that the 5 km to 1 km transformation derived from temperate Nimrod data (see Equation 4.1)), and the link between 1 km $R_{0.01\%}$ and the point one-minute $R_{0.01\%}$ may not be accurate in the Tropics, as Nimrod data cover the UK from 50° to 56° north. The transformation depends upon the fine scale spatial variation of rain rate and hence on the mix of convective and stratiform rain. Although the transformation was successfully applied to tropical rain data in section 4.2.2, a question remains whether a better transformation exists. This is tested by optimising the transformation parameters to yield the best fit with DBSG3 data. Furthermore, the fit to S&A $R_{0.01\%}$ data from literature, but not in DBSG3, is also reported.

To achieve this, the γ and δ parameters in Equation (4.1) are adjusted to minimize an error measuring the difference between downscaled TRMM $R_{0.01\%}$ and observed site data. The error is defined to be the mean absolute difference, as in Equation (4.4):

$$Error = mean(|RR_M - RR_O|) \qquad (4.4)$$

where RR_M and RR_O are the model rain rates and observed site rain rates.

4.5.1 Fitting TRMM 1 km distributions to DBSG3 data

Minimising Equation (4.4) where RR_M and RR_O are the downscaled TRMM $R_{0.01\%}$ predictions and the DBSG3 values respectively, and the constraint that γ ≥ 0, yields new parameters: γ = 0

and $\delta = 1.8462$. The constraint is required to maintain a monotonic transformation when fitting to just $R_{0.01\%}$ rather than the full distribution.

Table 4.3 contains TRMM $R_{0.01\%}$ derived from the optimised transformation with predictions of Rec. ITU-R P.837-7, and average site DBSG3 values for all the DBSG3 sites in the Tropics. Figure 4.12 shows the comparison between these values. Fitting metrics are provided in Table 4.5. The performance of TRMM is similar to Rec. ITU-R P.837-7.

Table 4.3

Rec837, OPTIMISED TRMM AND AVERAGE DBSG3 0.01% ANNUAL EXCEEDED RAIN RATES (mm/hr) FOR DBSG3 SITES					
SITE	LAT	LON	DBSG3	Rec.837-7	Optimised TRMM fitted to DBSG3
ALMERIA	36.85	-2.38	16.2	22.0	33.5
CADIZ	36.50	-6.26	36.6	31.7	45.7
MALAGA	36.67	-4.48	35.3	27.9	31.6
MELILLA	35.28	-2.92	28.9	26.7	41.3
TENERIFE NORTE	28.47	-16.32	32.9	32.2	41.5
DAEJON	36.37	127.36	87.7	59.2	88.1
TAEGU	35.88	128.62	57.9	54.1	67.8
PUSAN	35.10	129.03	93.7	61.5	102.8
CHONGQING	29.58	106.47	72.0	60.5	62.2
DONGXING	21.53	107.97	141.8	103.8	134.5
FUZHOU	26.08	119.28	85.3	65.7	110.1
GUANGZHOU	23.05	113.32	106.0	83.6	117.5
GUILIN	25.33	110.30	93.8	72.9	97.2
HAIKOU	20.03	110.47	122.4	86.7	83.4
HANGZHOU	30.32	120.20	61.1	63.7	54.4
JINAN	36.68	116.98	61.6	51.1	83.1
KUNMING	25.02	102.68	59.9	46.4	55.5
LANZHOU	36.05	103.88	24.1	24.4	28.9
NANCHANG	28.67	115.97	74.6	69.5	86.4
NANGJING	32.32	118.80	62.2	57.6	77.6
WUHAN	30.63	114.07	86.4	62.3	56.8
XIAN	34.30	108.93	30.6	36.7	31.9
YICHUN	27.80	114.38	63.4	67.6	114.9
ZHENGZHOU	34.72	113.65	57.9	46.5	48.5
PUSAN	35.10	129.03	93.7	61.5	102.8
BUKIT TIMA	1.30	103.90	124.8	99.7	95.9
HOUSTON	29.77	-95.73	93.8	58.8	69.1
JACKSONVILLE	28.34	-80.93	91.4	69.5	115.4
FLORIDA	28.34	-80.60	91.4	69.3	115.4
NORMAN	35.21	-97.44	64.7	50.4	92.1
WHITE	32.54	-106.61	38.8	28.4	59.0
TAMPA	28.06	-82.42	90.0	69.3	95.1
BELEM	-1.45	-48.48	126.9	103.9	111.3

BRASILIA	-15.48	-47.83	71.0	67.7	75.5
MANAUS	-3.15	-60.02	110.0	98.3	108.4
RIO DE JANEIRO	-22.92	-43.95	71.8	71.9	80.3
STA RITA DO SAPUCAI	-22.25	-45.72	70.0	60.3	84.5
SAO PAULO	-23.55	-46.63	67.1	63.3	104.5
PALAU PIG (SAINS)	5.35	100.30	123.8	104.1	127.7
KWAJALEIN	8.79	167.62	77.9	108.9	87.6
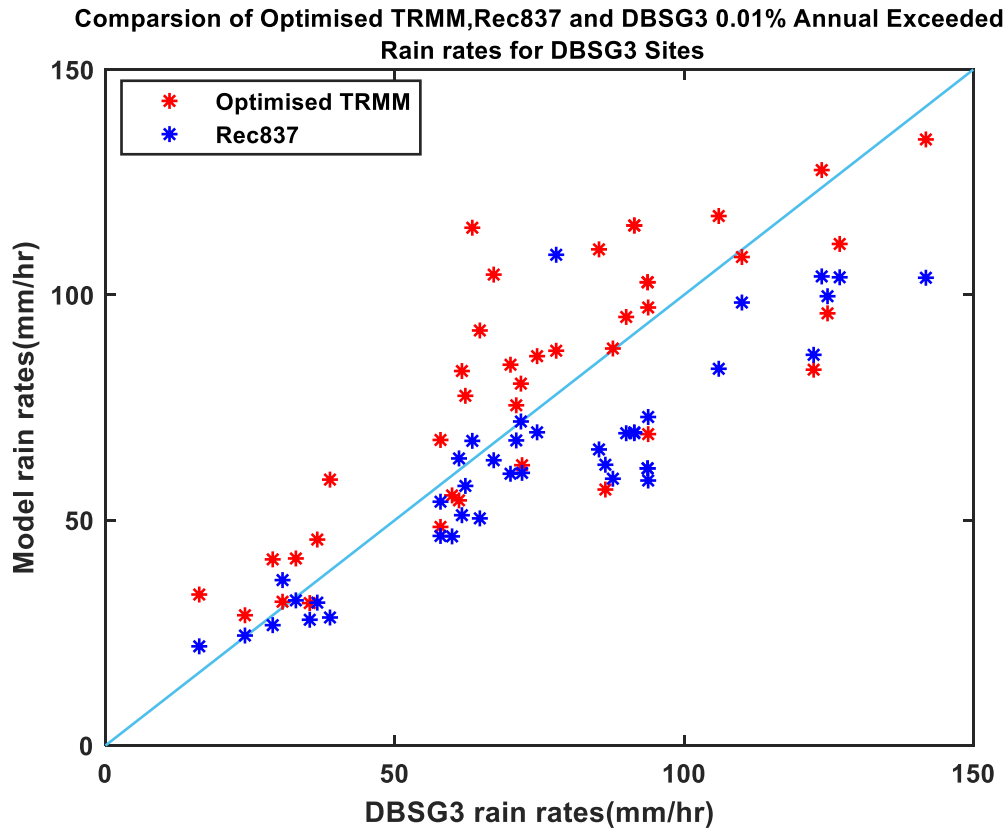
Figure 4.12. Comparison of $R_{0.01\%}$ from optimised TRMM 1 km distributions, DBSG3 and Rec837.

4.5.2 Fitting TRMM 1 km distributions to S&A Data

TRMM distributions were fitted to the S&A data, and the constrained optimisation yields new transformation parameters $\gamma = 0$ and $\delta = 2.0046$. The optimised TRMM $R_{0.01\%}$ for S&A sites are presented in Table 4.4

Figure 4.13 compares $R_{0.01\%}$ derived from the optimally downscaled TRMM distributions and from Rec.837-7, with average measured values for all the S&A sites that fall within the TRMM

boundaries. Rec. ITU-R P.837-7appears to have a strong under-estimation bias. The fitting metric

in Table 4.5 shows TRMM performing better than ITU-R P.837-7

Table 4.4

ITU-R P.837-7, OPTIMISED TRMM AND AVERAGE DBSG3 0.01% ANNUAL EXCEEDED RAIN RATES (mm/hr) FOR S&A SITES					
SITE	LAT	LON	S&A $R_{0.01\%}$	Rec. ITU-R P.837-7	Optimised TRMM fitted to S&A
BANDUNG	-6.91	107.61	120	93.9	148.3
AMRITSAR	31.63	74.87	48	63.3	92.6
THIRUVANANTHAPURAM	8.50	76.90	76	89.8	92.1
GANDAKI	13.50	79.20	68	67.0	83.6
KIANSAM	5.98	116.25	108	90.5	126.6
MIRI AIRPORT	4.31	113.98	117	105.	145.3
DALAS	6.03	116.48	110	89.6	122.1
BINTULULU	3.16	113.03	114	116.6	130.3
STAPANG	2.38	112.13	114	110.4	119.3
NTU, SINGAPORE	1.34	103.68	106	101.1	104.1
BUKIT TIMAH	1.33	103.80	75	100.2	104.1
USM	5.35	100.30	68	104.1	138.6
SKUDAI	1.45	103.75	120	101.1	104
NGURU	12.87	10.45	69.3	53.0	32.1
BORNO	11.50	12.97	72.5	57.7	78.1
KATSINA	12.98	7.62	74.9	55.0	91.9
GUSAU	12.16	6.67	78.1	66.0	79.0
SOKOTO	13.00	5.24	78.8	60.8	87.8
DIKWA	12.04	13.91	81.7	55.5	51.2
MAIDUGURI	7.73	13.15	84.0	68.8	109
GOMBE	10.24	11.16	86.1	65.4	75.0
BAUCHI	10.67	10.08	90.8	66.1	101
ADAMAWA	9.32	12.43	94.2	66.1	79.0
KANO	12.00	8.59	98.8	64.1	79.2
KADUNA	10.15	8.13	101.5	65.9	101.9
MINNA	9.58	6.54	101.9	72.0	91.9
ILE-IFE	7.49	4.55	106	73.4	108.8
ILORIN	8.47	4.54	103.4	69.2	85.0
ABUJA	9.07	7.39	104.5	73.44	96.7
JOS	9.89	8.85	108.4	65.1	96.2
MAKURDI	7.73	8.53	110	73.7	84.6
OGHOMOSO	8.12	4.24	114.1	68.9	85.0
LOKOJA	7.80	6.70	115.7	70.3	86.7
SAKI	8.67	3.39	118.2	69.1	100.9
OSOGBO	7.68	4.45	120.1	72.2	108.8
ABEOKUTA	7.14	3.35	121.9	73.2	82.4
AKURE	7.25	5.20	122.6	75.3	125.5
LAGOS	6.52	3.37	124.2	83.3	114
ABIA	5.43	7.52	127.3	88.1	85.9
ENUGU	6.45	7.54	129.8	83.2	77.4
BENIN	9.30	2.31	131	70.0	90.6
CALABAR	4.97	8.34	139.3	92.3	153.8
PORT HARCOURT	4.81	7.04	140.8	87.5	176.4
WARRI	5.55	5.79	145.2	97.4	139.5
GWANJU	35.16	126.86	90	59.1	101.8
DAEGU	35.87	128.60	60	54.3	73.7

BUSAN	35.18	129.08	90.00	60.84	111.60
ULSAN	35.54	129.31	65.40	57.23	111.60
PENANG	5.27	100.29	125.00	103.05	138.61
JOHOR BAHRU	1.30	103.43	114.00	102.05	104.08
ALOR STAR	6.15	100.25	107.00	98.05	108.79
KUALA LUMPUR	3.04	101.36	133.00	97.71	161.23
KOTOTABANG	-0.20	100.32	88.88	98.05	152.03
BUKIT JALIL	3.08	101.42	164.00	98.15	161.23
TAIPING	4.85	100.74	147.00	103.57	120.14
TEMERLOH	3.45	102.42	125.00	89.05	112.83

Table 4.5

GOODNESS OF FIT (GoF) METRIC (mm/hr) FOR MODEL 0.01% ANNUAL EXCEEDED RAIN RATES			
Fitting to DBSG3		Fitting to S&A	
TRMM	ITU-R P.837-7	TRMM	ITU-R P.837-7
14.55	15.00	20.41	28.52
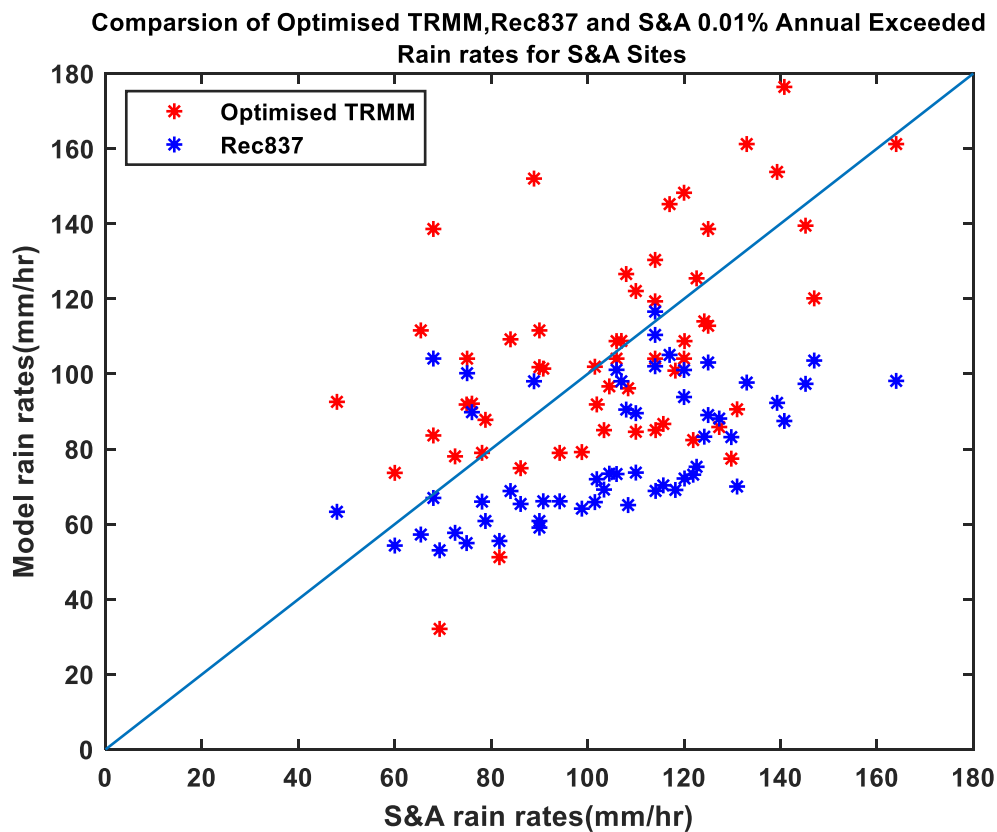
Figure 4.13. Comparison of optimised TRMM 1 km distributions, Rec837 and measured 0.01% exceeded rain rates for S&A sites.

4.6   Chapter summary

There are concerns that ITU-R models may not work accurately in the Tropics because of the lack of input and validating data from the Tropics. In this chapter, distributions of TRMM estimated surface rain rate data have been used to estimate the point-one-minute rain rate exceeded for a range of time percentages for sites in the Tropics.

Data from the UK Meteorological Nimrod system have been used to derive a method to transform the measured 5 km TRMM rain rates to 1 km rain rates. The transformation found was very similar to transformations calculated by optimal fitting of TRMM predicted exceeded rain rates to measured site data. The differences are likely to be due to the range of rain rates and exceedance probabilities i.e. the Nimrod transformation used exceedances in the range 1% to 0.001% while the transformations presented in this chapter used only 0.01%. However, the similarity suggests that the Nimrod derived transformation may be used in the Tropics.

Analysis has compared exceeded rain rates predicted by transforming distributions of TRMM rain rates to those generated by ITU-R models. Comparisons were also made with site data from the DBSG3 database, and an alternative S&A dataset. In general, P.837-7 performed better than P.837-6 when compared to DBSG3 data. Both tended to systematically under-estimate higher rain rates at several time percentages. In many comparisons the TRMM method yielded a better fit than the current Rec.837-7.

This chapter looked at using the measured distributions of TRMM rain rates directly. An alternative use of the same data is presented in the next chapter where TRMM data are used to estimate rain rate distributions conditional upon monthly accumulation and temperature. This allows the TRMM data to be used globally.

Chapter 5   Estimating Global Rain Rate Distributions Using Conditional Distributions of Measured TRMM Rain Rates

5.1   Introduction

The previous chapter used downscaled exceedance distributions of TRMM 5 km rain rates to estimate point one-minute rain rate distributions across the Tropics. This chapter explores the use of TRMM data to estimate rain rate exceedance probability distributions conditional upon local monthly rain accumulation and temperature, but not on location. These distributions were introduced in ITU-R P.837-7 (ITU-R, 2017b) as a part of the method to estimate distributions globally. This chapter looks at the estimation of these conditional probability distributions using TRMM data, the quality of rain rate distribution estimation using the Rec. P.837-7 method with TRMM conditional distributions, and a variety of sources for the accumulation and temperature data.

5.2   Conditional Distributions in Rec. ITU-R P.837-7

The current Recommendation ITU-R P.837-7 provides average annual, point one-minute rain rate distributions globally. The input data to Rec. ITU-R P.837-7 are digital maps of mean monthly surface temperatures (T) provided in Rec. ITU-R P.1510-1(ITU-R, 2017a) and mean monthly total precipitation accumulation (MT). Annual distributions are formed as weighted averages of monthly distributions, which are analytic lognormal distributions conditional upon T and MT: $XCD_{837}(R|T_{ii}, MT_{ii})$; with monthly T_{ii} and MT_{ii} available in data files associated with the Recommendation:

$$XCD(R) = \frac{1}{365.25} \sum_{ii=1}^{12} N_{ii} \times XCD_{837}(R|T_{ii}, MT_{ii}) \qquad (5.1)$$

where N_{ii} is the average number of days in month ii. A complication linked to the use of months is their variable length, meaning that monthly accumulation can be associated with different average daily accumulations. Rather than using MT_{ii} directly as implied by Equation (5.1) within the Recommendation, it is converted to mean daily accumulation: $MMDA_{ii} = MT_{ii}/N_{ii}$, to produce the conditional exceedance distribution.

5.3   Input Data to Rec. ITU-R P.837-7

The input data MT_{ii}, are derived from a global rain gauge network and reanalysis data i.e. the Global Precipitation Climatology Centre (GPCC) gridded rain gauge dataset over land and the European Centre for Medium-Range Weather Forecasts (ECMWF) ERA Interim database over water (ITU-R, 2017b). Monthly average temperatures are also derived from ERA Interim. These databases have been described in sections 3.3.4 and 3.3.5.

Annex 1 of Rec. ITU-R P.837-7 (ITU-R, 2017b) provides digital maps of monthly mean total rainfall and monthly mean surface temperatures. The maps of monthly accumulations have been formed by combining GPCC and ERA Interim data so as to cover both land and sea. Maps of average temperature derived from ERA Interim are also provided.

The Tropics are predominantly made up of countries where rain gauge networks are sparsely distributed and often located in urban areas. Therefore, these data often do not reflect geographic variation in rain distributions. For the GPCC dataset with the finest resolution, 0.25°, most grid squares will not contain a rain gauge and so results are generated by interpolation. These factors, as well as the errors associated with rain gauges discussed earlier, are likely to affect the performance of the ITU-R P.837-7 in the Tropics. In contrast, temperature exhibits much

smoother spatial and temporal variation than rain, is much easier to measure and so is likely to be significantly more reliable than the accumulation parameter.

5.4 Calculation of TRMM monthly one-minute rain rate distributions

The use of the Rec837 paradigm requires distributions of rain rates, conditional upon the monthly mean temperature and mean daily accumulation. These distributions were estimated using TRMM data i.e. nine years of TRMM 2A25 data, spanning 2004 to 2012, between latitudes -38° and +38° and all longitudes. The goal of the analysis was to estimate the TRMM conditional rain rate exceedance probability distributions: $XCD_{TRMM}(R\,|T,MT)$, the equivalent of the Rec837 distributions: $XCD_{837}(R\,|\,T,MT)$. This was achieved by aggregating data from the entire Tropics and the 9 years, from 1° grid squares that experience the similar monthly T and $MMDA$. The mean monthly daily accumulation, $MMDA$, was used so that rain rates from all months could be aggregated to estimate the conditional distributions. The process to derive TRMM conditional probability distributions is summarised as follows:

• Calculate histograms of 5 km TRMM rain rates for $1° \times 1°$ latitude and longitude squares, for each of the 108 months spanning 9 years

• Loop over each 1° square and for each month, acquire the T and $MMDA$ for each month from GPCC and ERA Interim data

• Aggregate rain rate histograms for each 1° square and month associated with a T and $MMDA$ bin

• Convert aggregated histograms, conditional upon T and $MMDA$, into TRMM 5km exceedance distributions

- Convert exceedance distributions of 5 km TRMM rain rates into 1 km rain rates using the quadratic transformation

This process is described in more detail below.

Monthly histograms of measured 5 km rain rates were calculated for every $1° \times 1°$ latitude and longitude square in the Tropics. Mean monthly temperatures (T) from ERA Interim data and mean monthly daily accumulations ($MMDA$) from the GPCC monthly precipitation, were calculated over the same array of $1° \times 1°$ squares. These three sets of data yield a histogram of TRMM rain rates, a T and a $MMDA$ for each $1°$ square and for each of $9 \times 12 = 108$ months. One-hundred equi-probable T bins were defined spanning 247.6 K to 313.6 K. Similarly, 100 equi-probable $MMDA$ bins were defined from 0 to 75.3 mm. TRMM 5km exceedance distributions were calculated by aggregating TRMM rain rates from all $1°$ squares with T and a $MMDA$ in the same bins. These provide estimates of exceedance distributions of 5 km rain rates conditional on a given T and $MMDA$: $XCD_{TRMM}(R \,|T, MT)$. The 5 km exceedance distributions were transformed to distributions of 1 km rain rates, using the quadratic transformation in section 4.2.1, yielding $XCD_{1km}(R \,|T, MT)$. The TRMM conditional distributions share the major characteristics with those of Rec837.

5.5 Methods Based on TRMM Conditional Distributions

Once these distributions were calculated, various tests were performed to determine how well they predict annual exceedance distributions in the Tropics. Two methods are considered in this study. Both methods use the Rec837 method (Equation (5.1)) but replace the conditional distribution with the equivalent transformed conditional TRMM distributions: XCD_{1km}. The two methods differ in the source of monthly mean temperature and accumulation, which are:

a)   Using the average annual T_{ii} and MT_{ii} available in Rec837 data files

b)   Using T_{ii} and MT_{ii} from ERA Interim and GPCC for the specific 108 months of TRMM data.

While method a) was expected to be more representative of average annual results, method b) was expected to be more consistent with the TRMM distributions as T and MT are from primary sources and are from the same period that the exceedance data was calculated.

5.5.1   Using Rec. ITU-R P.837-7 Input Data

Method a) uses the average annual T_{ii} and MT_{ii} from Rec837 data files, and the TRMM measured and downscaled conditional distributions XCD_{1km}, rather than XCD_{837}. In a second test, the downscaling transformation of TRMM values have also been optimised to fit DBSG3 (see section 4.5.1).

Rain rate distributions have been calculated for DBSG3 sites in the Tropics and the results are presented in Table 5.1. Figure 5.1 focuses on $R_{0.01\%}$ as this is the input parameter used in many other Recommendations. The sites in the DBSG3 database have been divided into two sets: sites with 4 or more years of data and those with less. Sites with four or more individual years of data allow the year-to-year variability to be estimated and so an estimate of the uncertainty in the estimate of the site average annual $R_{0.01\%}$ may be calculated. For the many sites with single years of data, it is difficult to say how close the rain rate values are to average annual. However, it is reasonable to assume that the average annual value is equally likely to be higher or lower than the single year measured value. Sites having 4 or more years of data are plotted with error bars of length: $\sigma_R/\sqrt{n}$ where σ_R is the standard deviation of annual DBSG3 $R_{0.01\%}$ measurements and n is the number of years. Due to temporal correlations in annual exceeded rain rates, the uncertainty is expected to be an under estimate.
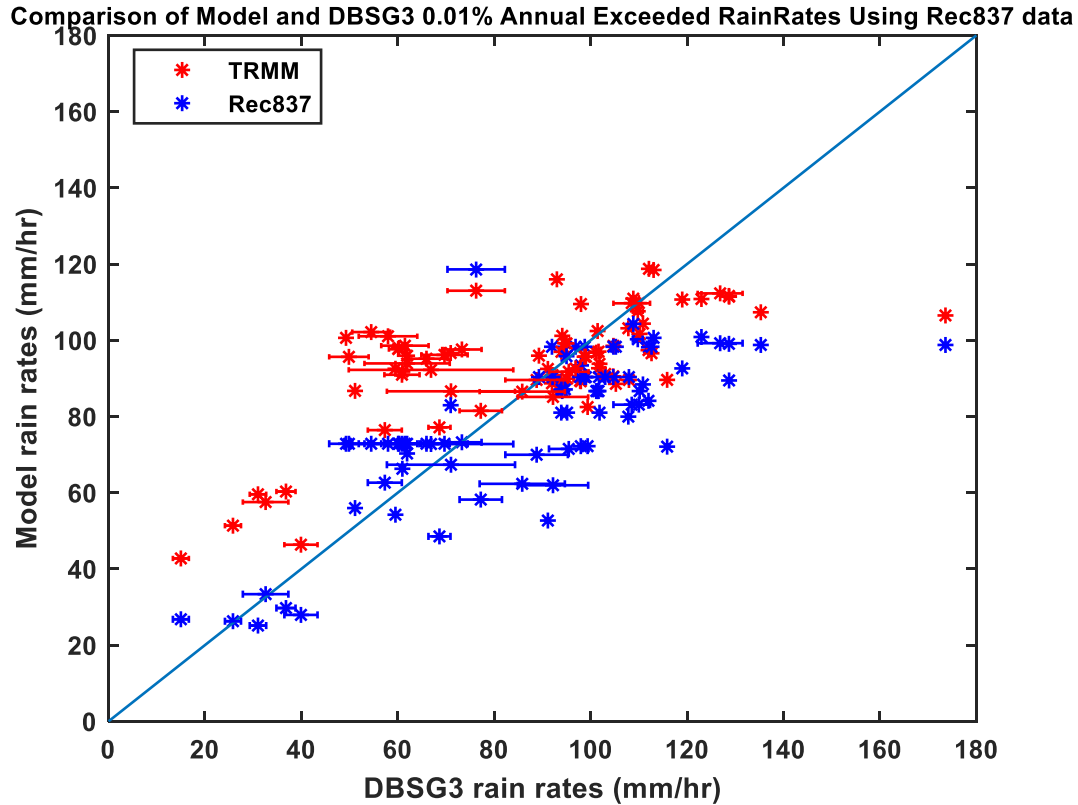
Figure 5.1. Comparison of Method a) $R_{0.01\%}$ and Rec837 exceeded rain rates with DBSG3 data for sites in the Tropics. Both models use Rec837 T_{ii} and MT_{ii} input data. The conditional monthly distributions are (blue): XCD_{837} and (red): XCD_{1km}. Sites with 4 or more years of data are plotted with error bars indicating the uncertainty in the DBSG3 estimate of average annual values. Red and blue error bars are at TRMM and Rec837 respectively.

If variation were purely random, two thirds of the error bars would be expected to span the line of equality. For both models, fewer than half the error bars span the line. This is probably due to the under-estimation of the uncertainty. Rec837 appears to under-estimate the higher rain rates while the TRMM method over-estimates the lower rain rates.

5.5.2 Using GPCC and ERA Interim Input Data

The same process described in 5.5.1 is followed but using T_{ii} and MT_{ii} from ERA Interim and GPCC for the specific 108 months of TRMM data, as inputs. Distributions were calculated using

both XCD_{837} and XCD_{1km}. This extends the test as both input data and conditional distributions now come from primary data sources, and the TRMM distributions are conditioned upon the accumulations and temperatures during which the rain rates were measured. The results are also presented in Table 5.1. Figure 5.2 mirrors Figure 5.1, comparing model 0.01% exceeded rain rates with DBSG3 site data. Most DBSG3 data come from outside the 9-year period providing the primary data.

Table 5.1

COMPARISON OF DBSG3 $R_{0.01\%}$ AND MODEL PREDICTIONS (mm/hr)							
				Method a)		Method b)	
SITE	LAT	LON	DBSG3	TRMM	Rec837	TRMM	Rec837
ALMERIA	36.85	-2.38	15.0	42.7	26.8	49.1	25.6
CADIZ	36.50	-6.26	36.8	60.3	29.7	60.7	32.6
MALAGA	36.67	-4.48	32.6	57.5	33.4	60.1	29.8
MELILLA	35.28	-2.92	25.8	51.3	26.3	56.8	30.2
TENERIFE NORTE	28.47	-16.32	31.0	59.6	25.1	53.2	29.3
DAEJON	36.37	127.36	77.2	81.5	58.2	84.5	64.8
TAEGU	35.88	128.62	57.3	76.4	62.6	83.9	66.5
PUSAN	35.10	129.03	85.8	86.5	62.3	83.2	60.7
SI RACHA	13.10	100.80	99.4	82.5	72.2	88.8	88.1
BANGKOK	13.70	100.50	98.0	89.2	72.2	88.8	88.1
CYBERJAYA FTA	2.92	101.66	135.3	107.3	98.8	109.4	102.1
CYBERJAYA MMU	2.93	101.64	173.6	106.5	98.8	109.4	102.1
BUKIT TIMA	1.30	103.90	123.0	110.8	100.9	112.7	106.7
HOUSTON	29.77	-95.73	92.2	85.1	62.0	82.8	61.7
JACKSONVILLE	28.34	-80.93	88.8	89.6	70.0	90.0	74.0
MIAMI	25.65	-80.43	115.9	89.6	72.1	91.5	80.1
NORMAN	35.21	-97.44	68.6	77.1	48.5	75.8	51.3
WHITE	32.54	-106.61	39.9	46.4	27.9	49.5	30.2
TAMPA	28.06	-82.42	95.5	91.7	71.5	89.2	69.2
AYURA	6.17	-75.57	60.3	98.0	72.8	108.3	75.1
CHORRILLOS	6.3	-75.51	60.1	97.7	72.8	108.3	75.1
CONVENTO	6.34	-75.52	58.0	101.1	72.8	108.3	75.1
CUCARACHO	6.29	-75.61	66.0	95.2	72.8	108.3	75.1
GERONA	6.23	-75.56	61.5	98.6	72.8	108.3	75.1
GIRARDOTA	6.39	-75.46	49.9	95.6	72.8	108.3	75.1
MANANTIALES	6.32	-75.54	54.5	102.1	72.8	108.3	75.1
PEDREGAL	6.31	-75.58	61.9	93.9	72.8	108.3	75.1
SAN ANTONIO DE PRADO	6.19	-75.66	69.7	96.2	72.8	108.3	75.1
SAN CRISTOBAL	6.28	-75.64	60.9	90.9	72.8	108.3	75.1
VILLA HERMOSA	6.26	-75.55	49.3	100.6	72.8	108.3	75.1
BELEM	-1.45	-48.48	126.9	112.3	99.2	113.6	111.1
BOA VISTA	2.78	-60.68	112.0	97.4	84.1	101.9	89.4
BRASILIA	-15.80	-47.83	71.0	86.6	67.3	93.8	69.5
CRUZEIRO DO SUL	-7.60	-72.67	128.7	111.4	89.5	106.0	90.3
CURITIBA	-25.42	-49.28	59.5	92.5	54.2	93.2	57.8
FORTALEZA	-3.77	-38.55	61.9	95.9	70.3	88.6	75.1
GOV.VALADARES	-18.85	-41.95	61.0	91.8	66.3	85.6	62.7
MACAPA	0.30	-51.10	119.0	110.7	92.6	107.2	93.7

MANAUS	-3.15	-60.02	109.8	107.6	100.3	108.5	98.8
MOSQUEIRO	-1.40	-50.69	128.7	111.6	99.1	111.3	103.8
NATAL	-5.70	-35.20	91.1	92.5	52.7	86.5	68.3
PONTA DAS LAGES	-3.20	-59.90	98.0	109.5	93.4	108.4	98.0
PORTO ALEGRE	-30.03	-51.22	51.1	86.7	56.0	89.1	57.3
RECIFE	-8.05	-34.90	71.0	96.6	83.0	104.3	96.7
RIO DE JANEIRO	-22.92	-43.95	73.3	97.6	73.2	96.2	71.2
SANTAREM	-2.50	-54.72	110.9	104.4	88.4	108.7	96.1
SAO GABRIEL DA CACHOEIRA	-0.12	-67.07	112.1	118.7	98.2	116.4	100.8
SAO PAULO	-23.53	-46.62	66.9	92.2	72.8	99.7	73.9
TABATINGA	-4.23	-69.94	113.1	118.4	100.6	118.6	107.7
LBA	-10.35	-62.58	107.8	103.1	80.0	100.0	80.0
KWAJALEIN	8.79	167.62	76.3	113.0	118.6	105.6	107.2
SUVA	-18.14	178.42	93.0	116.0	89.8	115.8	104.5
UNITECH LAE	-7.00	147.00	108.5	109.7	83.1	119.2	102.2
POST OFFICE LAE	-7.00	147.00	110.0	109.7	83.1	119.2	102.2
ANNABURROO	-12.91	131.67	108.0	89.6	90.3	98.8	100.7
BATCHELOR	-13.06	131.02	95.1	89.9	81.0	92.7	90.6
BATHURST	-11.77	130.62	94.1	101.2	86.7	102.5	101.1
BELLVILLE	-12.76	130.88	105.2	88.6	98.3	103.1	102.7
BERRIMAH	-12.46	130.93	112.6	96.6	98.3	103.1	102.7
CPFOUR	-11.77	130.03	101.2	96.8	86.7	102.5	101.1
CHARLESPOINT	-12.42	130.63	98.8	90.4	98.3	103.1	102.7
DARWINRIVERDAM	-12.83	130.97	92.0	88.7	98.3	103.1	102.7
DUMINMIRIE	-12.64	130.37	104.7	98.5	98.3	103.1	102.7
GARDENPTAIR	-11.40	130.42	110.2	101.7	86.7	102.5	101.1
GOODALLMINE	-13.22	131.38	93.9	88.7	81.0	92.7	90.6
GUNNPTPRISON	-12.16	131.02	104.7	90.5	90.3	98.8	100.7
HUMPTYDOO	-12.61	131.29	97.8	89.4	90.3	98.8	100.7
KOOLPINYAH	-12.39	131.18	101.7	92.7	90.3	98.8	100.7
LA BELLEAIRSTRIP	-13.12	130.49	94.7	99.2	87.1	99.7	101.0
LITCHFIELD	-13.43	130.48	93.9	97.0	87.1	99.7	101.0
MANDORAHJETTY	-12.44	130.76	96.9	92.6	98.3	103.1	102.7
MCMINNSLAGOON	-12.54	131.08	103.0	91.2	90.3	98.8	100.7
MTBUNDEY	-13.23	131.13	101.8	93.8	81.0	92.7	90.6
OLDPTSTUART	-12.36	131.81	98.8	95.7	90.3	98.8	100.7
PICKERTARAMOOR	-11.77	130.88	101.6	97.0	86.7	102.5	101.1
POINTSTUARTABBS	-12.59	131.76	92.1	90.9	90.3	98.8	100.7
SNAKEBAY	-11.42	130.65	101.5	102.4	86.7	102.5	101.1
SWIMCREEKPL	-12.36	131.81	99.0	95.7	90.3	98.8	100.7
WOOLNER	-12.38	131.47	89.3	96.0	90.3	98.8	100.7
BANDUNG	-6.90	107.60	108.9	110.9	104.3	111.7	101.1
MANILA (ADMU)	14.68	121.07	95.0	99.2	95.8	115.8	121.5
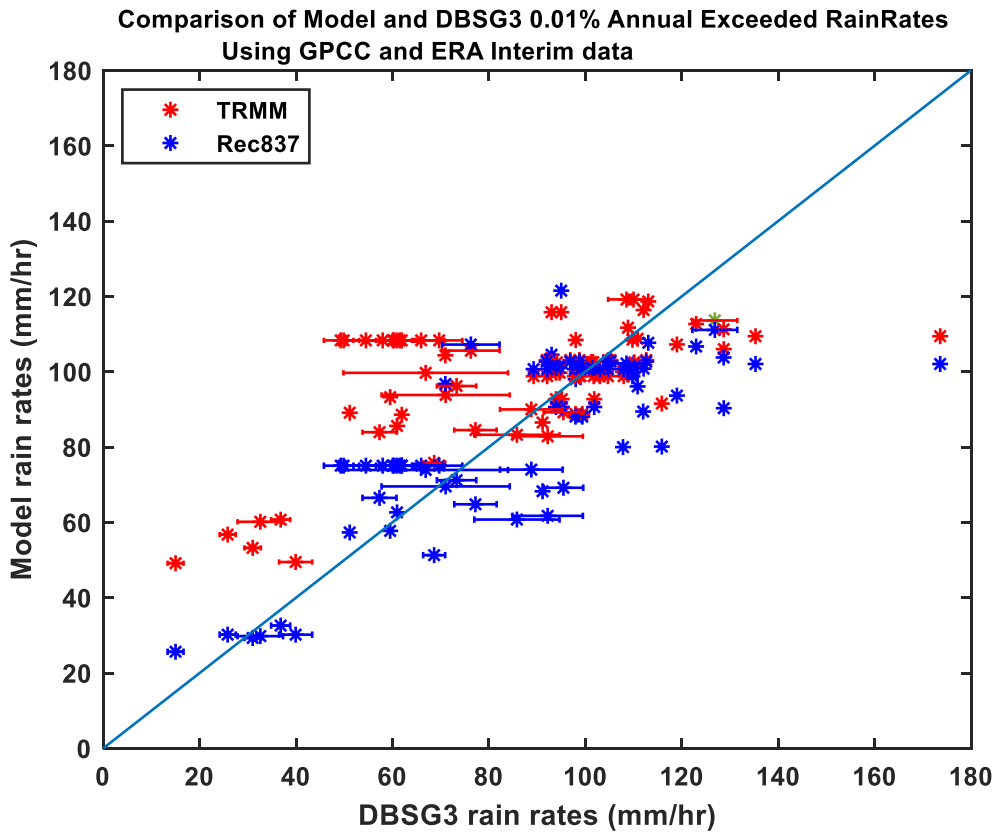
Figure 5.2. $R_{0.01\%}$ exceeded rain rates from Rec837 and Method b) i.e. GPCC and ERA input data and TRMM distributions. These are compared with DBSG3 data for all sites in the Tropics.

Oddly, Rec837 performs slightly better using these input data than those provided as part of the Recommendation. The Rec837 values are closer to the DBSG3 values from the Tropics as observed from the blue points in Figure 5.2 when compared to those in Figure 5.1. The TRMM method performs similarly well. Section 5.7 quantifies the goodness of fit between verification and model data. Again, goodness of fit metrics are calculated both with and without Ayura Valley data.

In Table 5.1, the site names are those used within DBSG3.

5.6 Comparing one-minute Rain Rates to Alternative Site data

Table 5.2 contains 0.01% TRMM and Rec837 annual exceeded rain rates calculated for the S&A sites described in section 4.5, using methods a) and b). The parameters for transforming TRMM from 5km to 1 km have been optimised to yield the best fit with S&A data (see section 4.5.2). Figure 5.3 and Figure 5.4 compare these calculated rain rates with S&A $R_{0.01\%}$

Table 5.2

COMPARISON OF S&A $R_{0.01\%}$ AND MODEL PREDICTIONS (mm/hr)							
				Method a)		Method b)	
SITE	LAT	LON	S&A R01%	TRMM	Rec 837-7	TRMM	Rec 837-7
BANDUNG	-6.91	107.61	120.0	121.1	104.3	121.3	101.0
AMRITSAR	31.63	74.87	48.0	74.1	52.0	71.5	62.0
THIRUVANANTHAPURAM	8.50	76.90	76.0	110.7	104.6	111.7	97.5
GANDAKI	13.50	79.20	68.0	84.9	69.1	93.6	78.3
KIANSAM	5.98	116.25	108.0	118.7	85.2	120.7	92.5
MIRI AIRPORT	4.31	113.98	117.0	129.7	109.3	124.3	118.4
DALAS	6.03	116.48	110.0	122.4	98.6	125.0	107.6
BINTULULU	3.16	113.03	114.0	135.2	115.4	132.9	119.2
STAPANG	2.38	112.13	114.0	132.1	108.7	137.2	126.2
NTU, SINGAPORE	1.34	103.68	106.0	120.7	100.9	122.3	106.7
BUKIT TIMAH	1.33	103.80	75.0	118.3	100.9	122.3	106.7
USM	5.35	100.30	68.0	119.9	106.7	121.7	104.6
SKUDAI	1.45	103.75	120.0	120.5	100.9	122.3	106.7
NGURU	12.87	10.45	69.3	63.9	56.0	68.9	55.1
BORNO	11.50	12.97	72.5	83.2	57.7	78.6	60.2
KATSINA	12.98	7.62	74.9	79.6	64.9	83.4	61.9
GUSAU	12.16	6.67	78.1	90.7	66.4	83.1	63.9
SOKOTO	13.00	5.24	78.8	73.9	61.2	70.1	56.6
DIKWA	12.04	13.91	81.7	71.8	58.6	67.2	55.9
MAIDUGURI	7.73	13.15	84.0	103.6	66.6	97.6	66.0
GOMBE	10.24	11.16	86.1	90.4	67.0	82.9	62.2
BAUCHI	10.67	10.08	90.8	93.3	65.9	90.7	69.3
ADAMAWA	9.32	12.43	94.2	92.8	64.7	87.3	65.3
KANO	12.00	8.59	98.8	88.5	63.4	84.3	66.5
KADUNA	10.15	8.13	101.5	94.4	66.2	94.2	66.5
MINNA	9.58	6.54	101.9	98.8	72.5	96.8	74.0
ILE-IFE	7.49	4.55	106.0	102.1	76.5	104.8	77.5
ILORIN	8.47	4.54	103.4	98.4	69.5	95.8	70.7
ABUJA	9.07	7.39	104.5	101.6	74.7	101.1	70.4
JOS	9.89	8.85	108.4	93.0	70.9	95.3	66.1
MAKURDI	7.73	8.53	110.0	99.4	81.7	99.4	78.3
OGHOMOSO	8.12	4.24	114.1	100.1	69.5	95.8	70.7
LOKOJA	7.80	6.70	115.7	93.9	81.3	98.2	75.4
SAKI	8.67	3.39	118.2	97.5	69.6	96.1	70.8
OSOGBO	7.68	4.45	120.1	100.7	76.5	104.8	77.5
ABEOKUTA	7.14	3.35	121.9	98.4	73.9	102.0	76.2
AKURE	7.25	5.20	122.6	102.4	77.9	102.7	76.3
LAGOS	6.52	3.37	124.2	110.0	81.5	109.6	86.4
ABIA	5.43	7.52	127.3	111.5	87.4	116.3	91.5
ENUGU	6.45	7.54	129.8	111.7	84.9	109.7	87.3

BENIN	9.30	2.31	131.0	89.3	69.7	95.2	70.9
CALABAR	4.97	8.34	139.3	121.1	102.6	121.7	100.6
PORT HARCOURT	4.81	7.04	140.8	112.4	91.6	117.9	93.7
WARRI	5.55	5.79	145.2	117.6	102.2	124.0	105.6
GWANJU	35.16	126.86	90.0	89.8	54.0	93.0	62.0
DAEGU	35.87	128.60	60.0	84.0	62.6	91.1	66.5
BUSAN	35.18	129.08	90.0	96.2	62.3	90.4	60.7
ULSAN	35.54	129.31	65.4	88.8	62.3	90.4	60.7
PENANG	5.27	100.29	125.0	115.1	106.7	121.7	104.6
JOHOR BAHRU	1.30	103.43	114.0	122.1	100.9	122.3	106.7
ALOR STAR	6.15	100.25	107.0	116.2	103.9	114.4	95.4
KUALA LUMPUR	3.04	101.36	133.0	119.3	95.0	123.5	105.6
KOTOTABANG	-0.20	100.32	88.9	127.8	117.6	128.7	108.7
BUKIT JALIL	3.08	101.42	164.0	118.6	95.0	123.5	105.6
TAIPING	4.85	100.74	147.0	127.1	113.7	122.8	103.2
TEMERLOH	3.45	102.42	125.0	119.1	92.3	117.7	96.5

Comparison of Model and S&A 0.01% Annual Exceeded RainRates Using Rec837 data
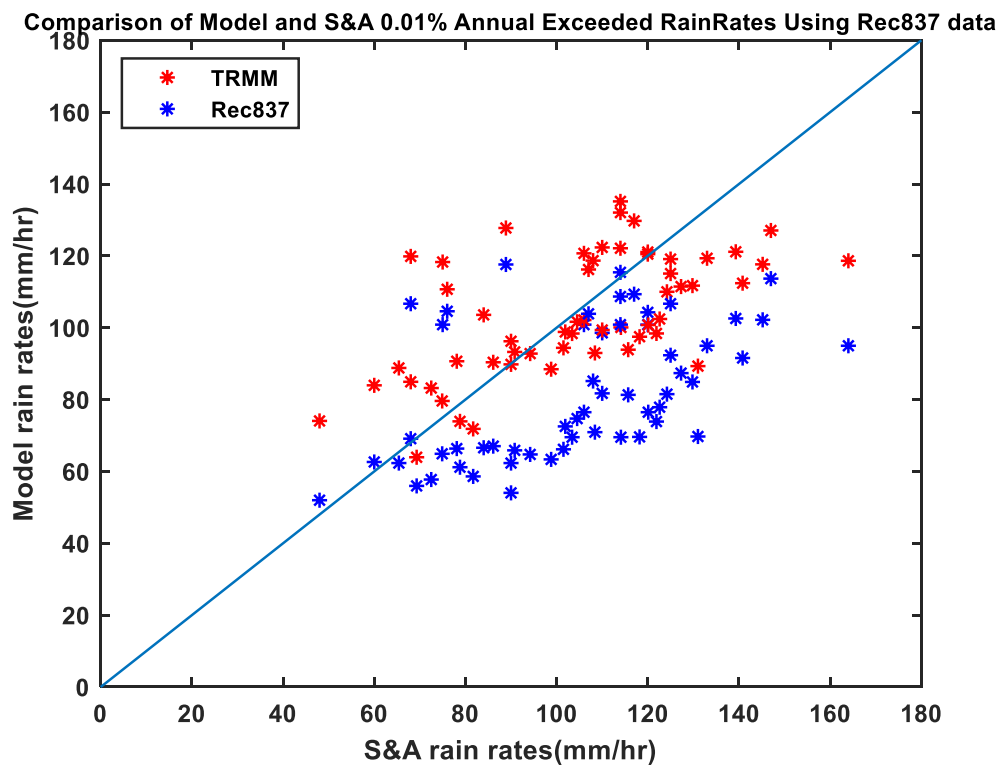
Figure 5.3. Comparison of Method a) $R_{0.01\%}$ and Rec837 exceeded rain rates with S&A site data
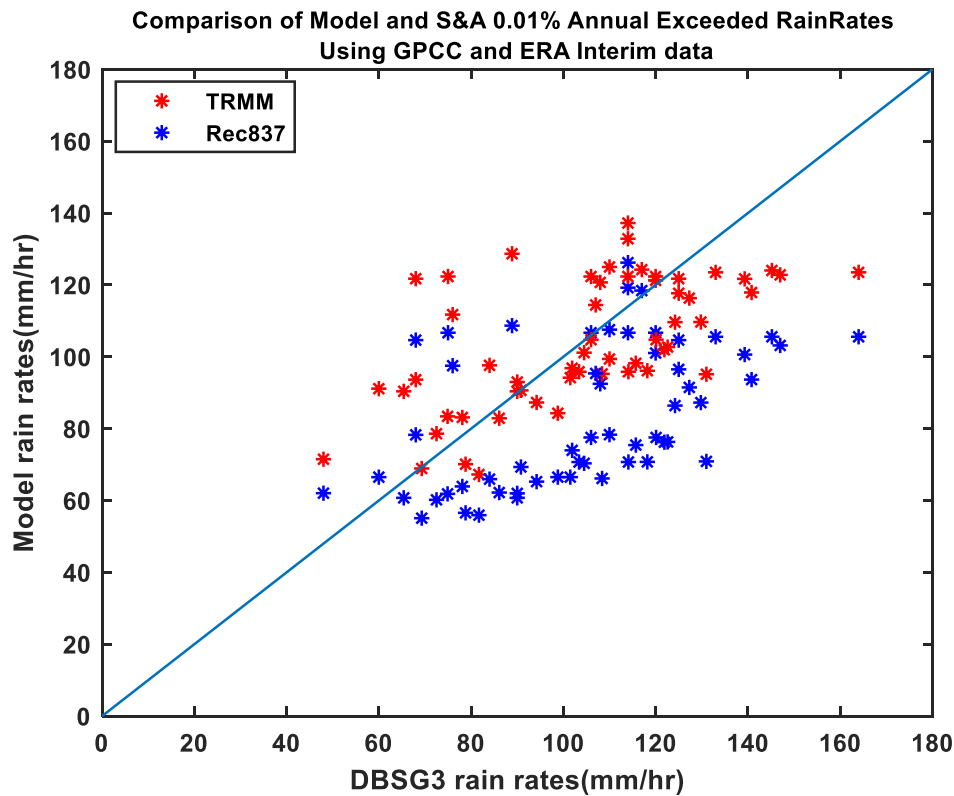
Figure 5.4. Comparison of Method b) $R_{0.01\%}$ and Rec837 exceeded rain rates with S&A site data

The TRMM method appears to perform much better than Rec837 against the S&A sites. Rec837 under-estimates for most sites for both sets of input data. The TRMM method appears to perform equally well using either set of inputs.

5.7 Comparison of TRMM and Rec837 annual 0.01% exceeded rain rates

Calculating $R_{0.01\%}$ using the methods a) and b) discussed in section 5.5 yields estimates of DBSG3 measured data that are comparable in quality to those provided by Rec837. Figure 5.1and Figure 5.2 suggest a general tendency for Rec837 to underestimate and for the TRMM results to overestimate. Table 5.3 presents the quality of TRMM and Rec837 predictions using a goodness of fit metric defined to be the mean absolute difference (Equation (4.4)).

The error metrics used by ITU-R Working Party 3J (ITU-R WP 3J, 2017) are based on mean and root-mean-square (RMS) relative errors:

$$\epsilon(i,j) = \frac{RR_E(P_j) - RR_O(P_j)}{RR_O(P_j)} \tag{5.2a}$$

$$E = \frac{\sum_{i=1}^{N_{st}} \sum_{j=1}^{n_i} \alpha_i \varepsilon(i,j)}{\sum_{i=1}^{N_{st}} n_i \alpha_i} \tag{5.2b}$$

$$RMS = \sqrt{\frac{\sum_{i=1}^{N_{st}} \sum_{j=1}^{n_i} \alpha_i \varepsilon^2(i,j)}{\sum_{i=1}^{N_{st}} n_i \alpha_i}} \tag{5.2c}$$

where N_{st} is the number of sites, n_i is the number of time percentages, and α_i is the number of years of data at the ith site. The 3J metrics indicate both bias and spread. Table 5.4 contains the ITU-R WP 3J errors.

Table 5.3

GOODNESS OF FIT (GoF) METRIC (mm/hr) FOR MODEL 0.01% ANNUAL EXCEEDED RAIN RATES				
	TRMM		Rec837	
	Fit to DBSG3 rain rates			
	ALL SITES	WITHOUT OUTLIERS	ALL SITES	WITHOUT OUTLIERS
Method a)	16.57	13.20	15.35	15.64
Method b)	17.92	13.05	12.55	12.04
	Fit to S&A rain rates			
Method a)	15.84		27.04	
Method b)	15.51		26.70	

Table 5.4

		WP3J	
		TRMM	Rec837
		Fit to DBSG3 rain rates	
		ALL SITES	ALL SITES
Method a)	E	0.20	0.00
	RMS	0.42	0.28
Method b)	E	0.28	0.05
	RMS	0.54	0.26
		Fit to S&A rain rates	
Method a)	E	-0.11	-0.19

	RMS	0.23	0.28
Method b)	E	-0.11	-0.17
	RMS	0.24	0.28

The different goodness of fit metrics provide alternative views of prediction accuracy. The mean absolute deviation provides an intuitive indication of the expected accuracy when predicting a rain rate distribution from climate data. However, it does not take into account the number of years of data at each site. Ideally, the fit to site data would be scaled by the uncertainty in the estimate of the average annual rain rate. However, it is not known how this uncertainty decreases with estimates derived from increasing numbers of years or how the uncertainty varies with exceedance percentage. Rain rates have been shown to exhibit complex long-term correlations spanning decades. These unknowns make the choice of GoF metric an art-form rather than a scientific certainty. The WP3J metrics are based on relative errors, in an attempt to account for the greater variation in higher rain rates. Both the mean and RMS metrics are weighted by the number of years of data at each site. This is equivalent to assuming that all site measurements are independent and so probably puts too much weight on sites with many years of data. The few sites in Spain and Korea with 10 to 20 years of data each, contribute significantly to the WP3J metric.

Table 5.3 compares the GoF metric for DBSG3 data, with and without the Colombian Ayura Valley (outlier) sites. Rec837 performs almost as well on both datasets, indicating the fit to the Ayura sites is similar in quality to the fit to other sites. As Ayura valley data are not representative of the rest of the 1° grid square, this suggests that Rec837 has been over-fitted to DBSG3 data and would not perform as well on other nearby sites. In contrast, both TRMM methods perform much better over sites excluding the Ayura valley.

For Rec837, using Rec837 input data corresponds to Method a). Oddly, Method b) using primary data sources, performs better for the tropical DBSG3 sites. This may not be true if non-tropical

sites were included in the analysis. There is a possibility that Method b) climate data from 2004 to 2012 are more representative for the more recently acquired site data than the long-term average used in Method a), due to climate change. However, there is insufficient data to conclude this.

When comparing to DBSG3 tropical data, the use of downscaled TRMM conditional distributions performs only slightly worse than Rec837 distributions i.e. by an average of about 1 mm/hr over all sites. This difference is probably insignificant given the spread and uncertainty in the data. The agreement is surprising given that the conditional distributions were derived by averaging over all of the Tropics, and the downscaling transformation was based on temperate UK Nimrod data. When S&A comparison site data is used, the methods using TRMM conditional distributions perform significantly better than Rec837. This is further evidence that Rec837 has been over-fitted to DBSG3 data. This suggests that the verification of Rec837 against DBSG3 may have reduced its accuracy.

5.7.1 One-Degree 0.01% Exceedance Maps

To further compare TRMM and Rec837 annual 0.01% exceeded rain rates, this section contains one-degree maps produced from downscaled TRMM and Rec837 distributions derived from methods a) - based on Rec837 data and b) – based on GPCC& ERA Interim data, and optimised to fit DBSG3 and S&A data respectively. GPCC data is monthly land-surface precipitation and is only available over land. As the GPCC and ERA Interim input data in method b) have no values for some locations (see Figure 5.7and Figure 5.10), a hybrid dataset has been created filling the missing values with Rec837 input data (Figure 5.6 and Figure 5.9). Comparing plots of $R_{0.01\%}$, Rec837 and TRMM distributions optimised using both DBSG3 and S&A site data yield similar results, suggesting that the method based on conditional distributions is robust. The

distributions fitted to S&A data shows TRMM much improved compared to Rec837 data. This again suggests that Rec837 has been over-fitted to DBSG3 site data.

a)

b)
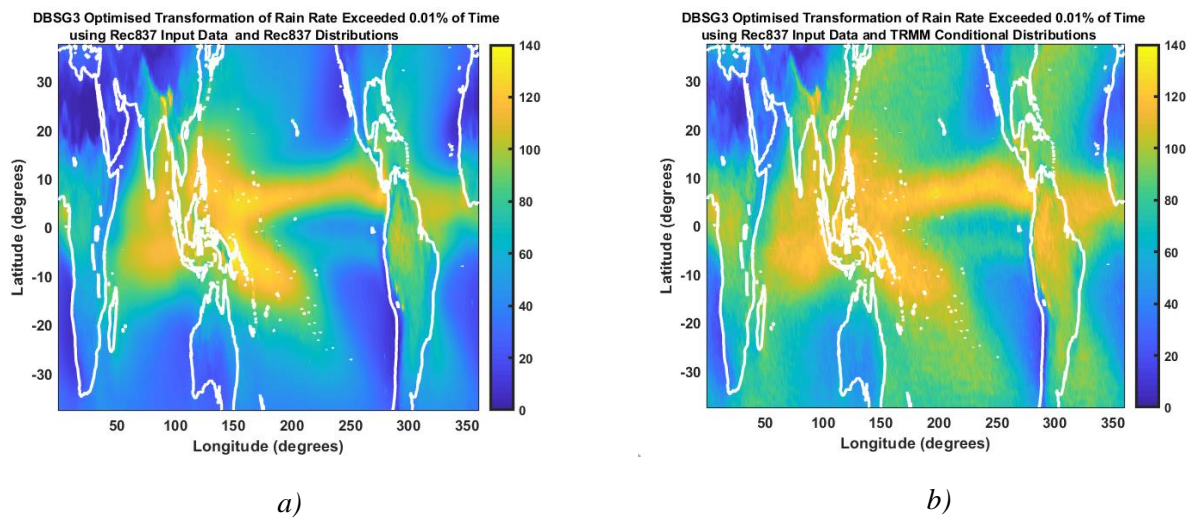
Figure 5.5. DBSG3 optimised Rec837 Input data using a) Rec837 distributions and b) TRMM conditional distributions

a)

b)
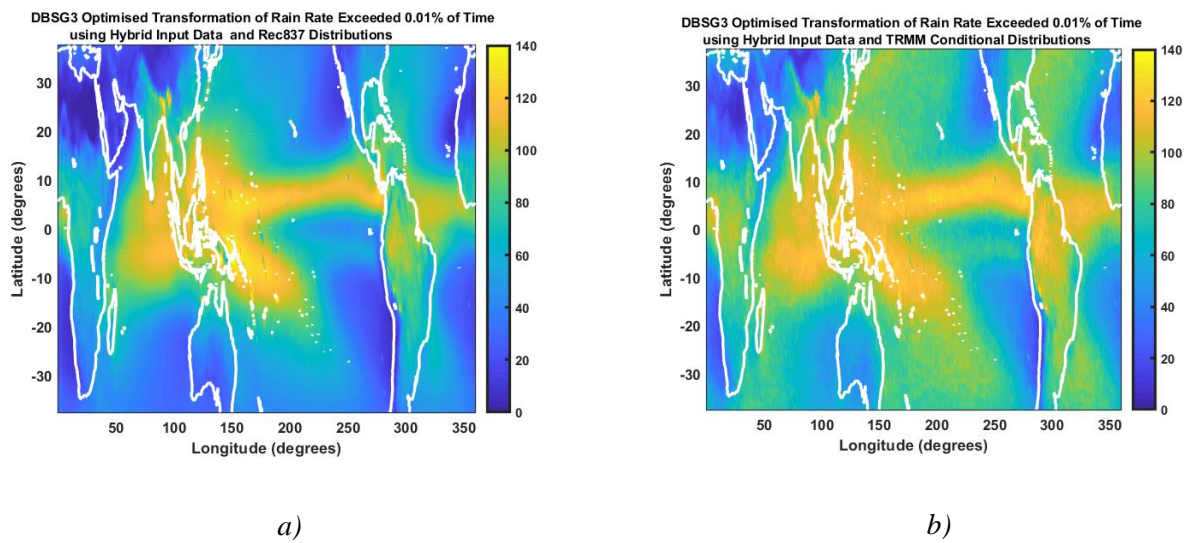
Figure 5.6. DBSG3 optimised hybrid Input data using a) Rec837 distributions and b) TRMM conditional distributions
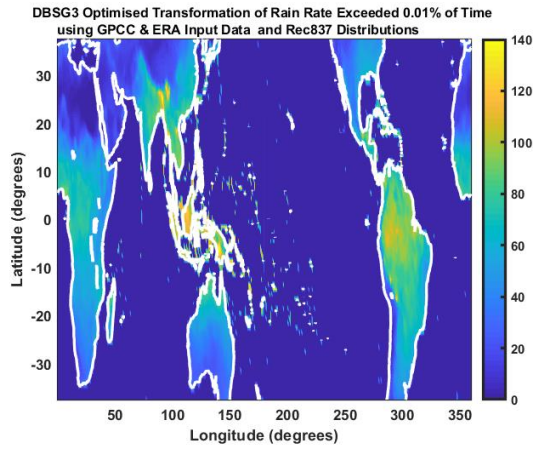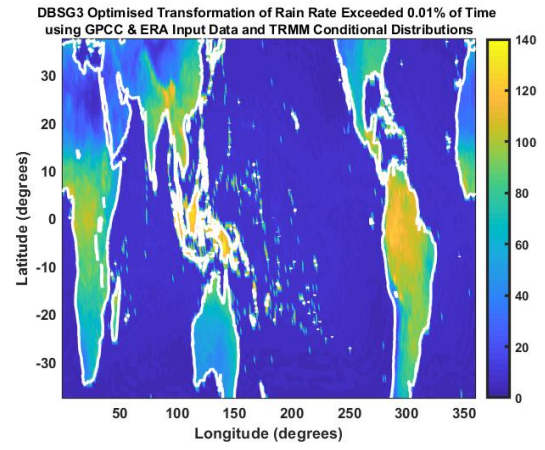
Figure 5.7. DBSG3 optimised GPCC and ERA Interim Input data using a) Rec837 distributions and b) TRMM conditional distributions
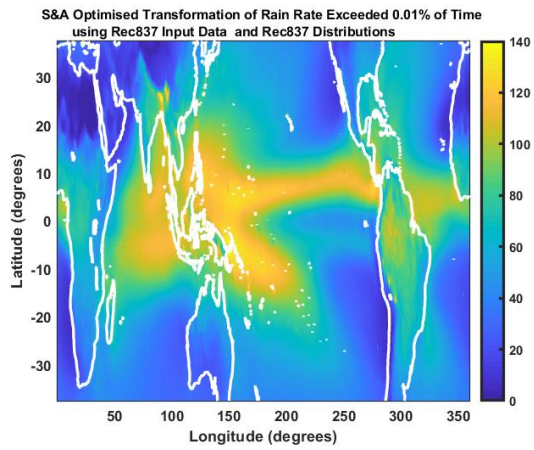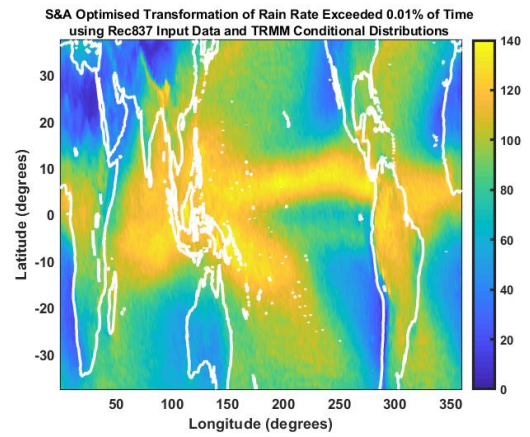
Figure 5.8. S&A optimised Rec837 Input data using a) Rec837 distributions and b) TRMM conditional distributions
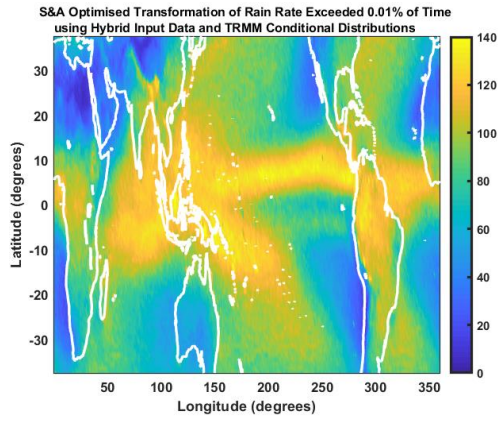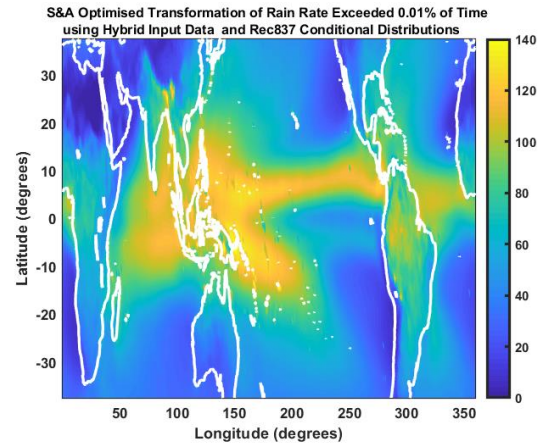
Figure 5.9. S&A optimised hybrid Input data using a) Rec837 distributions and b) TRMM conditional distributions
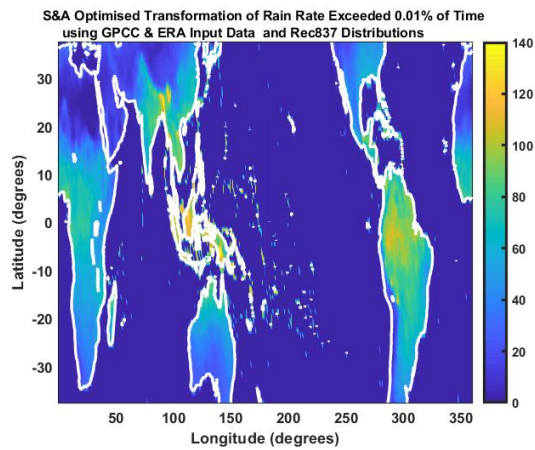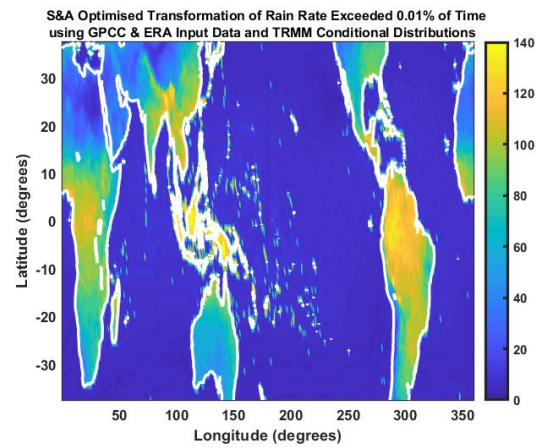
Figure 5.10. S&A optimised GPCC and ERA Interim Input data using a) Rec837 distributions and b) TRMM conditional distributions

5.8 Comparison of Global TRMM and Rec837 annual exceeded rain rates

To compare the performance of TRMM conditional distributions globally, they have been used to calculate exceedance distributions for all DBSG3 sites, tropical and temperate, as well as the S&A sites. Here, only Method a) is used for the comparison and annual exceeded rain rates at 0.1, 0.01 and 0.001% are considered. Figure 5.11 shows the rain rates exceeded for 0.1%, 0.01% and 0.001% of time (R1, R01 and R001 respectively) for 164 tropical and 91 temperate sites.

The goodness of fit metric presented in Table 5.5 shows how similar TRMM and Rec837 methods are in the Tropics, with TRMM performing slightly better than Rec837 for R1 and R01, and significantly better for R001, when the outliers are excluded. This is to be expected as Rec837 inputs have little from locations in the Tropics. In the temperate regions, Rec837 performs better than TRMM at all time-percentages. This is also to be expected as TRMM conditional distributions are from the Tropics. Table 5.6 contains the ITU-R WP 3J errors.

Comparing Conditional TRMM with Rec837 input data and Rec837 Annual Exceeded RainRates for all DBSG3 and S&A sites

Legend:
- ○ Tropical TRMM R1
- ▽ Temperate TRMM R1
- ✱ Rec837 R1
- ○ Tropical TRMM R01
- ▽ Temperate TRMM R01
- ✱ Rec837 R01
- ○ Tropical TRMM R001
- ▽ Temperate TRMM R001
- ✱ Rec837 R001
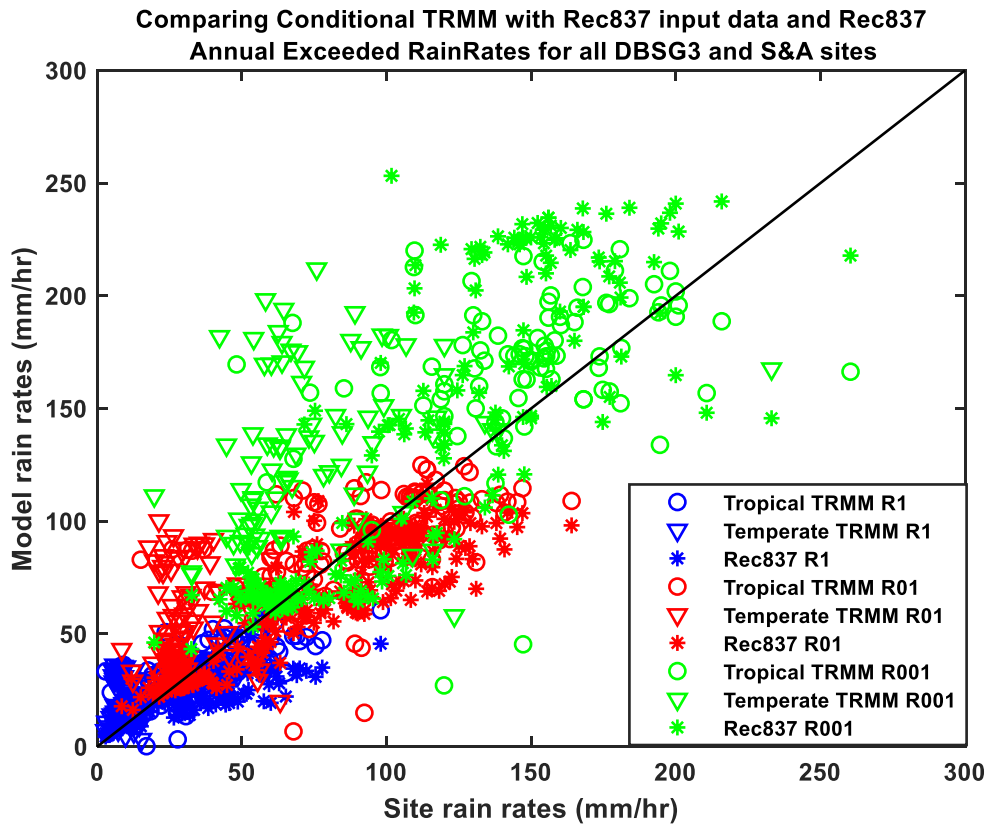
Figure 5.11. Comparisons between measured exceeded rain rates and model predictions for temperate and tropical sites.

Table 5.5

GOODNESS OF FIT (GoF) METRIC (mm/hr) FOR MODEL ANNUAL EXCEEDED RAIN RATES FOR ALL SITES						
	TROPICAL			TEMPERATE		
EXCEEDANCE	0.1	0.01	0.001	0.1	0.01	0.001
Rec837	12.33	19.38	46.11	2.33	6.88	14.76
TRMM	9.84	17.16	35.34	11.32	28.11	59.78

Table 5.6

		RELATIVE ERROR BY ITU-R WORKING PARTY 3J					
		TROPICAL			TEMPERATE		
	EXCEEDANCE	0.1	0.01	0.001	0.1	0.01	0.001
Rec837	E	-0.18	-0.14	0.19	0.15	0.01	0.04
	RMS	0.36	0.24	0.36	0.27	0.22	0.23
TRMM	E	0.60	0.25	0.34	1.65	1.14	1.01
	RMS	2.03	0.93	0.73	2.23	1.47	1.21

Figure 5.12 shows the same data as Figure 5.11 but only for $R_{0.01\%}$, the parameter of primary interest, as it is an input to models for microwave link fade distributions. It appears that Rec837

systematically underestimates at sites with higher exceeded rain rates. The TRMM method shows more scatter at lower rain rates.

In Table 5.7 the GoF metric shows that Rec837 performs better than TRMM on DBSG3 compared to S&A sites. Given that the fit to DBSG3 is the quality measure used by the ITU-R, this is to be expected. On the S&A sites, TRMM performs better than Rec837. This suggests that the verification of Rec837 against DBSG3 may have reduced its accuracy at other sites, inadvertently introducing a bias towards temperate areas at the expense of the Tropics.
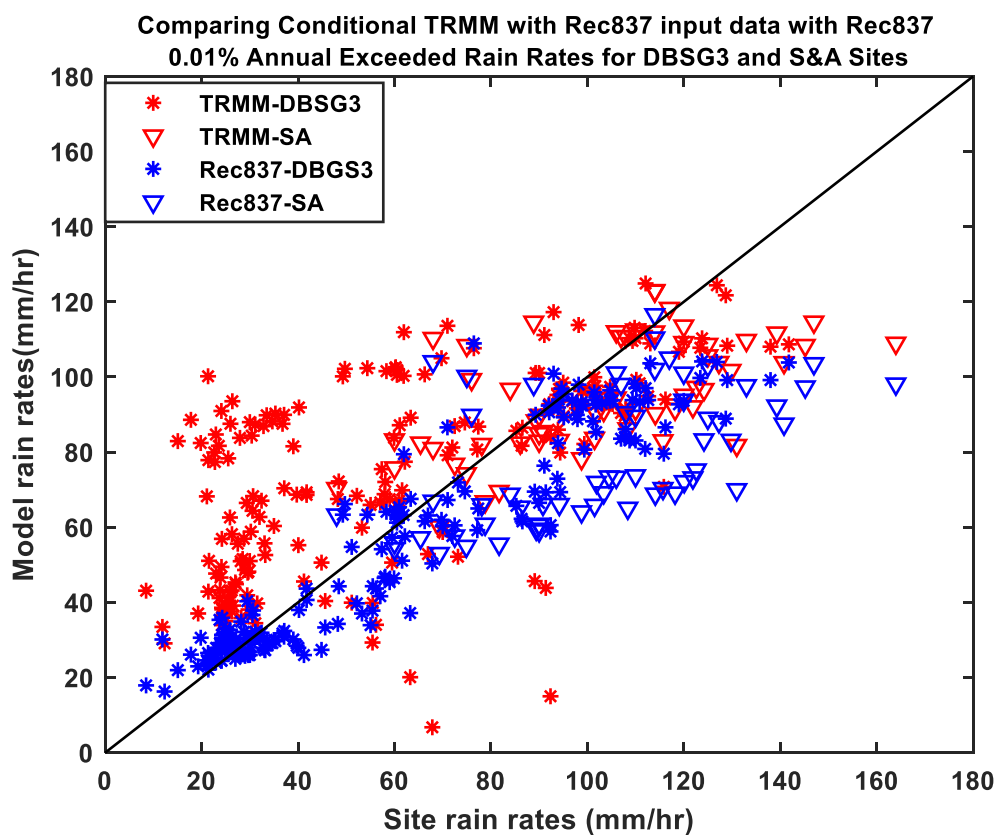
Figure 5.12. Comparison of TRMM and Rec. ITU-R P.837-7 $R_{0.01\%}$ for all sites

Table 5.7

GOODNESS OF FIT (GoF) METRIC (mm/hr) FOR MODEL ANNUAL EXCEEDED RAIN RATES FOR DBSG3 AND S&A SITES												
	S&A						DBSG3					
	Rec837			TRMM			Rec837			TRMM		
Exceedance	0.1	0.01	0.001	0.1	0.01	0.001	0.1	0.01	0.001	0.1	0.01	0.001

| | 22.23 | 28.14 | 41.12 | 11.79 | 17.32 | 35.33 | 5.00 | 9.97 | 31.10 | 10.66 | 23.72 | 50.41 |

Table 5.8

RELATIVE ERROR BY ITU-R WORKING PARTY 3J												
	S&A						DBSG3					
	Rec837			TRMM			Rec837			TRMM		
Exceedance	0.1	0.01	0.001	0.1	0.01	0.001	0.1	0.01	0.001	0.1	0.01	0.001
E	-0.45	-0.21	0.29	-0.18	-0.04	0.27	0.09	-0.02	0.09	1.44	0.91	0.83
RMS	0.47	0.29	0.39	0.26	0.21	0.34	0.27	0.20	0.28	2.29	1.37	1.10

5.9   Chapter Summary

This chapter has explored the application of conditional monthly rain rate distributions derived from TRMM data. The current Rec ITU-R P.837-7 uses these conditional distributions to estimate average annual distributions of point one-minute rain rates. TRMM conditional distributions have been used to replace the analytic distributions that are part of the current Rec. The subsequent predictions have been compared to databases of measured site data.

Rec837 relies on monthly accumulations derived from rain gauges, which are sparsely distributed in the Tropics. Furthermore, there is little validation data from the Tropics, and none from Africa. These factors could reduce the accuracy of the method in these countries that require the ITU-R model, as they often do not have historical rapid-response rain gauge data.

The DBSG3 data includes a group of sites in Ayura Valley Colombia that are unlikely to be representative of the region. Tests of goodness of fit to DBSG3 are considered with and without these outlier sites. Rec837 fits the DBSG3 data similarly well, with or without outliers, while the TRMM methods perform much better when these sites are excluded. This suggests that the Rec837 model may have been distorted by these data and so it may not represent the climate in the region outside the valley.

88

The Rec837 method works similarly well when the conditional distributions are replaced by distributions derived from TRMM. This suggests that the method based on conditional distributions is robust.

Estimation of $R_{0.01\%}$ from downscaled observed TRMM distributions, performs significantly better than Rec837 when compared to S&A data, and not as well when compared to DBSG3 data. This again suggests that the current Rec837 has been over-fitted to DBSG3 site data.

The algorithm that appears best depends upon the choice of GoF metric. Currently the uncertainty in estimate of average annual exceeded rain rates is not known, and so it is difficult to design a GoF metric that combines sites and exceedance percentages. The WP3J metrics may put too much weight on sites with many years of data and outliers.

Rain rate distribution data underpins the design and regulation of microwave networks. A method to estimate these distributions in the Tropics, based on rain rates measured from satellite, has been presented and validated. TRMM and future satellite missions should provide valuable data to improve the estimation of rain rate distributions globally. Particularly in the Tropics, these data could yield significantly improved estimations without the investment of resources and time in setting up networks of high resolution rain gauges. The methods and results developed in this chapter could benefit the economies of many equatorial countries.

Chapter 6   A Curve-Fit Approximation to Conditional Distributions of Measured TRMM Rain Rates

6.1   Introduction

In the previous chapter, TRMM distributions conditional upon accumulation and temperature were used to estimate point one-minute rain rates, and the performance of these were tested across tropical and temperate sites. Using TRMM conditional distributions, XCD_{TRMM}, yields a method that fits DBSG3 tropical sites data better than using XCD_{837}.   The TRMM conditional distributions yield a significantly better fit to the S&A site data than Rec837 distributions, suggesting that Rec837 method may have been distorted by the preponderance of temperate data in DBSG3.   The TRMM conditional distributions fit DBSG3 temperate data less well than Rec837.   This suggests that the conditional distributions may need another parameter, such as latitude, distinguishing tropical from temperate locations. In this chapter, the measured TRMM conditional distributions are replaced with analytic curves parameterised by monthly mean daily accumulation and temperature.

6.2   Curve Fit to TRMM Conditional Distributions

The use of TRMM conditional distributions provides a method that yields a better fit to tropical site data than Rec837.   However, it requires a database of discrete conditional exceedance distributions: $XCD_{TRMM}(R \mid T, MMDA)$, for a discrete list of rain rates and bins for T and $MMDA$.   Although perfectly feasible, this is not the preferred style for ITU-R Recommendations. Furthermore, it was noted in Rimven et al. (In press) that the use of TRMM conditional distributions yield a better fit to tropical site databases than using the TRMM location specific distributions directly.   This is probably because there were fewer $T - MMDA$ bins than latitude-

longitude bins, and so the conditional distributions are based on larger numbers of TRMM rain rate samples. This also suggest that some smoothing between $T - MMDA$ bin distributions may be of advantage.

To produce a model closer in format to standard ITU-R Recommendations, and to incorporate some inter-bin smoothing, parameterised analytic functions have been fitted to the discrete conditional TRMM distributions. A double exponential exceedance model was fitted to the distribution for each *T-MMDA* bin. The double exponential distribution was proposed by Salonen and Poiares-Baptista (Salonen & Poiares Baptista, 1997b) as a model rain rate exceedance distribution with global application. It was assumed in Rec. ITU-R P.837 from versions 2 to 6 inclusive. The distribution was written in a different format by Paulson (2017) where the parameters had physical interpretations and three of the four had units of rain rate:

$$XCD(R) = P_0 exp\left(-R\left(\left(\frac{R_0}{R+R_0}\right)\frac{1}{R_L} + \left(\frac{R}{R+R_0}\right)\frac{1}{R_H}\right)\right) \tag{6.1}$$

where P_0 is the probability of rain, often as a percentage. At low and high rain rates the distribution is approximately exponential of form $P_0 exp\left(-\frac{R}{R_L}\right)$ and $P_0 exp\left(-\frac{R}{R_H}\right)$ respectively. The transition between low and high rain rate is controlled by the R_0 parameter. Fitting Equation (6.1) to the TRMM conditional exceedance distribution for each $T - MMDA$ bin yields a set of four parameters: $\{P_0, R_L, R_0, R_H\}$ for each discrete $T - MMDA$ pair.

The second stage required experimentation with a range of closed-form expressions linking each of the four distribution parameters to the mean bin values of *T* and *MMDA*. After considerable effort, some expressions were found relating the climate parameters *T* and *MMDA* to SPB distribution parameters P_0, R_L. R_H and R_0 - the probability of rain, low, high and transition rain rates. 3D scatter plots were calculated for each SPB parameter versus *T* and *MMDA*, for all 1-degree latitude-longitude regions. Initially, the plots with the least scatter, or clear independence

from one input variable, were selected for curve fitting. Trial curve-fit expressions were selected by visual inspection and trial-and-error; and then fitted to the scatter plots to minimise the square error (MMSE). This was done for P_0 and R_L. The SPB parameters were fitted for a second time, but with the curve-fit P_0 and R_L parameters, yielding a new set of R_H and R_0. Curve-fit expressions for these parameters were then sought by MMSE fitting of likely expressions. Finally, all curve-fit expression coefficients were refined by MMSE curve-fitting of the parameterised SPB curves to rain distribution data. The expressions are as follows:

$$P_0 = 1.8 \times MMDA^{0.57} \tag{6.2a}$$

$$R_L = 1.46 + 0.819 \times MMDA \tag{6.2b}$$

$$R_H = 17.41 \tag{6.2c}$$

$$R_0 = max\big(4.39, k \times T + (7 - 300k)\big) \tag{6.2d}$$

where $k = \dfrac{1.225 \times MMDA - 23.85}{38}$

Although there is no physical model underpinning the relationships between distribution parameters and T and $MMDA$, some observations can be made. The probability of rain increases with accumulation but the sub-linear relationship implies that higher accumulation is associated with higher mean rain rates. Although there is no direct link to T in Equations (6.2a-c), the parameters T and $MMDA$ are positively correlated. The low and high rain rate exponential factors R_L and R_H, are close to independent from T and $MMDA$. In P.837 versions 2 to 6, the low rain rate exponent is fixed. The major complexity in the analytic curve-fit model is determining the transition rain rate R_0. The incidence of heavy rain rates is largely determined by this parameter.

Combining Equations (6.1) and (6.2) yields curve-fit conditional monthly exceedance distributions: $XCD_{curvefit}(R|T, MMDA)$. These can be used instead of XCD_{837} in Equation 5.1) to produce a prediction model. The quality of this prediction model can be measured by

comparing the predicted rain rates at specific exceedance probabilities with those measured at sites, specifically DBSG3 having sites globally but mainly temperate and S&A having only tropical sites. Figure 6.1 and Figure 6.2 are scatter plots of measured and predicted rain rates at exceedance percentages of 0.1%, 0.01% and 0.001%. Table 6.1 and

Table 6.3 present the goodness of fit measure based on the mean absolute difference between predicted and measured rain rates, while Table 6.2 and Table 6.4 give the error metric defined by the by ITU-R Working Party 3J.

Figure 6.1 presents a scatter plot of DBSG3 site exceeded rain rates at three time percentages: 0.1%, 0.01% and 0.001%, and the predicted rain rates using the standard Rec837 model with the Rec837 and TRMM curve-fit conditional distributions. The DBSG3 database contains many sites with average annual exceeded rain rates estimated from a small number of years, often one year. These estimates have large uncertainty and so scatter plots such as Figure 6.1 will always exhibit sizable scatter. However, it can be seen that the standard Rec837 model tends to under-estimate the higher rain rates at 0.01% and over-estimate at 0.001% time percentages. There are several possible reasons for this. One contributing factor is the lack of validation data in DBSG3 from the Tropics. This has the potential to bias the accepted models towards fitting temperate sites with lower rain rates. A second factor is the move from the SPB double exponential distribution model to lognormal. The more complex SPB model decays more slowly at high rain rates. The TRMM curve-fit method shows greater scatter at all time percentages, particularly for tropical sites. This is unexpected for a method devised using tropical data.

93
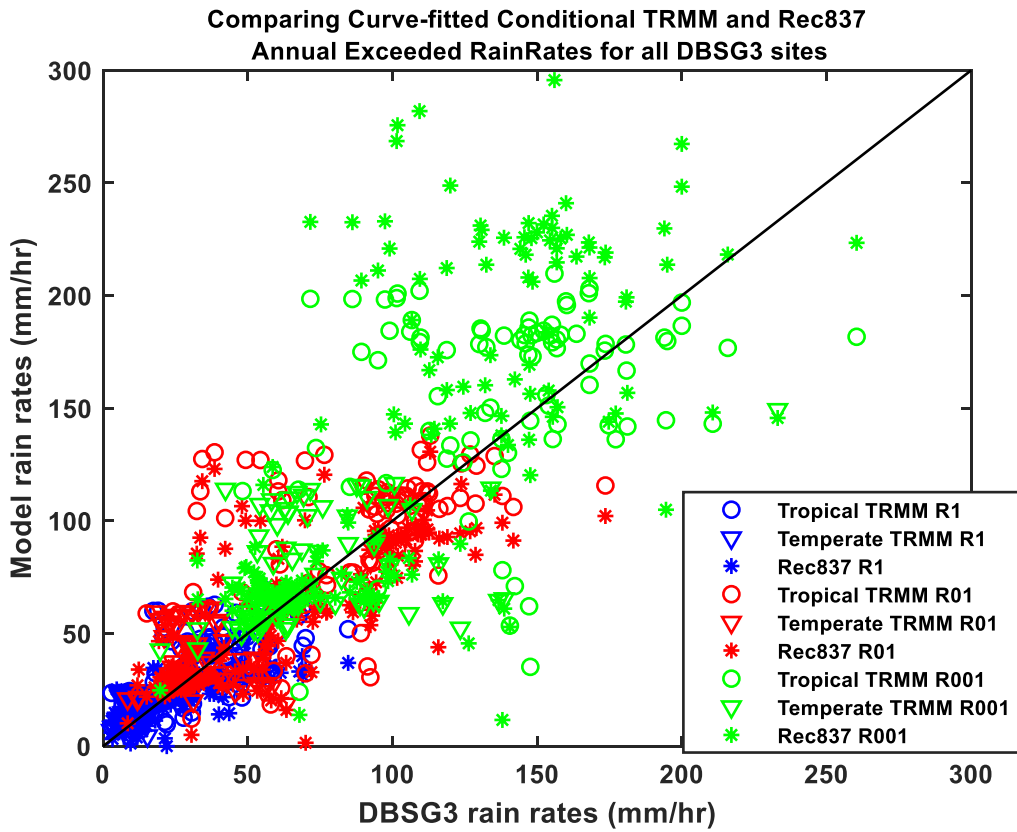
Figure 6.1. Scatter plot of DBSG3 site exceeded rain rates and predictions using the standard Rec837 conditional distributions and the curve-fit to TRMM distributions.

Table 6.1

GOODNESS OF FIT METRIC FOR MODEL ANNUAL EXCEEDED RAIN RATES FOR ALL DBSG3 SITES						
	TROPICAL			TEMPERATE		
EXCEEDANCE	0.1	0.01	0.001	0.1	0.01	0.001
Rec837	10.85	22.10	60.34	1.84	7.56	17.67
TRMM	11.06	22.96	40.95	7.07	14.05	21.54

Table 6.2

RELATIVE ERROR ITU-R WORKING PARTY 3J METRIC							
		TROPICAL			TEMPERATE		
EXCEEDANCE		0.1	0.01	0.001	0.1	0.01	0.001
	Rec837	-0.07	-0.06	0.19	0.19	0.03	0.06

94

		0.63	0.29	0.18	1.08	0.42	0.19
Mean error	TRMM						
	Rec837	0.44	0.47	0.58	0.48	0.32	0.31
RMS	TRMM	1.67	0.89	0.56	1.46	0.74	0.44

Figure 6.2 shows the same result for S&A sites. The exceeded rain rates for these sites have been calculated from at least 5-years of data, and so have much lower uncertainty than the majority of DBSG3 data. The Rec837 method systematically under-estimates at 0.1% and 0.01%, and over-estimates at 0.001%. The TRMM curve-fit method appears much more plausible at all three time percentages, but exhibits an over-estimation bias at 0.001%.
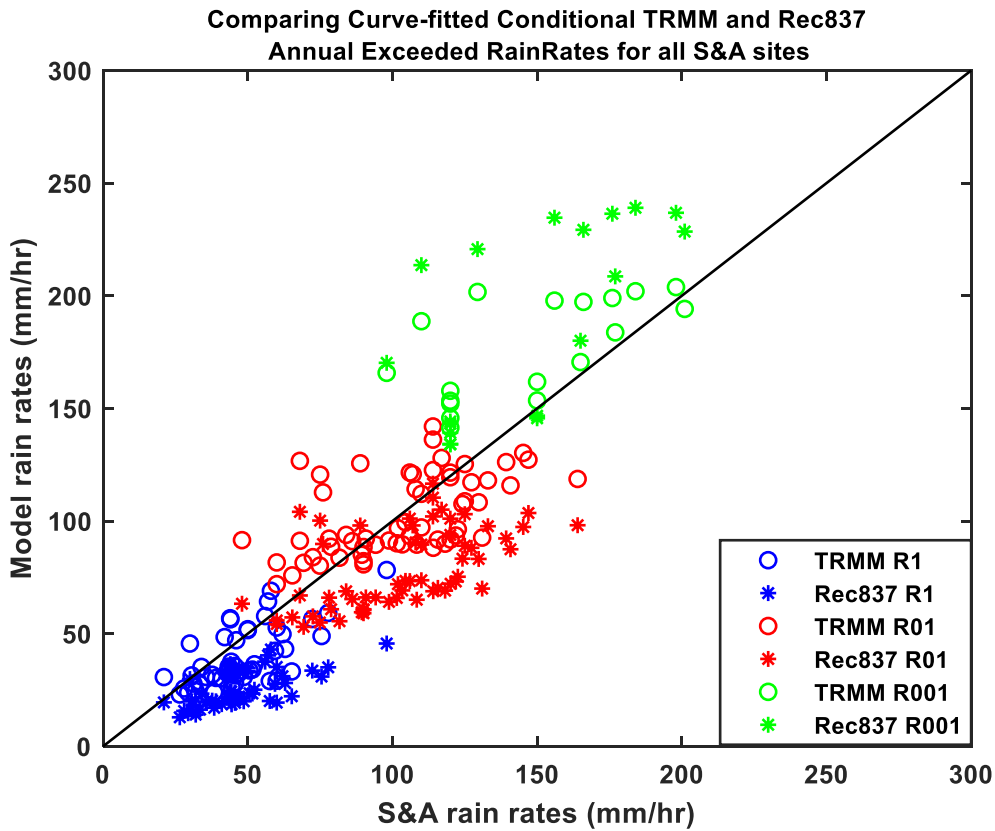
Figure 6.2. Scatter plot of S&A site exceeded rain rates and predictions using the standard Rec837 conditional distributions and the curve-fit to TRMM distributions.

Table 6.3

GOODNESS OF FIT (GoF) METRIC (mm/hr) FOR MODEL ANNUAL EXCEEDED RAIN RATES FOR ALL S&A SITES			
EXCEEDANCE	0.1	0.01	0.001
Rec837	22.23	28.15	41.12
TRMM	11.78	16.63	29.11

Table 6.4

RELATIVE ERROR USING ITU-R WORKING PARTY 3J METRIC				
EXCEEDANCE		0.1	0.01	0.001
Mean error	Rec837	-0.45	-0.21	0.29
	TRMM	-0.15	0.03	0.23
RMS	Rec837	0.47	0.29	0.39
	TRMM	0.28	0.25	0.31

The Goodness of Fit metrics presented in Table 6.1 shows that the TRMM method performs less well than Rec. ITU-R P837-7 in the temperate DBSG3 sites, and has a similar performance in the tropical sites at 0.1% and 0.01% of time. TRMM distributions are derived from tropical data while Rec. ITU-R P837-7 has been trained with little data from the Tropics. The WP3J metrics show the TRMM method appears to perform slightly better at 0.001% for both S&A and tropical DBSG3 sites. However, for S&A sites, the TRMM method performs better at all time percentages on tropical data.

6.3 Chapter Summary

In this chapter, conditional distributions of measured TRMM rain rates have been derived using a curve-fit approximation. This underpins the creation of an ITU-R style Recommendation based only on analytic functions and climate data.

The curve-fit TRMM method performs significantly better than Rec837 on S&A data but much worse on DBSG3 data. Once again, this suggests that fit to DBSG3 has driven the development of ITU-R models to a point where they may not fit other sites as well.

When comparing the curve-fit metric to the use of the observed conditional distributions, it can be seen that the curve-fit distributions have performed very similarly. For S&A data, the mean absolute error at 0.1%, 0.01% and 0.001% has increased by 0.01 mm/hr, 0.05 mm/hr and 5 mm/hr respectively. It was hoped that some smoothing introduced by curve-fitting would increase accuracy, but this has not been the case. The SPB distributions are very sensitive to the R_0 parameter, and the link between R_0 and the input parameters T and $MMDA$ is complex. There are likely to be better curve-fitting expressions 6.2a-d. Possibly the use of lognormal conditional distributions would yield better-fit or simpler curve-fit expressions. Maybe further conditional parameters are required.

This chapter has developed an ITU-R style model that performs better than Rec837 on S&A sites but worse on DBSG3 sites. The next chapter addresses this by building on the strengths of both models.

Chapter 7   A Hybrid Method for Tropical and Temperate Regions

7.1   Introduction

In chapter 5, the mean absolute variation goodness of fit metrics have shown the TRMM conditional distributions performing better than Rec837, at all time-percentages. Using the WP3J metrics, the TRMM method performs slightly better at 0.001% for both S&A and tropical DBSG3 sites. Furthermore, a closer examination of DBSG3 and S&A site data shows that for sites where Rec837 under-estimates, the TRMM method tends to over-estimate. This suggests that a combination of the two methods may perform better than either. In this chapter a hybrid method is developed that uses the TRMM curve-fit prediction for tropical regions and smoothly transitions to Rec837 values at temperate latitudes.

7.2   A Hybrid Method

Let $X_{837}(R)$ be the average annual exceedance distribution calculated using the standard Rec837 (Equation (5.1)), while $X_{TRMM}(R)$ is the same, but calculated using the TRMM curve-fit conditional distributions (6.2a-d). The hybrid method forms a weighted sum of the two distributions:

$$X_{TRMM}(R) = (1 - W) \times X_{TRMM}(R) + W \times X_{837}(R) \tag{7.1a}$$

where
$$W(lat) = S\left(\frac{|lat| - 25}{6}\right) \tag{7.1b}$$

and
$$S(x) = \frac{1}{1 + e^{-x}} \tag{7.1c}$$

$S(x)$ is the classic Sigmoid function that smoothly varies from 0 to 1 as the input varies from $-\infty$ to $+\infty$, passing through $\frac{1}{2}$ when $x = 0$. The weight function $W(lat)$ varies from close to zero at the equator where latitude is zero, to close to one at the poles.

Figure 7.1 shows the scatter plot of all DBSG3 and S&A exceeded rain rates versus the hybrid prediction. The GoF and ITU-R WP3J metrics are presented in Table 7.1 and Table 7.2. The hybrid method performs better than Rec837 or the TRMM methods for 0.001% of time on all databases. At 0.01% of time, the hybrid method performs significantly better than Rec837 and similar to TRMM on the S&A database while on the DBSG3 database, it performs significantly better than TRMM but much worse than Rec837. At 0.1% again the hybrid method performs slightly better than Rec837 but much worse than TRMM on the S&A database, and significantly better than TRMM but much worse than Rec837 on DBSG3.
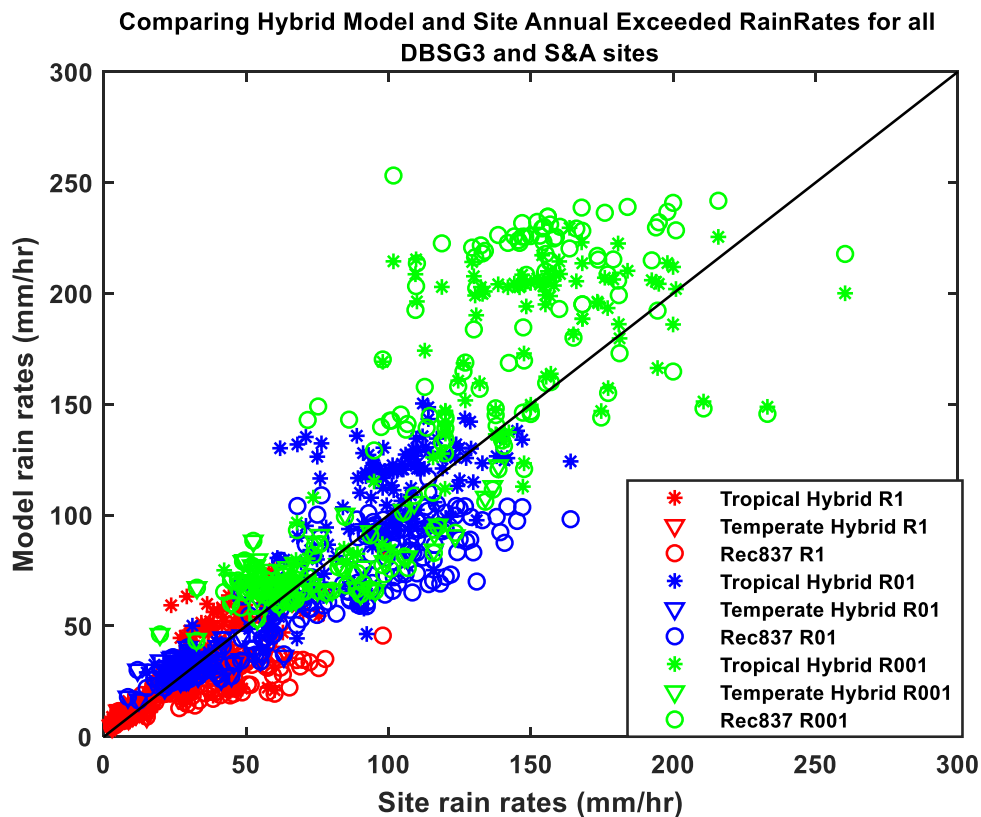
Figure 7.1. Scatter plot of DBSG3 and S&A site exceeded rain rates and predictions using the hybrid and Rec837 models.

Table 7.1

GOODNESS OF FIT METRIC FOR MODEL ANNUAL EXCEEDED RAIN RATES FOR ALL SITES (mm/hr)									
	Rec837			TRMM			Hybrid		
Database	0.1	0.01	0.001	0.1	0.01	0.001	0.1	0.01	0.001
DBSG3	6.54	15.01	39.69	13.07	27.85	48.16	8.01	18.69	36.43
S&A	22.14	27.82	41.12	10.20	16.34	38.30	12.09	16.01	30.59
Combined	8.53	14.09	32.00	12.61	23.93	44.30	7.95	15.08	31.16

Table 7.2

RELATIVE ERROR USING ITU-R WORKING PARTY 3J METRIC										
		Rec837			TRMM			Hybrid		
Database	Metric/Time Percentage	0.1	0.01	0.001	0.1	0.01	0.001	0.1	0.01	0.001
DBSG3	E	0.11	0.00	0.10	1.42	0.79	0.55	0.31	0.12	0.14
	RMS	0.52	0.37	0.41	2.12	1.23	0.80	0.67	0.47	0.41
S&A	E	-0.45	-0.21	0.29	-0.66	0.11	0.30	-0.12	0.04	0.23
	RMS	0.47	0.29	0.39	0.25	0.27	0.37	0.30	0.24	0.33
Combined	E	-0.18	-0.10	0.29	0.49	0.33	0.38	0.21	0.15	0.28
	RMS	0.33	0.24	0.42	1.01	0.63	0.58	0.50	0.37	0.46

7.3   Discussion

The current Rec837 under-estimates the higher exceeded rain rates at time percentages down to 0.01%. When validating, this under-estimation may have been masked by the preponderance of temperate sites in the DBSG3 database. In the previous chapter, an ITU-R Recommendation style method has been developed and presented, based on curve-fitting to measured TRMM

100

conditional exceedance distributions. This method performs significantly better than Rec837 against databases of tropical sites, but performs worse when using DBSG3. A weighted average of the two methods, where the weights depend upon latitude, is shown to perform significantly better than Rec837 on both site databases, particularly for time percentages below 0.01%.

The hybrid method transitions between using the TRMM derived SPB conditional distributions in the Tropics to standard Rec837 lognormal distributions in temperate latitudes. This has demonstrated the advantage of using conditional distributions that vary with latitude. Two locations with different latitudes but the same monthly accumulation and temperature, may be expected to have different conditional distributions due to the different mix of rain types. The stronger solar forcing near the equator is expected to lead to greater proportion of convective rain while the monthly temperature may be similar to places further from the equator due to the differences in maritime and continental climates or differences in altitude. Some of these variations will occur over finer scales than those available in the MT and T input data. Other climate features will be directly linked to latitude such as atmospheric circulations e.g. the roaring 40's, or ocean currents such as the Gulf Stream. Given enough data, conditional distributions could be linked to more parameters, such as altitude, topography (mountains or plains) and the proportion of the area covered with water. Currently, there is insufficient data to resolve the effects of these other parameters, or even to order their importance. However, latitude effects can be observed and this parameter can be used as a surrogate for others that are correlated.

The hybrid method has demonstrated that there is some advantage in using conditional distributions that vary with latitude. However, a more elegant solution would be to implement this directly using conditional exceedance distributions with a direct latitude dependence: $X_{837}(R|MT, T, lat)$. However, the derivation of such distributions was outside the resources of this thesis.

7.4   Chapter Summary

The hybrid method demonstrates that the distributions in Equation (5.1) require more conditional parameters. Including latitude is likely to yield a unified improved method that fits temperate and tropical site data equally well. The use of SPB distributions, rather than the lognormal currently used in Rec837, gives more flexibility to fit across all time percentages. In the future, satellite derived conditional rain rate distributions will be available over larger portions of the Earth. With more data at a resolution of kilometres, the conditional SPB distributions will be observable with higher confidence.

Chapter 8   Conclusions and Recommendations for Future Work

In section 1.4 the aims and objectives of this thesis were stated:

1. Review the ITU-R rain and rain fade models;

2. Evaluate current ITU-R method for estimating the average annual exceedance distribution of point one-minute rain rates R: $X(R| x)$, where x is position.

3. Evaluate the contribution that TRMM data can make to the estimation of $X(R)$ in the Tropics;

4. Develop a method for estimating $X(R)$ in the Tropics from TRMM data and evaluate against ground truth data;

5. Extend the method to sites in temperate regions and evaluate its performance

6. Create a new global Recommendation for the estimation of average annual exceedance distribution of point one-minute rain rates.

A major driver for the thesis was the need for accurate rain statistics in equatorial countries, as these are required for the design and optimisation of microwave telecommunications networks. These, in turn, are linked in a virtuous cycle with economic development. Concerns have been raised on the lack of rain data in the Tropics for testing models and as input data to prognostic methods. A possible solution was the use of satellite Earth observation data, such as that produced by TRMM.

This thesis has analysed TRMM rain data over a 9-year period where the orbit was stable. Objectives 2 to 6 have been addressed by this work and the conclusion drawn are presented in the sections below.

8.2   Main Conclusions

8.2.1 Estimation of point one-minute rain rates using measured distributions of TRMM in the Tropics

TRMM data have been used to calculate exceedance distributions of 5 km rain rates on maps of 1° squares across the Tropics. Previous work had shown that instantaneous rain rates averaged over 1 km squares provide an unbiased estimate of point one-minute rain rates exceeded 0.01% of the time. Nimrod data from the UK was used to calculate a quadratic downscaling transformation from distributions of 5 km to 1 km rain rates, and these were used as a proxy to point one-minute rain rates. The resulting method produced site exceeded rain rates that performed as well as Rec837 on DBSG3 sites and significantly better on S&A sites. This suggests that Rec837 may be over-fitted to the DBSG3 site data. The quadratic downscaling transformation was fitted to DBSG3 and S&A site data and yielded very similar transformations as that derived from Nimrod. This suggests that the quadratic downscaling transformation could be used in the Tropics and temperate zones. A major conclusion is that satellite data can be used directly to estimate local point one-minute rain rate distributions. This is likely to become the standard method in the future as more satellite data become available.

8.2.2   Estimation of point one-minute rain rates using conditional distributions of measured TRMM rain rates

The conditional distributions used in the current ITU-R P.837-7 have been replaced by distributions calculated from TRMM data. The purpose was to extend the use of tropical TRMM data to temperate zones. A further hope was that the extra smoothing produced by aggregating TRMM data into *T-MT* bins would result in more reliable distributions. The Rec837 method works similarly well when using Rec837 conditional distributions and those derived from TRMM. Rec837 using TRMM distributions performs better in the Tropics than in temperate

areas. This is largely to be expected as TRMM distributions are calculated using only tropical data, although the downscaling transformation is derived from temperate data.

8.2.3 A curve-fit approximation to conditional distributions of measured TRMM rain rates

Conditional distributions of measured TRMM rain rates have been derived using a curve-fit approximation. The performance of this method is slightly worse than when using the measured TRMM conditional distributions. However, the analytic functions in the curve-fit approximation are far more in the style of an ITU-R Recommendation.

8.2.4 A hybrid method for tropical and temperate regions

The Rec837 method performs better in the Tropics when using TRMM conditional distributions, but better in temperate zones using Rec837 distributions. The hybrid method moves smoothly from TRMM distributions near the equator to Rec837 distributions outside the Tropics. This method performs better than Rec837 globally. This suggests that the Rec837 conditional distributions need another conditional parameter, such as latitude.

8.3 Future work

This thesis has shown that satellite data can be used to estimate distributions of point one-minute rain rates. Much of the TRMM satellite data is now 20 years old and many new Earth observation satellites have been launched. Similarly, there has been considerable advances made on the algorithms used to estimate surface rain rates from space. A project that could be started immediately is a review of existing satellite measured rain rates and an extension of this project making use of the best and most recent data.

There is much to commend in the Rec837 method of estimating average annual rain rate distributions by averaging monthly conditional distributions. This method has been shown to be robust to changes in the conditional distributions. However, this thesis has shown that a set of conditional distributions calculated from Tropical data does not perform well in temperate zones. This strongly suggests that the distributions need to be conditional upon other parameters, probably latitude. The new satellite data identified in the first item of future work may provide the evidence to deduce the more complex conditional distributions.

Over the period spanned by this thesis, climate change has become increasingly evident. With 30 years of satellite-derived rain rates averaged over regions as small as 5 km across, there should be sufficient evidence to produce not just rain rate distributions, but trends in rain rate distributions. These trends are vital when designing radio systems with a life span of several decades or more.

APPENDIX A

SITES	LAT	LON	Measured Site Data			Rec. ITU-R P.837-7			Curve-fitted TRMM			Hybrid TRMM		
			R001	R01	R1	R001	R01	R1	R001	R01	R1	R001	R01	R1
GARDEMOEN SOR	60.2	11.1	61.6	27.0	6.3	59.6	25.0	8.5	58.1	29.9	13.4	58.1	29.9	13.4
HAMAR II	60.8	11.1	53.9	21.4	4.8	53.1	22.1	7.4	52.3	27.2	12.4	52.3	27.2	12.4
AS - RUSTADSKOGEN	59.7	10.8	67.4	29.7	8.5	61.8	26.0	8.9	60.1	30.9	13.8	60.1	30.9	13.8
OSLO - VESTLI	60.0	10.9	66.0	29.0	7.2	61.4	25.8	8.8	59.9	30.7	13.7	59.9	30.7	13.7
OSLO - BLINDEM PLU	59.9	10.7	65.2	28.1	9.2	61.8	26.1	9.0	60.8	31.1	13.9	60.8	31.1	13.9
GJETTUM	59.9	10.5	65.6	28.5	8.0	61.9	26.2	9.0	61.2	31.3	13.9	61.2	31.3	13.9
OVEROLL	59.9	10.6	61.0	27.5	7.1	61.9	26.1	9.0	61.1	31.2	13.9	61.1	31.2	13.9
KRISTIANSAND - SOMSKLEIVA	58.2	8.1	73.2	35.0	13.5	68.5	30.0	11.1	73.1	37.8	16.7	73.1	37.8	16.7
TIME - LYE	58.7	5.7	65.4	32.0	11.1	69.1	30.9	11.7	79.5	41.2	18.1	79.5	41.2	18.1
SANDNES - ROVIK	58.9	5.8	58.8	30.2	10.4	67.7	30.2	11.5	77.7	40.3	17.7	77.7	40.3	17.7
KRISTIANSUND - KARIHOLA	63.1	7.7	44.7	24.2	9.2	60.1	26.9	10.2	69.2	36.3	16.3	69.2	36.3	16.3
CHILBOLTON	51.1	358.6	49.7	23.0	6.8	51.3	23.1	8.8	57.0	31.2	14.6	57.0	31.2	14.6
BOLTON	53.6	357.6	63.5	29.7	9.4	46.6	20.7	7.8	51.6	28.6	13.6	51.6	28.6	13.6
CAVAN-BALLYHAISE	54.1	352.7	63.2	26.2	11.3	45.5	20.0	7.4	50.1	27.7	13.2	50.1	27.7	13.2
CAVON-OAK PARK	52.9	353.1	53.8	23.9	10.5	54.7	24.6	9.4	64.7	34.0	15.4	64.7	34.0	15.4
CORK-MOORE PARK	52.2	351.7	56.4	25.6	11.3	49.1	21.8	8.2	54.0	29.6	13.9	54.0	29.6	13.9
CORK-ROCHES POINT	51.8	351.8	53.5	25.5	11.8	49.8	22.2	8.3	54.7	29.9	14.1	54.7	29.9	14.1
CORK-SHERKIN ISLAND	51.5	350.6	48.9	23.7	11.5	50.2	22.3	8.4	55.0	30.0	14.1	55.0	30.0	14.1
DONEGAL-FINNER	54.5	351.8	53.4	25.0	11.5	44.5	19.5	7.2	49.0	27.2	12.9	49.0	27.2	12.9
DONEGAL-MALIN HEAD	55.4	352.7	47.9	24.2	11.7	43.3	18.9	6.9	47.8	26.6	12.7	47.8	26.6	12.7
DUBLIN-PHOENIX PARK	53.4	353.7	55.3	23.8	9.7	51.3	23.0	8.7	58.4	31.3	14.5	58.4	31.3	14.5
GALWAY-ATHENRY	53.3	351.2	64.1	31.5	12.4	46.9	20.8	7.7	51.6	28.4	13.4	51.6	28.4	13.4
GALWAY-MACE HEAD	53.3	350.1	49.5	24.3	11.8	46.6	20.5	7.6	51.1	28.2	13.3	51.1	28.2	13.3
KERRY-VALENTIA OBSERVATORY	51.9	349.8	52.5	29.5	13.4	49.3	21.9	8.1	53.9	29.5	13.8	53.9	29.5	13.8
MAYO-CLAREMORRIS	53.7	351.0	44.7	24.2	11.2	46.0	20.3	7.5	50.6	27.9	13.2	50.6	27.9	13.2
MAYO-NEWPORT	53.9	350.4	52.1	28.2	12.9	45.3	19.9	7.3	49.8	27.6	13.1	49.8	27.6	13.1

MEATH-DUNSANY	53.5	353.3	60.1	25.9	11.0	49.3	22.0	8.2	55.1	29.9	14.0	55.1	29.9	14.0
ROSCOMMON-MT DILLON	53.7	352.0	54.5	26.5	11.2	46.0	20.3	7.5	50.6	28.0	13.3	50.6	28.0	13.3
SLIGO-MARKREE	54.2	351.5	47.1	24.4	11.8	45.0	19.8	7.3	49.6	27.5	13.0	49.6	27.5	13.0
TIPPERARY-GURTEEN	53.1	352.0	51.4	25.1	10.3	47.4	21.0	7.8	52.1	28.7	13.6	52.1	28.7	13.6
WESTMEATH-MULLINGER	53.5	352.6	55.6	26.2	11.3	49.1	21.8	8.2	54.7	29.8	13.9	54.7	29.8	13.9
WEXFORD-JOHNSTOWN II	52.3	353.5	53.1	27.1	11.4	51.5	23.0	8.6	57.4	30.9	14.3	57.4	30.9	14.3
LUXEMBOURG	49.6	6.2	93.4	40.1	10.2	66.7	27.9	9.5	62.4	32.1	14.3	62.4	32.1	14.3
GOMETZ-LA-VILLE	48.7	2.1	88.8	44.9	15.1	66.5	27.4	9.0	60.9	30.9	13.6	60.9	30.9	13.6
LANNEMEZAN	43.1	0.4	82.4	37.1	13.8	76.5	32.4	11.3	71.8	36.4	15.8	71.8	36.4	15.8
TOULOUSE	43.6	1.5	63.4	26.3	6.2	72.6	29.7	9.7	66.5	33.0	14.2	66.5	33.0	14.2
ALICANTE	38.3	359.5	91.2	30.0	6.1	105.8	46.5	17.2	106.8	55.5	22.5	106.8	55.5	22.5
ALMERIA	36.9	357.6	48.2	15.1	2.9	111.8	48.7	17.7	110.0	57.0	22.7	110.0	57.0	22.7
AVILA	40.7	355.3	63.9	22.8	6.1	93.9	41.9	15.9	100.1	52.3	21.9	100.1	52.3	21.9
AVILES	43.6	354.0	53.3	25.9	9.5	75.3	33.9	13.0	82.7	43.4	19.1	82.7	43.4	19.1
BADAJOZ	38.9	353.0	67.0	27.9	8.3	104.5	46.3	17.3	108.8	57.0	23.3	108.8	57.0	23.3
CACERES	39.5	353.7	64.5	26.4	7.8	101.0	44.9	16.9	106.2	55.6	22.9	106.2	55.6	22.9
CADIZ	36.5	353.7	97.9	36.8	9.1	115.8	50.5	18.3	113.6	59.2	23.4	113.6	59.2	23.4
CASTELLON	40.0	359.9	106.8	39.0	9.1	97.3	43.1	16.2	101.3	52.7	21.8	101.3	52.7	21.8
CIUDAD REAL	39.0	356.1	58.2	21.3	6.0	102.3	45.2	16.9	105.6	55.0	22.5	105.6	55.0	22.5
CORDOBA	37.9	355.2	71.6	30.4	9.1	108.9	47.9	17.7	110.3	57.6	23.2	110.3	57.6	23.2
CUENCA	40.1	357.9	62.6	23.6	7.0	96.8	43.0	16.2	101.6	52.9	22.0	101.6	52.9	22.0
GIJON	43.5	354.4	68.7	32.4	11.2	75.9	34.2	13.1	83.5	43.8	19.2	83.5	43.8	19.2
GRANADA	37.2	356.2	42.3	17.8	5.5	111.1	48.6	17.8	110.7	57.5	23.0	110.7	57.5	23.0
GUADALAJARA	40.6	356.8	63.9	22.9	6.3	94.0	41.9	15.8	99.7	52.0	21.7	99.7	52.0	21.7
HUELVA	37.3	353.1	100.7	37.1	8.8	112.9	49.5	18.2	113.2	59.2	23.6	113.2	59.2	23.6
LA CORUNA	43.3	351.6	74.2	30.7	10.5	75.7	34.0	13.0	82.9	43.5	19.1	82.9	43.5	19.1
LEON	42.6	354.4	53.8	21.1	6.6	82.0	36.8	14.1	89.5	46.8	20.2	89.5	46.8	20.2
LERIDA	41.6	0.6	60.5	21.5	5.2	65.8	25.8	7.7	63.6	30.6	12.8	63.6	30.6	12.8
MADRID	40.4	356.3	57.8	22.6	6.3	95.2	42.4	16.0	100.6	52.5	21.9	100.6	52.5	21.9
MALAGA	36.7	355.5	85.3	32.8	8.4	113.7	49.5	18.0	111.9	58.1	23.1	111.9	58.1	23.1
MELILLA	35.3	357.1	67.5	26.0	6.7	117.0	50.3	17.9	111.3	57.1	22.2	111.3	57.1	22.2

MOLINA DE ARAGON	40.9	358.1	70.7	25.5	7.0	92.6	41.3	15.6	98.4	51.3	21.5	98.4	51.3	21.5
MORON DE LA FRONTERA	37.2	354.4	87.6	35.3	9.8	112.7	49.3	18.1	112.4	58.6	23.4	112.4	58.6	23.4
MURCIA	38.0	358.8	69.3	24.1	5.5	107.1	47.0	17.3	107.7	56.0	22.6	107.7	56.0	22.6
OVIEDO	43.4	354.1	63.2	29.4	9.8	76.7	34.5	13.2	84.3	44.2	19.3	84.3	44.2	19.3
SAN SEBASTIAN	43.3	358.0	84.7	41.8	15.0	78.7	35.4	13.6	86.2	45.2	19.7	86.2	45.2	19.7
SANTIAGO DE COMPOSTELA	42.9	351.6	93.6	41.8	15.2	78.5	35.2	13.5	85.9	44.9	19.6	85.9	44.9	19.6
SEVILLA	37.4	354.1	89.1	33.5	8.2	111.5	48.9	18.0	112.1	58.5	23.4	112.1	58.5	23.4
TENERIFE NORTE	28.5	343.7	73.6	31.1	8.6	147.9	60.0	18.8	133.1	68.9	23.4	133.1	68.9	23.4
TOLEDO	39.9	355.1	54.1	19.8	5.6	98.2	43.7	16.4	103.4	54.0	22.4	103.4	54.0	22.4
VALENCIA	39.5	359.6	98.5	34.7	7.5	99.8	44.2	16.5	103.0	53.6	22.1	103.0	53.6	22.1
ZARAGOZA	41.6	359.1	60.2	21.4	5.8	87.9	39.3	15.0	94.5	49.3	20.9	94.5	49.3	20.9
AVEIRO	40.6	351.3	75.9	40.2	12.6	94.7	42.3	16.1	102.3	53.6	22.4	102.3	53.6	22.4
CHEB	50.1	12.4	75.1	33.1	9.3	65.8	27.3	9.1	61.9	31.1	13.7	61.9	31.1	13.7
FRANTISKOVY LAZNE	50.1	12.4	95.3	33.2	8.1	65.7	27.3	9.1	61.8	31.1	13.7	61.8	31.1	13.7
PRAHA - KLEMENTINUM	50.1	14.4	90.2	41.2	8.7	64.3	26.0	8.2	59.8	29.5	12.7	59.8	29.5	12.7
PRAHA - TESTCOM	50.0	14.5	78.2	29.5	6.1	64.9	26.3	8.3	60.4	29.8	12.8	60.4	29.8	12.8
MSENO	50.4	14.6	80.2	30.0	8.6	65.9	26.9	8.6	61.2	30.3	13.2	61.2	30.3	13.2
SPINO DADDA	45.4	9.5	99.1	48.2	10.2	83.1	34.3	11.4	77.7	37.7	15.6	77.7	37.7	15.6
ROME	41.9	12.5	116.0	55.0	13.8	83.0	33.9	11.2	80.4	38.8	15.8	80.4	38.8	15.8
SEOUL	37.6	127.0	233.1	92.4	22.6	145.7	60.6	20.0	145.4	77.7	25.4	145.4	77.7	25.4
DAEJON	36.4	127.4	174.8	77.2	20.9	144.0	59.2	19.2	140.0	73.3	23.8	140.0	73.3	23.8
TAEGU	35.9	128.6	139.9	57.4	15.7	133.7	54.1	17.0	128.9	64.7	20.9	128.9	64.7	20.9
PUSAN	35.1	129.0	210.7	86.5	22.4	148.1	61.6	20.4	141.3	75.0	25.5	141.3	75.0	25.5
SI RACHA	13.1	100.8	180.9	99.4	28.3	199.2	80.7	24.8	169.3	98.9	36.8	169.3	98.9	36.8
BANGKOK	13.7	100.5	173.4	98.0	30.2	217.0	88.8	27.9	177.7	106.5	41.7	177.7	106.5	41.7
KUALA LUMPUR	3.2	101.7	194.0	138.0	70.0	229.8	99.2	34.7	180.8	110.2	46.3	180.8	110.2	46.3
BUKIT TIMA	1.3	103.9	195.0	123.4	47.5	232.1	99.7	34.6	181.3	110.6	46.4	181.3	110.6	46.4
ANQING	30.5	117.0	155.4	77.4	22.2	159.6	65.0	20.9	147.4	79.6	27.0	147.4	79.6	27.0
BEIJING	39.8	116.5	138.6	58.1	11.7	120.7	46.8	13.3	119.8	56.9	17.0	119.8	56.9	17.0
CHANGCHUN	43.9	125.2	105.2	52.2	11.6	101.1	39.8	11.7	101.2	45.7	14.9	101.2	45.7	14.9
CHONGQING	29.6	106.5	NaN	72.5	19.0	149.0	60.5	19.1	137.5	71.7	23.7	137.5	71.7	23.7

DALIAN	38.9	121.6	134.0	57.1	12.1	106.1	41.6	12.2	104.7	47.8	15.8	104.7	47.8	15.8
DONGXING	21.5	108.0	215.9	141.8	54.7	241.9	103.9	36.1	188.8	116.9	49.5	188.8	116.9	49.5
FUZHOU	26.1	119.3	157.0	85.3	26.2	160.0	65.7	21.3	145.9	78.8	27.1	145.9	78.8	27.1
GUANGZHOU	23.1	113.3	NaN	107.0	37.2	201.3	83.6	27.4	168.5	98.2	36.5	168.5	98.2	36.5
GUILIN	25.3	110.3	181.2	93.8	30.0	173.0	72.9	24.8	159.0	90.1	32.8	159.0	90.1	32.8
HAIKOU	20.0	110.4	NaN	116.2	40.1	208.4	86.6	28.3	171.0	100.4	38.0	171.0	100.4	38.0
HANGZHOU	30.3	120.2	132.0	61.1	17.5	157.0	63.8	20.5	144.6	77.3	26.2	144.6	77.3	26.2
HARBIN	45.7	126.6	117.4	53.3	11.3	94.8	37.0	10.7	94.2	41.9	14.1	94.2	41.9	14.1
JINAN	36.7	117.0	140.6	61.6	13.5	131.2	51.1	14.7	127.4	62.4	18.8	127.4	62.4	18.8
JING	32.0	118.8	NaN	72.0	18.0	145.3	57.7	17.6	136.0	69.7	22.3	136.0	69.7	22.3
KUNMING	25.0	102.7	115.7	59.9	18.1	110.1	46.4	15.6	110.1	53.9	19.1	110.1	53.9	19.1
LANZHOU	36.1	103.9	58.6	24.1	6.8	62.6	24.4	7.1	58.8	28.0	11.4	58.8	28.0	11.4
NANCHANG	28.7	116.0	147.6	74.6	22.1	169.8	69.6	22.7	156.1	87.2	30.7	156.1	87.2	30.7
NANGJING	32.3	118.8	137.7	62.2	15.5	145.1	57.6	17.6	135.8	69.5	22.1	135.8	69.5	22.1
SHENYANG	41.8	123.4	136.7	48.4	10.9	111.5	44.3	13.3	110.9	51.7	16.6	110.9	51.7	16.6
TAIYUAN	37.8	112.6	84.4	28.8	7.1	82.5	32.2	9.3	79.8	35.6	13.1	79.8	35.6	13.1
WUHAN	30.6	114.1	177.2	86.4	23.4	155.1	62.3	19.4	143.3	75.9	24.9	143.3	75.9	24.9
XIAN	34.3	108.9	67.9	30.6	9.5	93.2	36.7	10.9	88.5	40.3	14.7	88.5	40.3	14.7
XINXIANG	35.3	113.9	NaN	59.0	12.0	118.0	45.4	12.7	115.6	54.2	16.8	115.6	54.2	16.8
YICHUN	27.8	114.4	126.4	63.4	21.4	164.8	67.5	22.1	151.7	83.6	29.4	151.7	83.6	29.4
YINCHUAN	38.4	106.2	55.4	19.3	4.0	65.7	23.0	5.1	68.9	29.6	11.0	68.9	29.6	11.0
YINING	44.0	81.3	32.6	12.3	2.9	43.3	16.3	4.5	44.6	23.2	10.4	44.6	23.2	10.4
ZHENGZHOU	34.7	113.7	147.7	57.9	13.1	120.8	46.5	13.1	117.8	55.7	17.4	117.8	55.7	17.4
MONTREAL	45.5	286.4	105.7	45.6	7.6	55.1	19.4	4.3	54.8	24.8	9.7	54.8	24.8	9.7
VANCOUVER	49.3	236.8	32.7	11.9	5.2	53.0	18.6	4.6	58.8	26.6	11.0	58.8	26.6	11.0
OTTAWA	45.3	284.1	84.3	31.1	7.3	48.7	16.3	3.1	52.0	23.5	9.2	52.0	23.5	9.2
WALLOPS IS	37.8	284.5	NaN	55.5	14.5	62.5	22.1	5.0	64.6	28.3	10.7	64.6	28.3	10.7
CHICAGO	41.9	272.4	123.4	63.3	15.3	37.7	9.2	0.2	74.1	28.7	9.3	74.1	28.7	9.3
HOUSTON	29.8	264.3	147.2	92.4	27.8	22.3	8.7	2.4	31.6	18.0	8.3	31.6	18.0	8.3
JACKSONVILLE	28.3	279.1	NaN	89.1	31.0	57.6	24.5	8.4	59.9	30.1	13.0	59.9	30.1	13.0
MIAMI	25.7	279.6	194.5	115.9	43.6	102.1	43.7	15.1	103.8	50.7	18.7	103.8	50.7	18.7

FAIRBANKS	64.9	212.2	19.7	8.5	3.3	51.2	20.8	6.6	50.1	25.8	11.7	50.1	25.8	11.7
FLORIDA	28.3	279.4	142.3	91.4	30.7	54.4	22.9	7.6	56.9	28.5	12.3	56.9	28.5	12.3
NORMAN	35.2	262.6	119.9	67.9	17.0	8.4	2.8	0.5	25.2	14.8	6.6	25.2	14.8	6.6
RESTON	39.0	282.7	109.0	56.2	12.7	54.8	18.0	3.2	63.2	27.0	10.0	63.2	27.0	10.0
WHITE	32.5	253.4	NaN	39.7	4.7	173.4	65.6	17.8	164.1	92.7	30.1	164.1	92.7	30.1
TAMPA	28.1	277.6	NaN	94.4	36.9	102.6	46.3	17.6	142.3	77.2	27.8	142.3	77.2	27.8
MEDINA	41.2	278.2	116.1	55.4	9.8	45.8	13.9	1.8	58.2	24.8	9.2	58.2	24.8	9.2
AYURA	6.2	284.4	100.5	60.3	24.2	237.5	100.7	34.0	184.1	112.9	47.4	184.1	112.9	47.4
CHORRILLOS	6.3	284.5	104.3	60.2	24.3	237.8	100.8	34.1	184.3	113.0	47.4	184.3	113.0	47.4
CONVENTO	6.3	284.5	114.5	58.3	18.6	237.9	100.9	34.1	184.3	113.1	47.5	184.3	113.1	47.5
CUCARACHO	6.3	284.4	113.4	66.3	24.8	237.9	100.9	34.1	184.3	113.1	47.5	184.3	113.1	47.5
GERONA	6.2	284.4	101.1	61.9	23.0	237.7	100.8	34.1	184.2	113.0	47.4	184.2	113.0	47.4
GIRARDOTA	6.4	284.5	75.3	49.7	18.3	237.9	100.9	34.1	184.4	113.1	47.5	184.4	113.1	47.5
MANANTIALES	6.3	284.5	86.2	54.4	17.4	237.9	100.9	34.1	184.3	113.1	47.5	184.3	113.1	47.5
PEDREGAL	6.3	284.4	106.7	60.6	21.3	237.9	100.9	34.1	184.3	113.1	47.5	184.3	113.1	47.5
SAN ANTONIO DE PRADO	6.2	284.3	97.4	69.8	30.8	237.5	100.7	34.0	184.2	112.9	47.4	184.2	112.9	47.4
SAN CRISTOBAL	6.3	284.4	106.2	60.5	20.8	237.9	100.9	34.1	184.3	113.1	47.5	184.3	113.1	47.5
VILLA HERMOSA	6.3	284.4	71.6	49.3	19.0	237.7	100.8	34.1	184.3	113.0	47.4	184.3	113.0	47.4
BELEM	-1.5	311.5	167.9	126.9	61.4	251.2	111.1	40.7	194.4	123.0	56.2	194.4	123.0	56.2
BOA VISTA	2.8	299.3	160.0	112.0	45.8	261.1	112.9	39.6	193.3	121.6	54.5	193.3	121.6	54.5
BRASILIA	-15.8	312.2	112.8	71.0	24.2	186.7	73.2	21.0	166.8	96.0	33.4	166.8	96.0	33.4
CRUZEIRO DO SUL	-7.6	287.3	180.7	128.7	57.5	244.2	108.3	39.8	193.4	122.1	55.4	193.4	122.1	55.4
CURITIBA	-25.4	310.7	118.8	59.5	16.5	98.5	34.0	7.4	119.8	55.9	16.3	119.8	55.9	16.3
FORTALEZA	-3.8	321.5	109.5	61.9	23.7	215.0	94.9	34.6	179.1	109.1	46.3	179.1	109.1	46.3
GOV.VALADARES	-18.9	318.1	124.5	61.0	18.0	159.1	58.8	14.6	156.8	86.5	27.1	156.8	86.5	27.1
JI PARANA	-10.4	297.4	168.1	107.8	42.7	205.5	84.2	26.5	171.0	100.5	38.0	171.0	100.5	38.0
MACAPA	0.3	308.9	156.8	119.0	52.0	227.3	96.6	32.8	178.0	107.5	44.1	178.0	107.5	44.1
MANAUS	-3.2	300.0	168.1	109.8	55.6	202.7	90.5	33.7	179.0	109.1	46.5	179.0	109.1	46.5
MOSQUEIRO	-1.4	309.3	160.3	129.0	67.8	246.2	105.8	36.7	186.9	115.7	50.0	186.9	115.7	50.0
NATAL	-5.7	324.8	147.4	91.1	41.5	166.4	75.7	29.2	166.9	99.0	41.3	166.9	99.0	41.3
PONTA DAS LAGES	-3.2	300.1	NaN	98.2	49.7	203.3	90.2	33.3	176.2	106.5	44.8	176.2	106.5	44.8

PORTO ALEGRE	-30.0	308.8	94.9	51.1	13.3	61.1	21.6	5.0	71.4	32.1	12.2	71.4	32.1	12.2
RECIFE	-8.1	325.1	109.7	71.0	29.1	236.3	104.0	37.8	187.9	116.9	51.6	187.9	116.9	51.6
RIO DE JANEIRO	-22.9	316.1	127.0	73.2	27.6	117.1	40.0	8.3	143.2	73.9	20.6	143.2	73.9	20.6
STA RITA DO SAPUCAI	-22.3	314.3	138.0	70.0	22.0	114.7	40.5	9.1	129.5	63.4	18.3	129.5	63.4	18.3
SANTAREM	-2.5	305.3	155.2	110.9	57.5	228.3	96.6	32.5	179.0	108.3	44.3	179.0	108.3	44.3
SAO GABRIEL DA CACHOEIRA	-0.1	292.9	163.6	112.1	59.9	246.9	110.8	41.7	197.6	126.2	59.0	197.6	126.2	59.0
SAO PAULO	-23.5	313.4	137.7	66.9	18.4	105.6	37.0	8.3	123.4	58.7	17.1	123.4	58.7	17.1
SOBRAL	-3.7	319.7	200.0	90.0	28.4	172.8	76.1	27.7	154.1	87.8	34.3	154.1	87.8	34.3
TABATINGA	-4.2	290.1	156.0	113.1	56.1	245.1	105.0	36.2	187.5	116.1	50.0	187.5	116.1	50.0
LBA	-10.4	297.4	168.2	107.8	42.7	205.5	84.2	26.5	171.0	100.5	38.0	171.0	100.5	38.0
PALAU PIG (SAINS)	5.4	100.3	200.0	123.8	49.0	240.9	104.1	36.5	186.8	115.6	49.9	186.8	115.6	49.9
KWAJALEIN	8.8	167.6	101.8	76.5	36.3	253.2	108.9	37.8	190.3	118.8	52.1	190.3	118.8	52.1
SUVA	-18.1	178.4	154.0	93.0	40.0	229.4	100.9	36.6	184.8	114.1	49.4	184.8	114.1	49.4
UNITECH LAE	-7.0	147.0	NaN	108.8	56.8	183.8	83.1	31.7	171.6	103.1	43.7	171.6	103.1	43.7
POST OFFICE LAE	-7.0	147.0	130.0	110.0	69.0	183.8	83.1	31.7	171.6	103.1	43.7	171.6	103.1	43.7
ANNABURROO	-12.9	131.7	155.1	107.9	40.9	210.0	86.1	27.2	175.5	104.5	40.1	175.5	104.5	40.1
BATCHELOR	-13.1	131.0	130.5	95.1	36.8	216.4	89.3	28.5	178.3	107.0	41.9	178.3	107.0	41.9
BATHURST	-11.8	130.6	138.6	94.1	34.5	226.4	94.0	30.5	181.9	110.3	44.3	181.9	110.3	44.3
BELLVILLE	-12.8	130.9	147.1	105.2	41.5	225.7	93.8	30.5	182.2	110.7	44.5	182.2	110.7	44.5
BERRIMAH	-12.5	130.9	150.0	112.6	45.1	225.9	93.9	30.5	182.3	110.7	44.6	182.3	110.7	44.6
CPFOUR	-11.8	130.0	173.7	101.2	26.9	215.3	88.2	27.8	176.4	105.2	40.6	176.4	105.2	40.6
CHARLESPOINT	-12.4	130.6	158.1	98.8	38.4	224.8	93.3	30.2	181.5	110.0	44.0	181.5	110.0	44.0
DARWINRIVERDAM	-12.8	131.0	118.8	92.0	37.1	222.6	92.4	29.9	181.1	109.6	43.7	181.1	109.6	43.7
DUMINMIRIE	-12.6	130.4	156.8	104.7	47.4	231.2	96.4	31.5	184.2	112.5	45.9	184.2	112.5	45.9
GARDENPTAIR	-11.4	130.4	152.3	110.2	48.1	232.3	97.1	31.8	183.8	112.2	45.8	183.8	112.2	45.8
GOODALLMINE	-13.2	131.4	130.8	93.9	36.5	202.4	82.4	25.6	172.0	101.2	37.8	172.0	101.2	37.8
GUNNPTPRISON	-12.2	131.0	148.0	104.7	37.1	225.6	93.7	30.4	182.1	110.5	44.4	182.1	110.5	44.4
HUMPTYDOO	-12.6	131.3	260.4	97.8	32.0	217.9	89.9	28.8	179.2	107.8	42.4	179.2	107.8	42.4
KOOLPINYAH	-12.4	131.2	154.4	101.7	38.4	223.3	92.7	29.9	181.4	109.9	43.9	181.4	109.9	43.9
LA BELLEAIRSTRIP	-13.1	130.5	147.0	94.7	37.4	231.8	96.9	31.8	184.7	113.0	46.2	184.7	113.0	46.2
LITCHFIELD	-13.4	130.5	132.5	93.9	36.7	221.7	91.9	29.6	180.7	109.2	43.4	180.7	109.2	43.4

MANDORAHJETTY	-12.4	130.8	144.2	96.9	36.5	225.8	93.8	30.4	182.1	110.5	44.4	182.1	110.5	44.4
MCMINNSLAGOON	-12.5	131.1	145.6	103.0	45.8	223.9	93.0	30.1	181.6	110.1	44.1	181.6	110.1	44.1
MTBUNDEY	-13.2	131.1	148.4	101.8	31.0	208.4	85.3	26.9	174.8	103.8	39.6	174.8	103.8	39.6
OLDPTSTUART	-12.4	131.8	146.1	98.8	32.5	222.8	92.4	29.8	181.1	109.6	43.7	181.1	109.6	43.7
PICKERTARAMOOR	-11.8	130.9	153.2	101.6	38.3	226.1	93.9	30.5	181.9	110.4	44.3	181.9	110.4	44.3
POINTSTUARTABBS	-12.6	131.8	133.9	92.1	31.3	219.2	90.6	29.1	179.7	108.3	42.8	179.7	108.3	42.8
SNAKEBAY	-11.4	130.7	154.7	101.5	34.3	229.9	95.9	31.3	183.0	111.4	45.2	183.0	111.4	45.2
SWIMCREEKPL	-12.4	131.8	142.0	99.0	33.6	222.8	92.4	29.8	181.1	109.6	43.7	181.1	109.6	43.7
WOOLNER	-12.4	131.5	133.1	89.3	32.4	218.1	89.9	28.8	179.1	107.7	42.3	179.1	107.7	42.3
BANDUNG	-6.9	107.6	179.0	109.4	38.5	215.4	93.8	33.4	178.1	107.8	44.8	178.1	107.8	44.8
BANDUNG (BIT)	-6.9	107.6	192.5	120.0	48.0	215.0	93.6	33.3	177.8	107.6	44.7	177.8	107.6	44.7
MANILA (ADMU)	14.7	121.1	158.8	95.0	42.2	225.5	95.4	32.1	182.1	110.9	45.4	182.1	110.9	45.4
KUCHING	1.6	110.3	NaN	NaN	98.0	271.1	121.5	45.6	206.8	134.6	65.4	206.8	134.6	65.4
AKURE	7.2	5.2	165.0	NaN	NaN	180.1	75.8	25.3	157.5	89.4	33.2	157.5	89.4	33.2
BANDUNG	-6.9	107.6	NaN	120.0	50.0	215.4	93.8	33.4	178.1	107.9	44.9	178.1	107.9	44.9
AMRITSAR	31.6	74.9	NaN	48.0	NaN	168.8	63.3	16.6	164.3	92.9	30.0	164.3	92.9	30.0
THIRUVANANTHAPURAM	8.5	76.9	110.0	76.0	30.0	213.6	89.8	29.9	174.6	104.1	41.2	174.6	104.1	41.2
GANDAKI	13.5	79.2	98.0	68.0	21.0	170.2	67.0	19.5	158.5	88.9	30.5	158.5	88.9	30.5
KIANSAM	6.0	116.3	NaN	108.0	42.0	207.1	90.5	32.5	172.9	103.4	42.4	172.9	103.4	42.4
MIRI AIRPORT	4.3	114.0	NaN	117.0	56.0	240.5	105.1	37.6	187.4	116.4	50.9	187.4	116.4	50.9
DALAS	6.0	116.5	NaN	110.0	46.0	205.2	89.6	32.0	171.0	101.7	41.3	171.0	101.7	41.3
BINTULULU	3.2	113.0	NaN	114.0	58.0	262.5	116.6	43.0	199.4	127.7	59.8	199.4	127.7	59.8
STAPANG	2.4	112.1	NaN	114.0	57.0	249.9	110.4	40.4	194.0	122.6	55.8	194.0	122.6	55.8
NTU, SINGAPORE	1.3	103.7	156.0	106.0	60.0	234.7	101.1	35.2	182.4	111.7	47.3	182.4	111.7	47.3
BUKIT TIMAH	1.3	103.8	NaN	75.0	50.0	232.9	100.2	34.8	181.6	110.9	46.7	181.6	110.9	46.7
USM	5.4	100.3	NaN	68.0	44.0	240.9	104.1	36.5	186.7	115.6	49.9	186.7	115.6	49.9
SKUDAI	1.5	103.8	NaN	120.0	NaN	234.6	101.1	35.2	182.4	111.7	47.3	182.4	111.7	47.3
NIBONG TEBAL	5.2	100.4	NaN	NaN	NaN	232.3	100.0	34.7	182.1	111.4	46.9	182.1	111.4	46.9
NGURU	12.9	10.5	NaN	69.3	26.5	144.9	53.0	12.9	163.4	92.0	28.9	163.4	92.0	28.9
BORNO	11.5	13.0	NaN	72.5	28.0	150.8	57.7	15.7	157.1	86.9	27.5	157.1	86.9	27.5
KATSINA	13.0	7.6	NaN	74.9	29.4	144.5	55.0	14.7	150.9	81.6	25.0	150.9	81.6	25.0

GUSAU	12.2	6.7	NaN	78.1	30.6	164.6	66.0	20.0	157.2	87.9	29.9	157.2	87.9	29.9
SOKOTO	13.0	5.2	NaN	78.8	33.5	159.9	60.8	16.3	166.4	95.1	31.8	166.4	95.1	31.8
DIKWA	12.0	13.9	NaN	81.7	32.0	149.4	55.5	14.1	165.1	93.7	30.3	165.1	93.7	30.3
MAIDUGURI	7.7	13.2	NaN	84.0	34.0	162.2	68.8	23.4	152.3	85.1	30.9	152.3	85.1	30.9
GOMBE	10.2	11.2	NaN	86.1	35.5	163.8	65.4	19.6	157.0	87.7	29.6	157.0	87.7	29.6
BAUCHI	10.7	10.1	NaN	90.8	37.7	163.9	66.1	20.3	156.2	87.1	29.6	156.2	87.1	29.6
ADAMAWA	9.3	12.4	NaN	94.2	39.0	165.0	66.1	20.0	154.6	85.8	29.0	154.6	85.8	29.0
KANO	12.0	8.6	NaN	98.8	41.0	162.5	64.1	18.7	158.3	88.5	29.3	158.3	88.5	29.3
KADUNA	10.2	8.1	NaN	101.5	42.9	157.7	65.9	21.7	149.3	82.3	28.9	149.3	82.3	28.9
MINNA	9.6	6.5	NaN	101.9	43.4	174.5	72.0	23.1	160.2	91.2	32.9	160.2	91.2	32.9
ILE-IFE	7.5	4.6	NaN	106.0	43.9	175.3	73.3	24.2	153.9	86.4	31.5	153.9	86.4	31.5
ILORIN	8.5	4.5	NaN	103.4	44.0	168.6	69.2	22.0	152.1	84.4	29.9	152.1	84.4	29.9
ABUJA	9.1	7.4	NaN	104.5	44.3	175.0	73.4	24.4	160.2	91.5	33.6	160.2	91.5	33.6
JOS	9.9	8.9	NaN	108.4	44.7	155.0	65.1	21.7	147.8	81.1	28.6	147.8	81.1	28.6
MAKURDI	7.7	8.5	NaN	110.0	45.5	178.9	73.7	23.6	160.4	91.4	33.2	160.4	91.4	33.2
OGHOMOSO	8.1	4.2	NaN	114.1	45.8	167.1	68.8	22.0	149.8	82.7	29.3	149.8	82.7	29.3
LOKOJA	7.8	6.7	NaN	115.7	47.0	172.2	70.3	22.1	155.4	87.0	30.8	155.4	87.0	30.8
SAKI	8.7	3.4	NaN	118.2	46.3	168.8	69.1	21.8	152.7	84.9	30.0	152.7	84.9	30.0
OSOGBO	7.7	4.5	NaN	120.1	50.6	173.3	72.2	23.6	152.7	85.3	30.8	152.7	85.3	30.8
ABEOKUTA	7.1	3.4	NaN	121.9	51.6	177.4	73.2	23.4	155.7	87.6	31.6	155.7	87.6	31.6
AKURE	7.3	5.2	NaN	122.6	52.3	178.9	75.3	25.1	156.7	88.8	32.8	156.7	88.8	32.8
LAGOS	6.5	3.4	NaN	124.2	59.4	198.2	83.3	27.7	168.6	98.8	38.0	168.6	98.8	38.0
ABIA	5.4	7.5	NaN	127.3	62.0	203.2	88.1	31.1	175.6	105.5	43.1	175.6	105.5	43.1
ENUGU	6.5	7.5	NaN	129.8	62.9	196.5	83.2	28.1	169.3	99.6	38.7	169.3	99.6	38.7
BENIN	9.3	2.3	NaN	131.0	65.2	170.8	70.0	22.2	155.9	87.5	31.2	155.9	87.5	31.2
CALABAR	5.0	8.3	NaN	139.3	72.3	209.4	92.3	33.6	182.6	112.0	47.8	182.6	112.0	47.8
PORT HARCOURT	4.8	7.0	NaN	140.8	75.5	201.6	87.5	31.0	174.1	104.2	42.3	174.1	104.2	42.3
WARRI	5.6	5.8	NaN	145.2	77.8	222.2	97.4	35.1	187.0	115.9	50.2	187.0	115.9	50.2
GWANJU	35.2	126.9	120.0	90.0	45.6	143.2	59.1	19.3	138.4	72.3	23.9	138.4	72.3	23.9
DAEGU	35.9	128.6	120.0	60.0	38.4	134.0	54.3	17.1	129.2	64.9	21.0	129.2	64.9	21.0
BUSAN	35.2	129.1	150.0	90.0	57.6	146.8	60.8	20.1	140.0	73.9	25.0	140.0	73.9	25.0

SEOUL	37.6	127.0	150.0	90.0	48.6	145.6	60.5	20.0	145.4	77.6	25.3	145.4	77.6	25.3
ULSAN	35.5	129.3	120.0	65.4	44.4	139.2	57.2	18.6	133.1	68.4	22.9	133.1	68.4	22.9
INCHEON	37.5	126.7	120.0	89.4	60.0	144.2	59.5	19.4	142.4	75.1	24.3	142.4	75.1	24.3
CUNCHEON	37.9	127.7	120.0	60.0	31.2	134.2	55.9	18.5	137.8	71.7	23.2	137.8	71.7	23.2
PENANG	5.3	100.3	184.0	125.0	NaN	239.1	103.0	36.0	185.6	114.5	49.1	185.6	114.5	49.1
JOHOR BAHRU	1.3	103.4	176.0	114.0	NaN	236.4	102.0	35.7	183.4	112.6	47.9	183.4	112.6	47.9
ALOR STAR	6.2	100.3	166.0	107.0	NaN	229.3	98.1	33.7	181.6	110.7	46.2	181.6	110.7	46.2
KUALA LUMPUR	3.0	101.4	201.0	133.0	NaN	228.5	97.7	33.6	179.4	108.8	45.1	179.4	108.8	45.1
KOTOTABANG	-0.2	100.3	129.4	88.9	43.9	220.7	98.0	36.2	183.3	112.9	49.2	183.3	112.9	49.2
BUKIT JALIL	3.1	101.4	NaN	164.0	NaN	229.1	98.1	33.9	179.8	109.2	45.4	179.8	109.2	45.4
TAIPING	4.9	100.7	198.0	147.0	NaN	236.8	103.6	37.2	186.3	115.4	50.2	186.3	115.4	50.2
TEMERLOH	3.5	102.4	177.0	125.0	NaN	208.6	89.0	30.5	169.6	100.1	39.6	169.6	100.1	39.6

APPENDIX B

Estimating One-Minute Rain Rate Distributions in the Tropics From TRMM Satellite Data (October 2017)

Geraldine Rangmoen Rimven [ID], Kevin S. Paulson [ID], and Timothy Bellerby [ID]

Abstract—Internationally recognized prognostic models of rain fade on terrestrial and Earth-space extremely high frequency (EHF) links rely fundamentally on distributions of 1-min rain rates. In Rec. ITU-R P.837-6, these distributions are estimated from the data provided by Numerical Weather Products (NWPs). NWP yields rain accumulations over regions typically larger than 100 km across and over intervals of 6 h. Over the tropics, the Tropical Rain Measuring Mission (TRMM) satellite data yield instantaneous rain rates over regions 5 km across. This paper uses TRMM data to estimate rain rate distributions for telecommunications regulation over the tropics. Rain rate distributions are calculated for each 1° square between 35° south to 35° north. These distributions of instantaneous rain rates over 5 km squares are transformed to distributions over 1 km squares using a correction calculated from U.K. Nimrod radar data. Results are compared to rain distributions in DBSG3, the database of ITU-R Study Group 3. A comparison with the new Rec. ITU-R P.837-7 is also presented. A table of 0.01% exceeded rain rates over the tropics is provided as associated data.

Index Terms—Link budget, microwave, propagation, rain, rain fade, satellite data, spectrum planning.

I. Introduction

RAIN-INDUCED attenuation is a major impairment for wireless line of sight communications operating above 10 GHz, such as terrestrial and Earth-space links and links to high-altitude platforms (HAPs) and unmanned airborne vehicles (UAVs). A fundamental input parameter to the International Telecommunications Union - Radio Section (ITU-R) models of rain fade on terrestrial and Earth-space links, Rec. ITU-R P.530-16 [1] and Rec. ITU-R P.618-12 [2], respectively, is the 1-min rain rate exceeded for 0.01% of an average year, R0.01%. Many parts of the world do not have measured data of 1-min rain rates and so rely upon distributions provided by Rec. ITU-R P.837-6 [3]. This recommendation is based on work by Salonen and Poiares-Baptista (SPB), [4], [5], and The ITU-R

Study Group 3 [6]. It assumes that the average annual 1-min rain rate complementary cumulative probability function (CCPF or exceedance), globally, is well approximated by a double exponential distribution. Furthermore, the SPB method links the four distribution parameters to three output parameters from Numerical Weather Products (NWP). These NWP output parameters are 6-h precipitation accumulations over regions typically 100 to 200 km square. The SPB method has serious deficiencies, described in [7]. A fundamental problem is that the NWP outputs are precipitation accumulations over regions much larger than convective rain events, and over intervals that are much longer than their life-time. These convective events typically produce the moderate or heavier rain than leads to outage on telecommunications links. A second major problem is that the annual accumulations used by the SPB method are very poorly correlated to any parameter of 1-min rain rate distributions. Due to these and other problems, the 0.01% exceeded rain rates derived from the SPB method deviate from measured results in the ITU-R Study Group 3 database by an average of 30% [8], [9]. There are particular concerns about the accuracy of the SPB method in the tropics, where 0.01% exceeded rain rates are high and there is little data in the database of ITU-R Study Group 3, DBSG3.

The Tropical Rain Measuring Mission (TRMM) was a joint USA–Japanese satellite-based Earth observation mission, which carried, alongside other instruments, a spaceborne precipitation radar (PR) with a nominal spatial resolution ~5 km and a spatial coverage spanning 35° north and south of the equator [10]. Compared to NWP, the 5-km PR pixels are closer to the typical convective rain cell, which is reported to have an average diameter of about 2.6 km in [11] and between 1.2 and 1.5 km in [12]. However, these diameters were for regions experiencing rain rates well above the 0.01% exceeded rain rate of principal interest for radio system regulation. The 5 km pixels are much closer than NWP data to the point 1-min data required for telecommunications regulation. Paulson [7] has shown that the instantaneous rain rates averaged over 1 km squares, as produced by the U.K. Nimrod radar network, provide an unbiased estimate of point 1-min rain rates exceeded 0.01% of the time.

TRMM data have been validated through a ground validation programme by the National Aeronautical Space Agency (NASA) using several sources of rain data collected from four primary sites [13], including Kwajalein in the Pacific. TRMM data have been used to estimate 1-min rainfall rates in some studies [14], [15]. However, these are not direct estimations of point 1-min rain rate distributions. TRMM data were used to

estimate thunderstorm ratio and the average annual total rainfall, and these parameters have been correlated with parameters of point 1-min rain rate distributions such as the 0.01% exceeded rain rate.

This paper develops estimates of average annual point 1-min rain rate distributions for the tropics using TRMM data. Section II introduces the TRMM and Nimrod data, and the DBSG3 database. Section III describes the calculation of distributions of 5 km instantaneous rain rates, and presents some data. In Section IV, Nimrod data are used to calculate the correction required to estimate point 1-min rain rates from the 5 km instantaneous rain rates. Section V compares the predicted rain rate distributions with those in the DBSG3 database. Conclusions are drawn in Section VI.

II. DATA USED

A. TRMM 2A25

The TRMM data product 2A25 [16] is the primary input data for this study. This dataset provides instantaneous attenuation-corrected near-surface rainfall from the TRMM PR. The spatial resolution changed due to an orbit boost on August 2001. The satellite had pre- and post-boost orbital periods of 91.5 and 92.5 min, yielding about 16 orbits per day, with spatial resolutions ~4.3 and ~5.0 km, respectively. The data span the interval from December 1997 to April 2015. The retrieval algorithm [17] has continuously evolved and been enhanced [18]. The current algorithm is 2A25 version 7 (V7) [19]. As with terrestrial radar, PR rainfall estimates are sensitive to the local variation in the reflectivity/rainfall (Z/R) relationship, ground clutter, and other factors such as calibration errors [20], path attenuation, and bright-band effects [21]. Retrieval errors are sensitive to both rainfall rate and meteorological regimes [22].The changes in TRMM 2A25 V7 have not only improved the Z/R relationship over preceding versions but also contains corrections for attenuation, as well as nonuniform beam-filling effects [23]. TRMM PR estimates have been compared to other types of precipitation data in numerous studies.

B. Nimrod

The U.K. Meteorological Office Nimrod system combines data from a network of 15 C-band radars with satellite data, together with surface reports and numerical weather prediction (NWP) fields. Composite rain field images are produced, with a 5-min sample interval and presented on a 1-km spatial Cartesian grid, spanning the U.K. and parts of Western Europe. These are available from the British Atmospheric Data Centre from April 2004 to the present. Although presented on a uniform grid, the actual spatial averaging is limited by the distance from a point to the nearest radar. The Nimrod system, radar calibration, and the formation of composite rain field data is described in [24]. Distributions of Nimrod rain rates have been shown to be good estimates of distributions of 1-min rain rates derived from networks of rapid-response rain gauges [7]. Furthermore, Nimrod data can be spatially integrated to compare rain rate distributions over 1 and 5 km squares, for the same rain fields. Rain
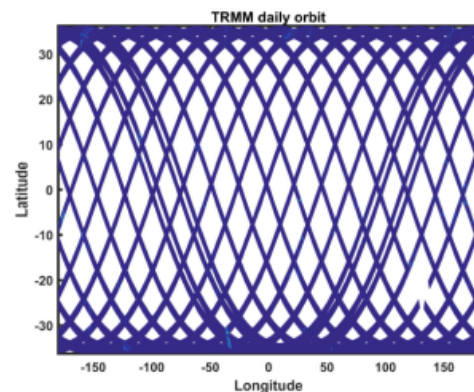

Fig. 1. Typical coverage captured in one day from the 16 orbits of TRMM satellite.

data from five regions have been extracted from the Nimrod dataset. The five regions are 200 km squares and cover southern England (SE), the Midlands (ML), northern England (NE), Southern Scotland (SS), and Northern Scotland (NS).

C. DBSG3

The database of the ITU-R Study Group 3, DBSG3, contains 1127 records of annual rain rate distributions collected since 1959. A selection of rain rates exceeded at time percentages from 1% to 0.001% are presented for each site and for each measurement interval. Often, individual years are reported as well as results derived by accumulating data from several consecutive years. The data have been provided by the national spectrum regulators of many countries. However, the database contains no data from Africa, and much of the data is from developed countries in temperate regions of Europe, Asia and the Americas. Furthermore, there is no information in the database of measurement reliability. Rain gauges are difficult to site, particularly in urban areas and can provide biased measurements when in the wind shadow of buildings, trees, etc. Measurements of low-probability rain rates are also very sensitive to temporary blockage, due to insects or plant matter in the funnel. Finally, several authors have published evidence of temporal trends in R0.01% [7], [25], [26] starting in the 1980s. The non-stationarity of R0.01% needs to be taken into account when comparing estimates measured in different decades.

III. CALCULATION OF 5-KM RAIN RATE DISTRIBUTIONS

Each orbit of the TRMM satellite yields a 247-km-wide swath of ~5 km rain rate measurements under an orbit that extends 35° north and south of the equator (see Fig. 1). The satellite orbits just less than 16 times a day, and the orbit path shifts around the world, giving near universal coverage over the tropics, but with irregular return times.

TRMM 2A25 data from 9 years, 2004 to 2012, were downloaded and analyzed. Each rain rate measurement was allocated to a single 1° by 1° square by its latitude and longitude. Histograms of measurements were calculated for each 1° square,
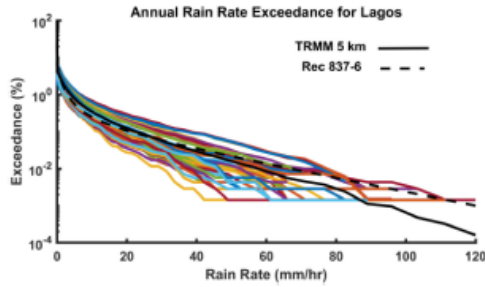
Fig. 2. Exceedance distributions of 5 km rain rates from TRMM, with Rec. ITU-R P. 837-6 prediction for Lagos, Nigeria. Colored lines are for individual years, while the black solid line is derived from all the nine years of data.

and these were transformed into exceedance distributions. Fig. 2 shows the exceedance distribution of 5 km rain rates for Lagos, Nigeria (6.52 °N, 3.38 °E). This is compared with the Rec. ITU-R P.837-6 prediction. The 5-km rain rates are smaller than point 1-min rain rates as averaging reduces the incidence of extremes. A correction needs to be applied to TRMM derived distributions to approximate distributions with less spatial averaging. It is known that spatial averages over 1 km squares yield unbiased estimates of the point 1-min rain rate exceeded 0.01% of the time in the U.K. Therefore, in the next section, a transformation will be developed between distributions of 5 and 1 km instantaneous rain rates.

IV. TRANSFORMATION FROM 5 TO 1 KM RAIN RATE DISTRIBUTIONS UNITS

In this section, we compare distributions of 1 and 5 km rain rates derived from the same Nimrod rain rate fields. Each Nimrod composite rain rate map yields 200×200 rain samples at approximately 1 km resolution, each 5 min, for each of the five regions. When the rain rate samples in 5×5 arrays are averaged, they yield an estimate of the rain rate averaged over a 5-km square. Each region, for each composite rain field, yields 196×196 not-independent 5 km rain rates. Over a year, there are $365 \times 24 \times 12$ maps yielding 4.2×10^9 1 km rain rates and 4.0×10^9 5 km rain rates. These data allow annual distributions of 1 and 5 km rain rates to be compared down to very low exceedance probabilities.

Ten years of Nimrod data have been analyzed, from 2005 to 2014 inclusive. Fig. 3 shows the relationship between 1 and 5 km exceeded rain rates, for the same exceedance probabilities, for the Midlands region. The blue lines are for each of the ten individual calendar years, and the red line is the best-fit quadratic to these relationships.

Figure 4 shows the best-fit quadratic equiprobable 5 and 1 km rain rate relationships, derived from ten years of data, for the five regions considered. An average has been taken of the relationships for the four southern regions (SS, NE, ML, and SE) and this may be expressed as

$$R_{0.01\%}^{1\,km} = \left(0.0126\,R_{0.01\%}^{5\,km} + 1.0619\right) \times R_{0.01\%}^{5\,km}. \quad (1)$$
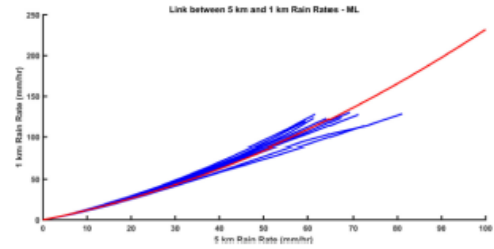

Fig. 3. Equiprobable 1 and 5 km rain rate relationships for the ten years in the Midlands region (blue) and the best-fit quadratic (red).
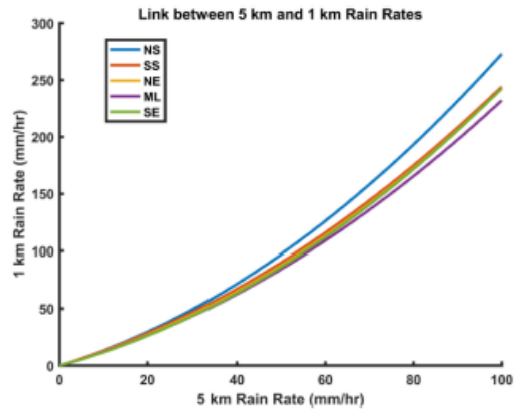

Fig. 4. Equiprobable 5 and 1 km rain rate relationships for the five U.K. regions.

The climate across the five U.K. regions varies from Northern Scotland dominated by stratiform rain off the Atlantic to Southern England with a large proportion of heavy convective events origination in continental Europe. Despite this, there is little variation in the equi-probably 1 km–5 km exceeded rain rate relationships and no discernible trend in the four southern-most regions. This suggests that the average relationship may be applicable to tropical regions. This is clearly speculative, and we would have more confidence in a transformation based on data from the tropics. Ideally, the estimation of TRMM to 1-min transformation requires 1-min rain data, which are not available even from the validation sites. The radar data from the TRMM ground validation site at Kwajalein, could be used to calculate a 5- to 1-km transformation, but the link between Kwajalein 1 km data and 1-min data has not been demonstrated.

V. PREDICTIONS OF POINT 1-MIN RAIN RATE DISTRIBUTIONS

A. Comparison to Rec. ITU-R P.837-6

Applying the transformation (1) presented in Section IV to the 5-km rain rate distributions calculated in Section III yields estimates of the 1 km distributions, and hence, the point 1-min distribution, for each 1° square in the tropics. The 0.01% exceeded rain rates can be estimated directly from these
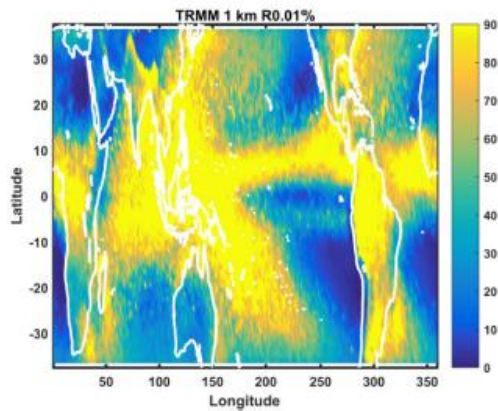
Fig. 5.　0.01% exceeded rain rates derived from distributions of TRMM 5 km rain rates transformed using (1).

Fig. 7.　Comparison of 0.01% exceedance from 1 km TRMM distribution and Rec. ITU-R P.837-6 prediction, with DBSG3 data from the tropics.

between the TRMM rain rates and Rec. ITU-R P.837-6 predictions.

The 0.01% exceeded rain rates derived by this process can also be compared with those in the DBSG3 database. Sites with at least four individual years of measurements have been selected, yielding 50 sites out of 64 that fall within the TRMM boundary. Selection has been performed as the year-to-year variability provided by the four or more years of results allows the standard error in the R0.01% to be estimated.

Figure 7 compares the R0.01% predicted using the TRMM data and Rec. ITU-R P.837-6, with the average DBSG3 value for each site. Table I lists the Rec. ITU-R P.837-6 prediction and that derived from TRMM and the average over at least four years of DBSG3 site data.

Using the *t*-test, Table II shows the probability that the TRMM estimates differ from the DBSG3 values only by chance. *N* gives the number of years over which the data are collected, and *the* standard errors in the values were estimated from year-to-year variation. This probability is just an indication as it assumes that 0.01% exceeded rain rates are normally distributed and independent from year to year. However, the high probabilities of observing the difference between DBSG3 and the TRMM estimates provide some confidence in the method. The low values are for a group of sites in Colombia that are quite close together.

Figure 7 shows that the TRMM method yields generally better estimates of DBSG3 values than Rec. 837-6. The Rec. 837-6 values show a bias at high rain rates that the TRMM values do not have. The notable outliers are the group of sites where TRMM estimates R0.01% to be 120 mm/h compared to the DBSG3 values around 60 mm/h. All these sites are close together in Colombia, within the Ayura valley and in the wind shadow of the Central Range mountains. Within the valley, the terrain may also lead to biased TRMM rain rate estimates due to clutter returns. It is likely that the TRMM values are more representative of the region over the 100-km resolution of the method. Furthermore, it is likely that ITU-R Recommendations are artificially biased by taking the fit to these sites as a measure of improved quality of a method.
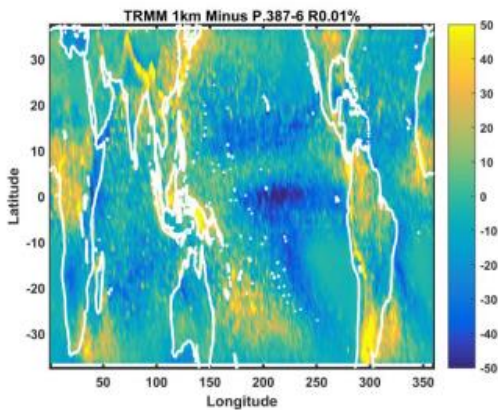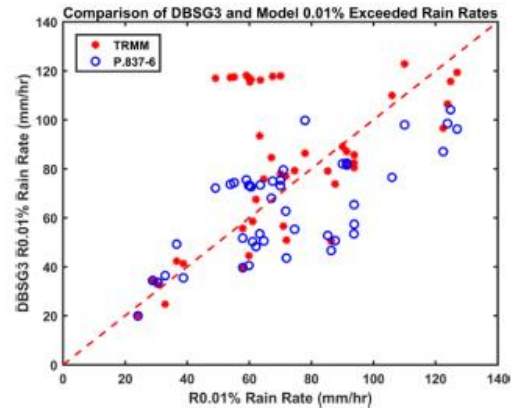

Fig. 6.　Difference between 0.01% exceeded rain rates derived from transformed TRMM 5 km rain rates and Rec. ITU-R P.837-6 prediction.

distributions. Fig. 5 shows the 0.01% exceeded rain rates derived from the transformed distributions of TRMM 5 km rain rates. The spatial variation of R0.01% is similar to that provided by Rec. ITU-R P.837-6, but with significant regional differences. For example, regions along the lower coastal regions of West Africa extending to locations in central Africa, coastal areas of Southern Africa, as well the island of Madagascar have been shown by TRMM distributions to have rain rates between 80 and 90 mm/h. This is much higher than the Rec 837-6 values around 20–30 mm/h along the coast of Southern Africa and 60–70 mm/h for the West and central African regions. The TRMM distributions also show high rain rates over the areas around Argentina in South America. Coordinates of locations over the Pacific and the North Atlantic also show rain rates higher than the Rec. ITU-R P.837-6 predictions. These and other differences are shown in Fig. 6, which is a plot of the difference

TABLE I
REC. ITU-R P.837 PREDICTION, TRMM 1 KM DISTRIBUTION, AND AVERAGE DBSG3 MEASUREMENT FOR POPULATION CENTERS IN TROPICS

LOCATION	LAT	LON	DBSG3	TRMM	Rec837-6	Rec837-7
ALMERIA	36.85	-2.38	16.18	20.6	31.1	22.0
CADIZ	36.5	-6.26	36.6	44.1	49.2	31.7
MALAGA	36.67	-4.48	35.33	33.7	35.9	27.9
MELILLA	35.28	-2.92	28.9	36.6	34.4	26.7
TENERIFE NORTE	28.47	-16.32	32.89	25.8	36.4	32.2
DAEJON	36.37	127.36	87.66	71.1	50.7	59.2
TAEGU	35.88	128.62	57.89	62.8	51.7	54.1
PUSAN	35.1	129.03	93.70	83.9	53.4	61.5
CHONGQING	29.58	106.47	71.96	50.7	43.6	60.5
DONGXING	21.53	107.97	141.80	144.2	82.4	103.8
FUZHOU	26.08	119.28	85.28	77.5	52.8	65.7
GUANGZHOU	23.05	113.32	105.98	114.4	76.5	83.6
GUILIN	25.33	110.3	93.79	85.4	57.4	72.9
HAIKOU	20.03	110.47	122.42	105.1	87.0	86.7
HANGZHOU	30.32	120.2	61.09	49.9	50.2	63.7
JINAN	36.68	116.98	61.58	48.5	44.1	51.1
KUNMING	25.02	102.68	59.91	45.5	40.5	46.4
LANZHOU	36.05	103.88	24.12	15.3	20.0	24.4
NANCHANG	28.67	115.97	74.59	84.2	55.3	69.5
NANGJING	32.32	118.8	62.15	70.7	48.3	57.6
WUHAN	30.63	114.07	86.37	43.6	46.6	62.3
XIAN	34.3	108.93	30.55	22.6	33.6	36.7
YICHUN	27.8	114.38	63.36	98.5	53.4	67.6
ZHENGZHOU	34.72	113.65	57.94	38.7	39.7	46.5
PUSAN	35.1	129.03	93.70	83.9	53.4	61.5
BUKIT TIMA	1.3	103.9	124.79	100.8	104.1	99.7
HOUSTON	29.77	-95.73	93.75	83.0	65.3	58.8
JACKSONVILLE	28.34	-80.93	91.40	89.7	81.5	69.5
FLORIDA	28.34	-80.602	91.38	89.7	82.3	69.3
NORMAN	35.21	-97.44	64.68	78.3	50.6	50.4
WHITE	32.54	-106.61	38.79	41.7	35.5	28.4
TAMPA	28.06	-82.42	90.01	84.2	82.0	69.3
AYURA	6.1689	-75.5681	60.21	120.1	73.1	63.3
CHORRILLOS	6.2991	-75.5061	60.55	120.1	72.6	64.4
CONVENTO	6.3378	-75.5163	59.76	120.1	73.2	64.1
CUCARACHO	6.2869	-75.6119	67.52	120.1	75.0	61.6
GERONA	6.2342	-75.5583	63.57	120.1	73.4	63.2
GIRARDOTA	6.3855	-75.4575	49.12	120.1	72.2	66.1
MANANTIALES	6.3209	-75.5436	53.90	120.1	73.7	63.3

TABLE I
CONTINUED.

PEDREGAL	6.3074	-75.5777	55.15	120.1	74.4	62.4
SAN ANTONIO DE PRADO	6.1877	-75.6649	70.03	120.1	75.4	62.0
SAN CRISTOBAL	6.2837	-75.639	59.07	120.1	75.5	61.2
BELEM	-1.45	-48.48	126.9	120.7	96.2	103.9
BRASILIA	-15.48	-47.83	71	57.5	79.5	67.7
MANAUS	-3.15	-60.02	110	133.1	97.9	98.3
RIO DE JANEIRO	-22.92	-43.95	71.78	78.9	62.7	71.9
STA RITA DO SAPUCAI	-22.25	-45.72	70	82.9	73.1	60.3
SAO PAULO	-23.55	-46.63	67.11	88.0	68.1	63.3
PALAU PIG (SAINS)	5.3546	100.3012	123.8	108.3	98.5	104.1
KWAJALEIN	8.79	167.62	77.93	88.4	99.7	108.9

TABLE II
COMPARISON OF POINT 1-MIN RAIN RATES FOR MULTIYEAR 1 KM TRMM AND DBSG3

	DBSG3			TRMM			PROBABILITY OF DIFFERENCE
LOCATION	N	STDEV(σ)	MEAN	N	STDEV(σ)	MEAN	
ALMERIA	20	7.40	15.01	9	8.38	20.38	0.24
CADIZ	5	4.85	36.81	9	22.16	44.04	0.44
MALAGA	10	14.93	32.58	9	10.15	31.67	0.91
MELILLA	18	7.09	25.40	9	8.29	35.61	0.03
TENERIFE NORTE	14	6.38	31.00	9	14.41	26.59	0.50
DAEJON	10	18.07	83.79	9	51.18	78.07	0.81
TAEGU	10	11.15	57.31	9	15.80	59.28	0.82
PUSAN	10	27.94	85.81	9	29.93	80.26	0.77
HOUSTON	8	20.65	92.19	9	25.77	76.76	0.33
JACKSONVILLE	8	18.35	88.80	9	28.35	81.82	0.66
NORMAN	4	4.57	68.64	9	15.63	79.33	0.15
WHITE	5	7.69	39.91	9	11.72	40.03	0.99
TAMPA	4	8.21	95.46	9	26.64	81.05	0.27
AYURA	4	0.45	60.26	9	38.66	130.38	0.00
CHORRILLOS	4	3.83	60.08	9	38.66	130.38	0.00
CONVENTO	4	12.14	57.97	9	38.66	130.38	0.00
CUCARACHO	4	8.72	65.95	9	38.66	130.38	0.00
GERONA	4	9.82	61.48	9	38.66	130.38	0.00
GIRARDOTA	4	8.18	49.86	9	38.66	130.38	0.00
MANANTIALES	4	7.86	54.49	9	38.66	130.38	0.00
PEDREGAL	4	17.69	61.93	9	38.66	130.38	0.00
SAN ANTONIO DE PRADO	4	9.60	69.69	9	38.66	130.38	0.00
SAN CRISTOBAL	4	7.29	60.87	9	38.66	130.38	0.00
BELEM	7	12.31	126.86	9	31.61	121.74	0.74
BRASILIA	4	26.58	71.03	9	20.20	61.86	0.65
MANAUS	7	2.71	109.78	9	39.01	132.94	0.10
RIO DE JANEIRO	11	11.19	58.80	9	27.30	84.10	0.04
KWAJALEIN	7	16.70	63.95	9	24.64	83.16	0.19

Rec. ITU-R P.311 provides the procedure for the acquisition, presentation, and analysis of data in studies of radiowave propagation [27]. Of importance is the goodness of fit (GoF) metric, which measures the distance between pairs of fade exceedance distributions. It is calculated using the logarithm of the ratio of rain rates exceeded at the same time percentage, which results in a statistic that is approximately normally distributed where a value close to zero indicates a good fit.

The GoF for the 0.01% exceeded rain rate for TRMM compared to DBSG3 data was 0.1304, while for Rec. ITU-R P.837-6 was 0.0931. Excluding the outliers, the GoF for TRMM improves remarkably to a value of 0.0374 while the GoF for Rec. ITU-R P.837-6 is 0.1030. A validation was done using all 120 tropical sites regardless of the number of years of data, and the GoF for TRMM and Rec. ITU-R P.837-6 were 0.0881 and 0.0776, respectively. Without the outliers, the values

121

were 0.0471 and 0.0789 for TRMM and Rec. ITU-R P.837-6, respectively.

B. Comparison to Rec. ITU-R P.837-7

Shortly before the submission of this paper, the ITU-R published Rec. ITU-R P.837-7. The recommendation uses inputs derived from a global rain gauge network and reanalysis data, i.e., the Global Precipitation Climatology Centre (GPCC) gridded rain gauge dataset and the European Centre for Medium-Range Weather Forecasts (ECMWF) ERA Interim database, over land and water, respectively. The new recommendation is therefore not affected by the problems observed with the SPB method used in the Rec. ITU-R P.837-6 model. However, the issues associated with rain gauges still apply. Moreover, it has been reported that developing countries, which constitute a large part of the tropics, have a sparse distribution of rain gauges [28]. It is expected that this lack of data will limit the resolution and accuracy of Rec.ITU-R837-7 in the tropics.

VI. CONCLUSION

Rec. ITU-R P.837-6 is based on input data with severe and fundamental limitations and is known to perform poorly in the tropics. Similarly, its recent replacement, Rec. ITU-R P.837-7, relies upon rain gauge data that are very sparse in the tropics. Data from the TRMM satellite mission yield a large amount of data derived from integration regions smaller that the convective cells that are fundamentally important for radio system design and regulation. This paper has developed a method to estimate point 1-min rain rate distributions over the tropics from TRMM data. Radar data, either terrestrial or satellite based, yield rain rate estimates with systematic errors due to fine-scale rain variation, partial beam filling, and drop size distribution variations. TRMM dataset 2A25 V7 tries to mitigate many of these errors but still yields estimates with some error and uncertainty [34]. Despite these errors, the proposed method still performs better than ITU-R Recommendations on the DBSG3 validation data.

A transformation from 5 km rain rate distributions to 1 km distributions has been derived from U.K. data and applied in the tropics. No north–south variation was found in the transformation, and so it has speculatively been applied to tropical data. The validity of this has been tested against the DBSG3 database of rain rate distributions. Future work will explore the use of data from the TRMM ground validation sites to refine this transformation. Future research can also address the limitations associated with the validation dataset.

This paper has highlighted the importance of regional representation of data in DBSG3. The Colombian sites are not representative of their region due to orographic effects. If the evolution of ITU-R Recommendations is driven by their fit to the database, then such sites will introduce bias into the recommendations. When these sites are excluded from consideration, the TRMM method performs significantly better than P.837-6 and P.837-7. Furthermore, the TRMM method relies on more recent data than methods based on ERA40 and other reanalysis data and so is more likely to match the present-day climate.

The method developed will be applicable to other satellite precipitation datasets as they become available in the future. It is expected that higher resolution data covering more of the globe will be available in the near future and that these data will be the best starting point for the estimation of distributions of point 1-min rain rate distributions for radio regulation.

REFERENCES

[1] Propagation Data and Prediction Methods Required for the Design of Terrestrial Line-of-Sight Systems, Recommendation ITU-R p. 530–16, 2016.
[2] Propagation Data and Prediction Methods Required for the Design of Earth-Space Telecommunication Systems, Recommendation ITU-R p. 618–12, 2016.
[3] Characteristics of Precipitation for Propagation Modelling, Recommendation ITU-R p. 837–6, 2015.
[4] E. T. Salonen and J. P. V. Poiares Baptista, "A new global rainfall rate model," presented at ICAP'97, Edinburgh, U.K., Jan. 1997, doi: 10.1049/cp:19970359.
[5] J. P. V. Poaires Baptista and E. T. Salonen, "Review of rainfall rate modelling and mapping," presented at CLIMPARA'98, Ottawa, ON, Canada, 1998.
[6] ITU-R Propagation Prediction Methods for Interference and Sharing Studies, ITU-R Study Group 3, 2012.
[7] K. S. Paulson, "Evidence of trends in rain event size effecting trends in rain fade: Trends in rain event size effecting fade," Radio Sci., vol. 51, no. 3, pp. 142–149, 2016.
[8] K. S. Paulson, C. Ranatunga, and T. Bellerby, "Estimation of trends in distributions of one-minute rain rates over the UK," presented at EuCAP 2014, The Hague, The Netherlands, doi: 10.1109/EuCAP.2014.6901749.
[9] G. Blarzino, L. Castanet, L. Luini, C. Capsoni, and A. Martelucci, "Development of a new global rainfall rate model based on ERA40, TRMM, GPCC and GPCP Products," presented at EUCAP 2009, Berlin, Germany.
[10] README Document for the Tropical Rainfall Measurement Mission. [Online]. Available: https://disc2.gesdisc.eosdis.nasa.gov/data/TRMM_L2/TRMM_2A23.7/doc/TRMM_Readme_v3.pdf. Accessed on: Feb. 7, 2017.
[11] H. Sauvageot, F. Mesnard, and R. S. Tenório, "The relation between the area-average rain rate and the rain cell size distribution parameters," J. Atmos. Sci., vol. 56, no. 1, pp. 57–70, 1999.
[12] N. H. H. Khamis, J. Din, and T. A. Rahman, "Determination of rain cell size distribution for microwave link design in Malaysia," presented at Radio and Microwave 2004, Selangor, Malaysia, doi: 10.1109/RFM.2004.1411069.
[13] D. B. Wolff et al., "Ground validation for the tropical rainfall measuring mission (TRMM)," J. Atmos. Ocean. Technol., vol. 22, no. 4, pp. 365–380, 2005, doi: 10.1175/JTECH1700.1.
[14] T. V. Omotosho and C. O. Oluwafemi, "One-minute rain rate distribution in Nigeria derived from TRMM satellite data," J. Atmos. Sol. Terr. Phys., vol. 71, no. 5, pp. 625–633, 2009.
[15] T. V. Omotosho et al., "Distribution of one-minute rain rate in Malaysia derived from TRMM satellite data," Ann. Geophys., vol. 31, pp. 2013–2022, 2013.
[16] TRMM 2A25. [Online]. Available: https://search.earthdata.nasa.gov/?q = TRMM+2A25&ok = TRMM+2A25. Accessed on: Mar. 17, 2017.
[17] T. Iguchi, T. Kozu, R. Meneghini, J. Awaka, and K. I. Okamoto, "Rain-profiling algorithm for the TRMM precipitation radar," J. Appl. Meteorol., vol. 39, no. 12, pp. 2038–2052, 2000.
[18] D. B. Wolff and B. L. Fisher, "Comparisons of instantaneous TRMM ground validation and satellite rain rate estimates at different spatial scales," J. Appl. Meteorol. Climatol., vol. 47, no. 8, pp. 2215–2237, 2008.

[19] Tropical Rainfall Measuring Mission (TRMM) Precipitation Radar Algorithm. Instruction Manual for Version7. [Online]. Available: http://www.eorc.jaxa.jp/TRMM/documents/PR_algorithm_product_informati on/pr_manual/PR_Instruction_Manual_V7_L1.pdf. Accessed on: Sep. 23, 2017.

[20] P. Kirstetter et al., "Toward a framework for systematic error modeling of spaceborne precipitation radar with NOAA/NSSL ground Radarâ Based National Mosaic QPE," J. Hydrometeorol., vol. 13, no. 4, pp. 1285–1300, 2012.

[21] D. B. Wolff and B. L. Fisher, "Comparisons of instantaneous TRMM ground validation and satellite rain-rate estimates at different spatial scales," J. Appl. Meteorol. Climatol., vol. 47, no. 8, pp. 2215–2237, 2008.

[22] Y. Duan, A. M. Wilson, and A. P. Barros, "Scoping a field experiment: Error diagnostics of TRMM precipitation radar estimates in complex terrain as a basis for IPHEx2014," Hydrol. Earth Syst. Sci., vol. 19, no. 3, pp. 1501–1520, 2015.

[23] P. Kirstetter et al., "Comparison of TRMM 2A25 products, version 6 and version 7, with NOAA/NSSL ground Radarâ based national mosaic QPE," J. Hydrometeorol., vol. 14, no. 2, pp. 661–669, 2013.

[24] S. H. Chan, R. R. Halterman, and D. G. Long, "Cross-validation of Jason-1 and QuikSCAT wind speeds," presented at IGARSS 2004, Anchorage, AK, USA, doi: 10.1109/IGARSS.2004.1369866.

[25] L. S. Chiu et al., "Comparison of TRMM and water district rain rates over New Mexico," Adv. Atmos. Sci., vol. 23, no. 1, pp. 1–13, 2006.

[26] M. N. Islam and H. Uyeda, "Use of TRMM in determining the climatic characteristics of rainfall over Bangladesh," Remote Sens. Environ., vol. 108, no. 3, pp. 264–276, 2007.

[27] Y. Fu et al., "Recent trends of summer convective and stratiform precipitation in Mid-Eastern China," Sci. Rep., vol. 6, p. 33044, 2016.

[28] Q. Cao et al., "Statistical and physical analysis of the vertical structure of precipitation in the mountainous west region of the United States using 11+ years of spaceborne observations from TRMM precipitation radar," J. Appl. Meteorol. Climatol., vol. 52, no. 2, pp. 408–424, 2013.

[29] D. L. Harrison, S. J. Driscoll, and M. Kitchen, "Improving precipitation estimates from weather radar using quality control and correction techniques," Meteorol. Appl., vol. 7, no. 2, pp. 135–144, 2000.

[30] K. S. Paulson, C. Ranatunga, and T. Bellerby, "Estimation of trends in distributions of one-minute rain rates over the UK," presented at EuCAP 2014, The Hague, The Netherlands, doi: 10.1109/EuCAP.2014.6901749.

[31] T. Tjelta and J. Mamen, "Climate trends and variability of rain rate derived from long-term measurements in Norway," Radio Sci., vol. 49, no. 9, pp. 788–797, 2014.

[32] Acquisition, Presentation and Analysis of Data in Studies of Radiowave Propagation, Recommendation ITU-R P. 311-16, 2016.

[33] T. Islam, M. A. Rico-Ramirez, D. Han, K. P. Srivastava, and M. A. Ishak, "Performance evaluation of the TRMM precipitation estimation using ground-based radars from the GPM validation network," J. Atmos. Solar Terr. Phys., vol. 77, pp. 194–208, 2012, doi: 10.1016/j.jastp.2012.01.001.

[34] P. Kirstetter et al., "Impact of sub-pixel rainfall variability on spaceborne precipitation estimation: Evaluating the TRMM 2A25 product: Impact of Sub-Pixel Rainfall Variability on TRMM 2A25," Q. J. R. Meteorol. Soc., vol. 141, no. 688, pp. 953–966, 2015.

Geraldine Rangmoen Rimven received the B.Eng. degree in electrical/electronic engineering from Abubakar Tafawa Balewa University, Bauchi, Nigeria, in 2000, and the M.Sc. degree in personal, mobile, and satellite communication from the University of Bradford, Bradford, U.K., in 2011. She is currently working toward the Ph.D. degree from the School of Engineering and Computer Science, University of Hull, Hull, U.K.

She worked in various computing and electrical support roles before joining the University of Jos, Nigeria, as a Systems Engineer for its Network and Internet Services. Since 2014, she has been a Lecturer in the Electrical/Electronic Department, Faculty of Engineering, University of Jos.

Kevin S. Paulson received the B.Sc. and M.Sc. degrees in atmospheric physics from the University of Auckland, Auckland, New Zealand, in 1983, and 1985, respectively, and the Ph.D. degree in mathematics from the Oxford Brookes University, Oxford, U.K., in 1991.

He was Leader of the Terrestrial Systems in the Radio Communications Research Unit of Rutherford Appleton Laboratory until 2004 when he joined the University of Hull, Hull, U.K., as a Senior Lecturer in telecommunications.

Timothy Bellerby received the B.Sc. degree in applied mathematics from the University of Warwick, Warwick, U.K., in 1986, and the Ph.D. degree in geophysics from the University of Sheffield, Sheffield, U.K., in 1991.

He is a Senior Lecturer in Geography in the School of Environmental Sciences, University of Hull, Hull, U.K. He has formerly been a Research Associate at the University of Bristol Centre for Remote Sensing, U.K., and a Contactor to the United States National Weather Service. He was a Consultant to the United Nations Food and Agricultural Organization. His current research interests include the application of artificial intelligence and machine vision approaches to satellite cloud monitoring, precipitation estimation, and the development of ensemble and probabilistic representations of uncertainty in precipitation estimates. He has an interest in monitoring and forecasting the River Nile.

123

APPENDIX C

A Comparison of Tropical One–Minute Rain Rate Distributions Derived From TRMM with Rec. ITU-R P.837-7

Geraldine R. Rimven, Kevin S. Paulson, Timothy Bellerby

Abstract— Knowledge of the average annual exceedance distribution of point one-minute rain rates is essential for the design and regulation of microwave telecommunications networks. The current internationally recognised method for estimating these distributions globally is Rec. ITU-R P.837-7. The method is based on averaging monthly exceedance distributions, each conditioned upon mean monthly temperature and rain accumulation. The method is expected to be less accurate over the tropics than in temperate zones, due to lack of data for conditioning and verification from developing equatorial countries. This project uses TRMM satellite derived rain rates to estimate distributions over the tropics. TRMM data have been used in two ways. Initially, TRMM data from 9-years is aggregated to estimate monthly distributions on 1° squares across the tropics. The second method uses TRMM data to estimate conditional monthly probability distributions, as in Rec. ITU-R P.837-7. The TRMM distributions are downscaled to estimate point one-minute distributions by optimised fitting. Two sets of verification data are used: the database of ITU-R Study Group 3 (DBSG3) and data collected from 56 tropical sites in Africa and Asia.

Index Terms— Link budget, microwave, propagation, rain fade, satellite data, spectrum planning

I. INTRODUCTION

Wireless line-of-sight communication systems operating above 10 GHz, such as terrestrial and Earth-space telecommunications links, suffer rain-induced attenuation. Optimization of spectrum efficiency requires a balance between the power that systems transmit to overcome attenuation and the interference they cause each other. The International Telecommunications Union – Radiocommunication Section (ITU-R) maintains a set of recommendations with internationally recognized models to predict rain attenuation on terrestrial and Earth-space links: ITU-R P.530-17 [1] and ITU-R P. 618-13 [2] respectively. A fundamental input parameter for these prediction methods is the average annual point one-minute rain rate exceeded for 0.01% of an average year: $R_{0.01}$. An accurate knowledge of rainfall statistics with one-minute integration times is required to predict rain attenuation in order to design robust links and to optimize spectrum efficiency.

The current recommendation ITU-R P.837-7 [3] provides average annual, point one-minute rain rate distributions globally; although it states that if local data are available, these should be used. For locations with reliable data but measured using longer integration times, the Recommendation provides a method of conversion to distributions of one-minute rain rates. Version 7 is radically different from versions 2 to 6. While ITU-R P.837-6 predicts rainfall rate at a

given exceedance probability, ITU-R P.837-7 predicts the exceedance probability at a given rainfall rate. The ITU-R P.837-7 method was first published in [4] where it was evaluated alongside ITU-R P.837-6 and another method known as MORSE [5] against local data in Ireland. Other published works include [6] and [7]. ITU-R P.837-7 is the only version of the Recommendation considered in this paper and it will be referred to as Rec837.

The previous versions used three input parameters derived from Numerical Weather Prediction (NWP) reanalysis models: the average annual convective and total accumulation, and the proportion of 6-hour periods in which it rained. The input data to Rec837 consists of digital maps of mean monthly total precipitation accumulation (MT), and mean monthly surface temperatures (T) provided by Rec. ITU-R. P1510-1, for each calendar month. Annual exceedance probability distributions of one minute rain rates R are calculated from weighted averages of monthly distributions, which are analytic distributions conditional upon T and MT: XCD_{837} ($R / T, MT$). The average annual rain rate exceedance at any location is calculated from 24 parameters being the monthly T_{ii} and MT_{ii} for month ii = 1 to 12:

$$P(R > R_{ref}) = \frac{1}{365.25}\sum_{ii=1}^{12} N_{ii} \times XCD_{837}(R_{ref} / T_{ii}, MT_{ii}) \quad (1)$$

N_{ii} are the average number of days in a month where for February N_2 = 28.25. A complication linked to the use of months is their variable length, meaning that monthly accumulation can be associated with different average daily accumulations. Rather than using MT_{ii} directly, as implied by (1), it is converted to monthly mean daily accumulation: $MMDA_{ii} \equiv MT_{ii}/N_{ii}$, to produce the conditional exceedance distribution. This was necessary when aggregating TRMM data, as described in Section III.

The input data, T_{ii} and MT_{ii}, are derived from a global rain gauge network and reanalysis data: the Global Precipitation Climatology Centre (GPCC) gridded rain gauge dataset and the European Centre for Medium-Range Weather Forecasts (ECMWF) ERA Interim database over land and water respectively [3]. [8] have documented the GPCC global archive of monthly precipitation data, which provides global gridded products with spatial resolutions of 0.25°, 0.5°, 1°, and 2.5°, and also review GPCC products, processing and reliability issues. The GPCC version 15 dataset used by the Rec837 has been derived from a network of 75000 weather stations, with input from more countries and island/atoll regions than previous versions. Furthermore, additional levels of quality control that have been introduced, resulting in a significant improvement compared to previous versions [9].

Rain gauges are often considered to provide rain accumulation ground truth, but they are affected by many errors [10]-[12] arising from wind effects, shadowing and evaporation. Different electronic gauge mechanisms e.g. syphon, drop-counting and weighing gauges yield different systematic and random errors. They all suffer from blockages and are difficult to site in rough terrain (such as urban areas)

3

and at sea. Rain gauge networks are labor intensive and require considerable attention if they are to give accurate results. The rain gauges in the tropics are sparsely distributed, often located in urban areas, and may not provide a sufficiently dense geographic distribution of rainfall rate statistics. For the GPCC dataset with the finest resolution, 0.25°, most grid squares will not contain a rain gauge and so results are generated by interpolation. These factors may affect the performance of the Rec837 in the tropics.

Due to the sparsely distributed rainfall rate data, Rec837 may be less accurate in the tropics than in temperate regions where there is geographically dense rainfall rate data. Tropical regions also experience much higher and more variable $R_{0.01\%}$. For these reasons, it has become imperative that other methods are explored to estimate one-minute rain rate distributions. This paper seeks to compare distributions derived from satellite measurements with Rec837 predictions and site data, over the tropics. Unlike other works, satellite data are used directly. Rec837 style conditional distributions are calculated from satellite data and compared to the original Rec837 distributions. Satellite derived rain rate measurements have the advantage of consistent coverage over large global regions.

This paper uses data from the Tropical Rainfall Measuring Mission (TRMM). TRMM was a joint USA-Japanese satellite based Earth observation mission. The satellite was launched in 1997 and was in operation until 2015 with a nominal spatial resolution of ~5 km and a spatial coverage spanning 35° north and south of the equator [13]. With an orbital period of about 92.5 minutes, TRMM completed just less than 16 orbits in a day, giving an average return time of about one and a half hours for most places in the tropics.

Rain rates derived from satellite-based radars have random and systematic errors due to many factors, and rely upon calibration and validation from ground based measurements and rain gauges. This paper explores two quite different ways of using TRMM data to estimate tropical one-minute rain rate distributions. A previous paper, [14], used downscaled TRMM rain rate distributions derived from aggregating 9 years of TRMM data. In Section IV, this process is again tested but with different downscaling transformations and validation data. Before that, two new methods based on the Rec837 paradigm are tested. Section III presents the results of using (1) with TRMM derived conditional probability distributions and two alternative sets of monthly input data. This is different from the method used in [14] where the measured distribution is used. Section V quantitatively compares the performance of the algorithms against the two sets of validation data, while conclusions are drawn in Section VI. To begin, Section II introduces the datasets used in this project.

II. DATA USED

A. TRMM 2A25

TRMM data have been validated through a ground validation programme run by the National Aeronautical Space Agency (NASA), using several sources of rain data collected over four primary sites - Kwajalein Atoll, Republic of the Marshall Islands; Melbourne, Florida; Houston, Texas; and Darwin, Australia [15]. To use TRMM data, a relationship needs to be found between distributions of instantaneous rain rates over 5 km squares and point one-minute rain rates. [16] has shown that the instantaneous rain rates averaged over 1 km squares, as produced by the UK Nimrod radar network, provide an unbiased estimate of point one-minute rain rates exceeded 0.01% of the time. A transformation from 5 km to 1 km rain rate distributions, derived from Nimrod data, has been reported in [14].

TRMM 2A25 is instantaneous attenuation-corrected near-surface rainfall collected by the precipitation radar (PR) on-board the TRMM satellite, with a geographic coverage of -38° and +38° and all longitudes [17]. Compared to GPCC data, the 5 km PR pixels are closer to the diameter of a typical convective rain cell: about 2.6 km in [18] and between 1.2 and 1.5 km in [19]. However, these diameters were given for regions experiencing rain rates well above $R_{0.01\%}$ of principal interest for radio system regulation. Although PR data have errors arising from the local variation of the rainfall/reflectivity (Z/R) relationship, path attenuation and ground clutter, the current TRMM 2A25 V7 contains improvements to the Z/R relationship and corrections for attenuation, as well as non-uniform beam-filling effects [20]. Despite these improvements, it still produces estimates with errors and uncertainty [21].

B. Rec. ITU-R P.837-7 data

Annex 1 of Rec837 [3] provides digital maps of monthly mean total rainfall and monthly mean surface temperatures at 2 metres above the surface of the Earth, also provided by Rec. ITU-R P.1510-1. These are long-term averages derived from the ERA and GPCC databases, and are the input data used to determine one-minute rain rate exceedance values for specific locations.

C. ERA Interim 2 m temperature

The European Centre for Medium-range Weather Forecasts (ECMWF) is an independent intergovernmental organization founded in 1975 and provides a range of numerical weather predictions and forecasts. The 2 m temperature dataset is the mean surface temperature 2 m above the surface of the Earth, and is one of the parameters, T, required by Rec837 [3].

D. GPCC Full Data Monthly Product Version 7.0

The GPCC was established in 1989 and provides gridded gauge-analysis products derived from quality controlled station data The GPCC Full Data Monthly Product Version 7.0 is monthly land-surface precipitation accumulation based on 75,000 rain gauges. It covers the period 1901 to 2013, with global coverage, and is available in spatial resolutions of 0.5°× 0.5°, 1.0° × 1.0° and 2.5° × 2.5° by latitude/longitude. It is the most accurate in situ precipitation reanalysis data set of the GPCC [22].

E. DBSG3

This is the database of the ITU-R Study Group 3, version 7 release 2, which contains annual rain rate distributions collected from 198 sites globally. The data accepted in to the database are specified in ITU-R P.311-17 [23]. Rain rates exceeded at 0.001%, 0.01% and 1% of time are provided for individual years and, in some cases, for numbers of consecutive years. ITU-R member administrations provide the data; however, these are predominantly from countries in temperate regions of Europe, Asia and the Americas, with none from Africa. The database may be biased because of the errors in rain gauges. With the evidence of temporal trends in $R_{0.01\%}$ starting in the 1980s as published by several authors [16], [24], [25], trends in $R_{01\%}$ should be taken into account when estimates from different decades are compared. ITU-R rainfall rate and rain attenuation prediction methods are tested by comparing their predictions with DBSG3 measured data. For this study, the 81 sites that fall within the TRMM boundaries are selected. Of the 81 sites, 53 have 4 or more years of data with only 30 of those having data for individual years. The 81 sites are predominantly in South-Eastern Asia, with a few in Europe, America and no sites in Africa.

125

III. CALCULATION OF TRMM MONTHLY ONE-MINUTE RAIN RATE DISTRIBUTIONS

The use of the Rec837 paradigm (1) requires a) monthly mean total rainfalls (MT_{ii}), b) monthly mean surface temperatures (T_{ii}), as input data. From these are calculated the monthly probability of rain, and monthly exceedance probability distributions of rainfall rate conditioned on monthly mean total rainfall and monthly mean surface temperature. These conditional probability distributions have been estimated using TRMM data. Nine years of TRMM 2A25 data were acquired, spanning 2004 to 2012, between latitudes -38° and +38° and all longitudes. The goal of the analysis was to estimate the TRMM conditional rain rate exceedance distributions $XCD_{TRMM}(R /T, MT)$, the equivalent of the Rec837 distributions: $XCD_{837}(R / T, MT)$. This was achieved by combining data from the entire tropics and the 9 years, from 1° grid squares that experience the similar monthly T and $MMDA$. TRMM data comes from two distinct periods separated by an orbit boost on August 2001. To ensure consistency in the derived rain rates, only the 9 years from the later period is considered.

Monthly histograms of measured 5 km rain rates were calculated for every 1°× 1° latitude and longitude square in the tropics. ERA Interim temperatures and GPCC precipitation data were also acquired for the same period and area. Mean monthly temperatures (T) from ERA Interim data and mean monthly daily accumulations ($MMDA$) from the GPCC monthly precipitation, were calculated over the same array of 1°× 1° squares. These three sets of data yield an exceedance distribution of TRMM rain rates, a T and a $MMDA$ for each 1° square and for each of $9 \times 12 = 108$ months. One-hundred equiprobable T bins were defined spanning 247.6 K to 313.6 K. Similarly, 100 equiprobable $MMDA$ were defined from 0 to 75.3 mm. Exceedance distributions were calculated by aggregating TRMM rain rates from all 1° squares that experienced T and $MMDA$ in the same bins. These provide estimates of exceedance distributions of 5 km rain rates conditional on a given T and $MMDA$: $XCD_{TRMM}(R /T, MMDA)$. The 5 km exceedance distributions were transformed to distributions of 1 km rain rates, using the quadratic transformation in [14] yielding $XCD_{1km}(R /T, MMDA)$. Deriving TRMM conditional probability distributions can be summarized as follows:

- Calculate histograms of 5 km TRMM rain rates for 1°× 1° latitude and longitude squares, for each of the 108 months spanning 9 years;
- For each 1° square and for each month, acquire the T and $MMDA$ from GPCC and ERA Interim data;
- Aggregate rain rate histograms for each 1° square and month within the same T and $MMDA$ bin;
- Convert aggregated histograms, conditional upon T and $MMDA$, into exceedance distributions;
- Convert exceedance distributions of 5 km TRMM rain rates into 1 km rain rates using the quadratic transformation.

The TRMM conditional distributions share the major characteristics with those of Rec837. Where sufficient data was available, the high rain rate tail tended to yield higher probabilities. Once these distributions have been calculated, various tests can be performed to see how well they can be used to predict annual exceedance probability distributions in the tropics. Two methods based on conditional distributions have been considered in this study. Both methods use the Rec837 method (1) but replace the conditional probability distribution with the equivalent transformed conditional TRMM distributions:XCD_{1km}. The two methods differ in the source of monthly mean temperature and accumulation, which are:

a.   Using the mean monthly T_{ii} and MT_{ii} available in Rec. ITU-R P.1510-1 and Rec837 data files
b.   Using T_{ii} and MT_{ii} from GPCC and ERA Interim for the specific 9 years of TRMM data.

While method a) might be expected to be more representative of average annual results, method b) is expected to be more consistent with the TRMM distributions as MT and T are from primary sources spanning the period the TRMM distributions were measured. For comparison with specific site data, monthly T_{ii} and MT_{ii} were interpolated from the gridded data in the respective datasets.

A. Using Rec. ITU-R P.837-7 Input Data

This method uses the monthly average T_{ii} and MT_{ii} from Rec837 data files and the TRMM measured and downscaled XCD_{1km} rather than XCD_{837}. Rain rate distributions have been calculated for DBSG3 sites in the tropics and the results are presented in Table 1. Fig 1 compares the $R_{0.01\%}$ predicted by this method to DBSG3 data for all sites.

The sites in the DBSG3 database have been divided into two sets: sites with 4 or more years of data and those with less. Sites with multiple individual years of data allow the year-to-year variability to be estimated and so an estimate of the uncertainty in the estimate of the site average annual $R_{0.01\%}$ may be calculated. For the many sites with single years of data, it is difficult to say how close the rain rate values are to average annual. It is reasonable to assume that the average annual value is equally likely to be higher or lower than the single year measured value. Sites having 4 or more years of data are plotted with error bars of length: $\sigma_R/\sqrt{n}$ where σ_R is the standard deviation of annual $R_{0.01\%}$ measurements and n is the number of years. Due to temporal correlations in annual exceeded rain rates, the uncertainty is expected to be an under estimate.
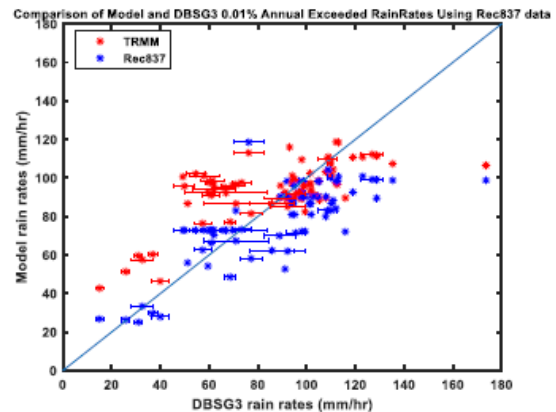
Fig. 1: Comparison of Method a) $R_{0.01\%}$ and Rec837 exceeded rain rates with DBSG3 data for sites in the tropics.

Both models use Rec837 MT_{ii} and MA_{ii} input data. The conditional monthly probability distributions are (blue) XCD_{837} and (red) XCD_{1km}. Sites with 4 or more years of data are plotted with error bars indicating the uncertainty in the DBSG3 estimate of average annual values. Red and blue error bars are for TRMM and Rec837 respectively. The two methods yield similar results. Rec837 tends to under-estimate for the higher rain rates, while this is less pronounced for the TRMM method.

B. GPCC and ERA Interim Input Data

The same process described in a) is followed but using T_{ii} and MT_{ii} from GPCC and ERA Interim for the specific 108 months of TRMM data. This extends the test as both input data and conditional probability distributions now come from primary data sources. The results are also presented in Table 1. Fig. 2 mirrors Fig. 1, comparing model 0.01% exceeded rain rates with DBSG3 site data. Most DBSG3 data come from outside the 9-year period providing the primary data. Oddly, Rec837 performs better using these input data than those provided as part of the Recommendation. The Rec837 values are closer to the DBSG3 values as observed from the blue points in Fig. 2 when compared to those in Fig. 1. The TRMM method performs similarly well. Section V quantifies the goodness of fit (GoF) between verification and model data.

It can be observed in Table 1 that a group of sites with latitude ~6° and longitude ~-75° yield very different 0.01% exceeded rain rates from DBSG3 (60 mm/hr) compared to TRMM based methods (e.g. 105 mm/hr). These sites are in Colombia within the Ayura valley and in the wind shadow of the Central Range Mountains. The DBSG3 site data is not representative of the 1° square it inhabits. These sites dominate measures of agreement between DBSG3 and models and reliance on these measures can lead to misleading results. For this reason, GoF metrics in Table 3 are calculated both with and without these outliers.
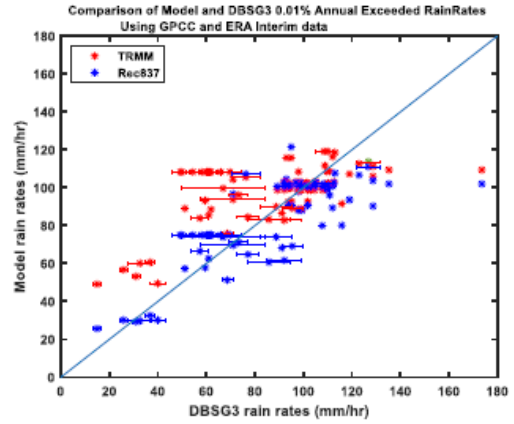
Fig. 2: R0.01%exceeded rain rates from Rec837 and Method b) i.e. GPCC and ERA input data and TRMM distributions. These are compared with DBSG3 data for all sites in the tropics.

TABLE 1

COMPARISON OF DBSG3 R0.01% AND MODEL PREDICTIONS

SITES	LAT	LON	DBSG3	Method a) TRMM	Method a) Rec837	Method b) TRMM	Method b) Rec837	Optimised TRMM fitted to DBSG3
ALMERIA	36.85	-2.38	15.01	31.34	26.78	37.2	25.64	31.14
CADIZ	36.50	-6.26	36.81	48.12	29.73	48.55	32.59	42.46
MALAGA	36.67	-4.48	32.58	45.34	33.37	47.97	29.79	29.38
MELILLA	35.28	-2.92	25.81	39.28	26.27	44.55	30.19	38.36
TENERIFE NORTE	28.47	-16.32	31.00	47.39	25.13	41.08	29.31	38.51
DAEJON	36.37	127.36	77.21	71.42	58.19	75	64.8	81.79
TAEGU	35.88	128.62	57.31	65.55	62.63	74.32	66.51	62.99
PUSAN	35.10	129.03	85.81	77.44	62.33	73.5	60.74	95.44
SI RACHA	13.10	100.80	99.38	72.59	72.21	80.21	88.08	83.85
BANGKOK	13.70	100.50	97.96	80.77	72.21	80.21	88.08	83.85
CYBERJAYA FTA	2.92	101.66	135.3	104.3	98.77	107.2	102.1	103.8
CYBERJAYA MMU	2.93	101.64	173.6	103.2	98.77	107.2	102.1	103.8
BUKIT TIMA	1.30	103.90	123.0	109.2	100.9	111.8	106.7	89.01
HOUSTON	29.77	-95.73	92.19	75.75	61.95	73.03	61.73	64.19
JACKSONVILLE	28.34	-80.93	88.80	81.19	69.96	81.7	74.00	107.1

MIAMI	25.65	-80.43	115.9	81.22	72.09	83.62	80.12	77.21
NORMAN	35.21	-97.44	68.64	66.37	48.53	64.84	51.29	85.57
WHITE	32.54	-106.61	39.91	34.60	27.93	37.50	30.18	54.80
TAMPA	28.06	-82.42	95.46	83.87	71.49	80.73	69.19	88.29
AYURA	6.17	-75.57	60.26	91.82	72.84	105.7	75.05	109.8
CHORRILLOS	6.30	-75.51	60.08	91.47	72.84	105.7	75.05	109.8
CONVENTO	6.34	-75.52	57.97	95.87	72.84	105.7	75.05	109.8
CUCARACHO	6.29	-75.61	65.95	88.21	72.84	105.7	75.05	109.8
GERONA	6.23	-75.56	61.48	92.62	72.84	105.7	75.05	109.8
GIRARDOTA	6.39	-75.46	49.86	88.83	72.84	105.7	75.05	109.8
MANANTIALES	6.32	-75.54	54.49	97.32	72.84	105.7	75.05	109.8
PEDREGAL	6.31	-75.58	61.93	86.63	72.84	105.7	75.05	109.8
SAN ANTONIO DE PRADO	6.19	-75.66	69.69	89.5	72.84	105.7	75.05	109.8
SAN CRISTOBAL	6.28	-75.64	60.87	82.89	72.84	105.7	75.05	109.8
VILLA HERMOSA	6.26	-75.55	49.26	95.32	72.84	105.7	75.05	109.8
BELEM	-1.45	-48.48	126.9	111.2	99.23	113.1	111.1	103.4
BOA VISTA	2.78	-60.68	112.0	91.11	84.11	97.02	89.42	102.6
BRASILIA	-15.80	-47.83	71.03	77.54	67.34	86.5	69.54	70.09
CRUZEIRO DO SUL	-7.60	-72.67	128.7	110.0	89.45	102.5	90.31	101.76
CURITIBA	-25.42	-49.28	59.52	84.86	54.22	85.77	57.75	65.74
FORTALEZA	-3.77	-38.55	61.93	89.21	70.28	79.95	75.11	57.01
GOV.VALADARES	-18.85	-41.95	60.95	83.94	66.27	76.33	62.65	44.05
MACAPA	0.30	-51.10	119.0	109.0	92.62	104.2	93.65	86.27
MANAUS	-3.15	-60.02	109.8	104.7	100.27	105.9	98.75	100.7
MOSQUEIRO	-1.40	-50.69	128.7	110.3	99.06	109.7	103.8	100.0
NATAL	-5.70	-35.20	91.13	84.81	52.69	77.42	68.25	53.83
PONTA DAS LAGES	-3.20	-59.90	98.00	107.3	93.40	105.8	98.01	105.5
PORTO ALEGRE	-30.03	-51.22	51.13	77.67	55.96	80.60	57.32	76.89
RECIFE	-8.05	-34.90	70.97	90.12	82.96	100.3	96.74	69.89
RIO DE JANEIRO	-22.92	-43.95	73.3	91.33	73.23	89.53	71.19	74.54
SANTAREM	-2.50	-54.72	110.9	100.3	88.41	106.3	96.09	99.77
SAO GABRIEL DA CACHOEIRA	-0.12	-67.07	112.1	120.4	98.17	117.0	100.8	112.4
SAO PAULO	-23.53	-46.62	66.89	84.49	72.77	94.09	73.91	97.02

TABATINGA	-4.23	-69.94	113.1	120.0	100.6	120.3	107.7	122.3
LBA	-10.35	-62.58	107.8	98.65	79.96	94.49	79.98	95.28
KWAJALEIN	8.79	167.62	76.26	112.2	118.6	101.9	107.2	81.30
SUVA	-18.14	178.42	93.00	116.45	89.83	116.2	104.5	67.64
UNITECH LAE	-7.00	147.00	108.5	107.7	83.10	121.0	102.2	105.1
POST OFFICE LAE	-7.00	147.00	110.0	107.7	83.10	121.0	102.2	105.1
ANNABURROO	-12.91	131.67	108.0	81.18	90.34	92.92	100.7	87.22
BATCHELOR	-13.06	131.02	95.12	81.62	81.00	85.10	90.63	81.91
BATHURST	-11.77	130.62	94.12	96.02	86.67	97.80	101.1	132.6
BELLVILLE	-12.76	130.88	105.2	79.93	98.29	98.59	102.7	109.2
BERRIMAH	-12.46	130.93	112.6	90.04	98.29	98.59	102.7	109.2
CPFOUR	-11.77	130.03	101.2	90.26	86.67	97.80	101.1	132.6
CHARLESPOINT	-12.42	130.63	98.78	82.16	98.29	98.59	102.7	109.2
DARWINRIVERDAM	-12.83	130.97	91.98	80.1	98.29	98.59	102.7	109.2
DUMINMIRIE	-12.64	130.37	104.7	92.57	98.29	98.59	102.7	109.2
GARDENPTAIR	-11.40	130.42	110.2	96.7	86.67	97.80	101.1	132.6
GOODALLMINE	-13.22	131.38	93.91	80.16	81.00	85.10	90.63	81.91
GUNNPTPRISON	-12.16	131.02	104.7	82.38	90.34	92.92	100.7	87.22
HUMPTYDOO	-12.61	131.29	97.82	80.92	90.34	92.92	100.7	87.22
KOOLPINYAH	-12.39	131.18	101.7	85.03	90.34	92.92	100.7	87.22
LA BELLEAIRSTRIP	-13.12	130.49	94.66	93.49	87.10	94.13	101.0	97.41
LITCHFIELD	-13.43	130.48	93.94	90.54	87.10	94.13	101.0	97.41
MANDORAHJETTY	-12.44	130.76	96.87	84.94	98.29	98.59	102.7	109.20
MCMINNSLAGOON	-12.54	131.08	103.0	83.16	90.34	92.92	100.7	87.22
MTBUNDEY	-13.23	131.13	101.8	86.50	81.00	85.1	90.63	81.91
OLDPTSTUART	-12.36	131.81	98.75	88.90	90.34	92.92	100.7	87.22
PICKERTARAMOOR	-11.77	130.88	101.6	90.60	86.67	97.80	101.1	132.6
POINTSTUARTABBS	-12.59	131.76	92.1	82.80	90.34	92.92	100.7	87.22
SNAKEBAY	-11.42	130.65	101.45	97.70	86.67	97.80	101.1	132.6
SWIMCREEKPL	-12.36	131.81	99.02	88.90	90.34	92.92	100.7	87.22
WOOLNER	-12.38	131.47	89.28	89.23	90.34	92.92	100.7	87.22
BANDUNG	-6.90	107.60	108.9	109.3	104.3	110.4	101.1	126.8
MANILA (ADMU)	14.68	121.07	95.00	93.40	95.81	116.2	121.5	160.7

A study by [26] contains values of measured 0.01% exceeded rain rates collected from various published works. Fifty-six tropical sites from Africa and Asia, within the boundaries of TRMM data, were selected for this study, and are referred to as the S&A sites. Table 2 contains 0.01% TRMM and Rec837 annual exceeded rain rates calculated for S&A sites using methods a) and b). Figures 3 and 4 compare the TRMM calculated rain rates using methods a) and b), with S&A $R_{0.01\%}$. Both methods exhibit an under-estimation bias that increases with rain rate. Otherwise, the performance of the methods is very similar.
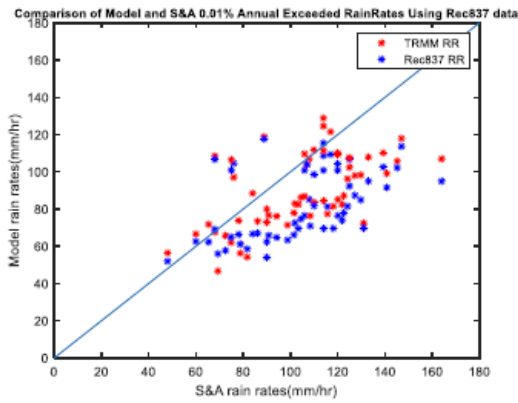

Fig. 3: Comparison of Method a) $R_{0.01\%}$ and Rec837 exceeded rain rates with S&A site data
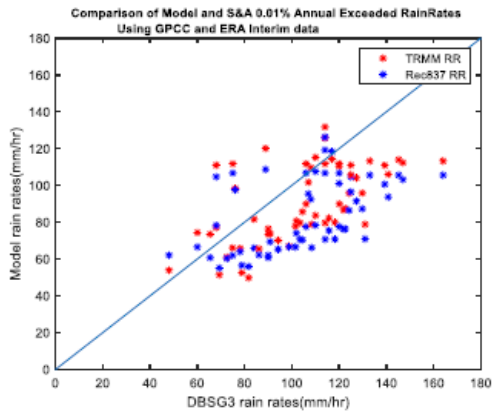

Fig. 4: Comparison of Method b) $R_{0.01\%}$ and Rec837 exceeded rain rates with S&A site data

Figures 5 to 8 compare 0.1%, 0.01% and 0.001% exceeded rain rates from TRMM and Rec837 using methods a) and b) for DBSG3 and S&A sites. For both datasets, both methods tend to over-estimate at 0.001%. For DBSG3, there is less bias using the TRMM methods at 0.1%, although both methods under-estimate the higher rain rates at

this probability level. For both datasets, both methods under-estimate at 0.1% and over-estimate at 0.001%.
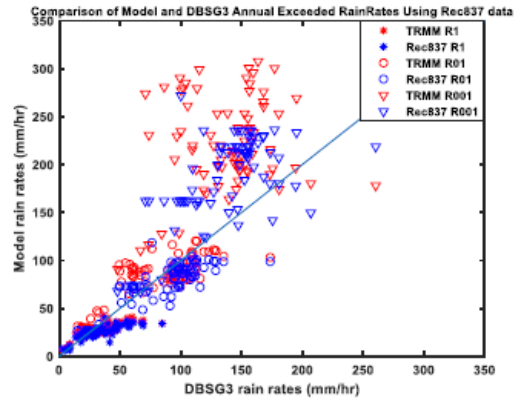

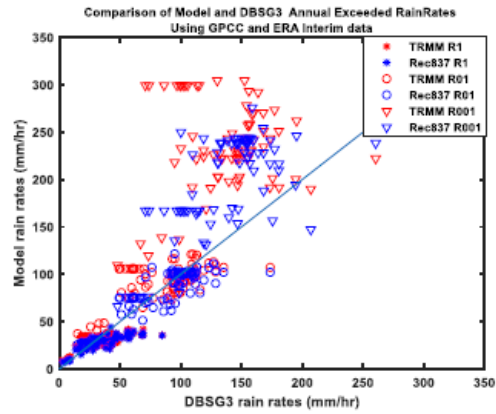Fig 5: Comparison of Method a) and Rec837 exceeded rain rates for DBSG3 sites

Fig 6: Comparison of Method b) and Rec837 exceeded rain rates for DBSG3 sites
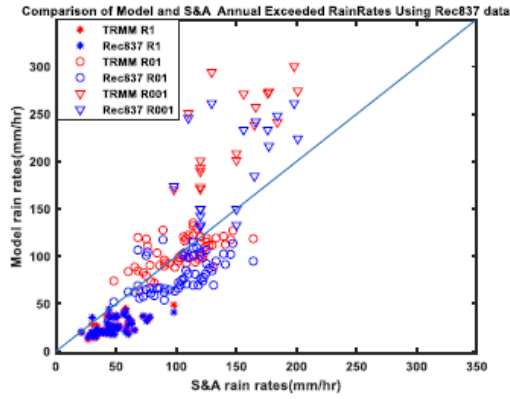
3

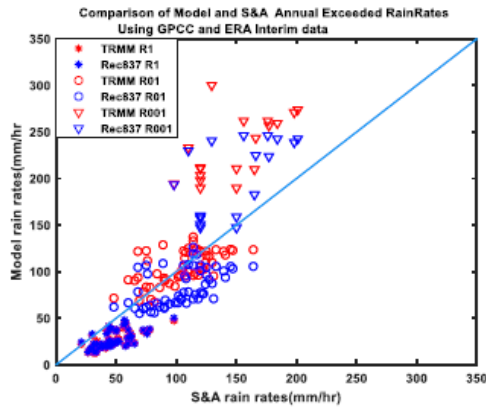Fig.7: Comparison of Method a) and Rec837 exceeded rain rates for S&A sites

Fig. 8: Comparison of Method b) and Rec837 exceeded rain rates for S&A sites

IV. TESTING THE TRANSFORMATION OF TRMM TO ONE-MINUTE RAIN RATE DISTRIBUTIONS

This section explores a method that does not rely upon conditional monthly probability distributions. The nine-years of TRMM data is used to calculate the average annual distributions of TRMM 5 km rain rates over 1° squares. These distributions are then transformed to the expected distribution of point one-minute rain rates, which have been assumed to be the same as instantaneous 1 km rain rates. There are legitimate concerns that the 5 km to 1 km transformation derived from temperate Nimrod data [14] may not be accurate in the tropics. This is tested by optimizing the transformation parameters to yield the best fit with DBSG3 data. Furthermore, the fit to $R_{0.01\%}$ data from literature, but not in DBSG3, is also reported.

A. Fitting TRMM 1 km distributions to DBSG3 data

A quadratic transformation, from distributions of 5 km to 1 km rain rates, was developed from composite Nimrod rain rates in [14], shown in (2).

$$R_{1km} = (\alpha R_{5km} + \beta) \times R_{5km} \qquad (2)$$

where $\alpha = 0.0126$ and $\beta = 1.0619$. These data cover the UK from 50° to 56° north. The transformation depends upon the fine scale spatial variation of rain rate and hence on the mix of convective and stratiform rain. Although [14] successfully applied the transformation to tropical rain data, a question remains whether a better transformation exists. To test this, the α and β parameters in (2) are adjusted to minimize an error measuring the difference between downscaled TRMM $R_{0.01\%}$ and DBSG3 data. The error is defined to be the mean absolute difference, as in (3):

$$Error = mean\left(abs\left(RR_E(P_j) - RR_O(P_j)\right)\right) \qquad (3)$$

where RR_E and RR_O represent model and measured rain rates, and P_j is the time percentage. The error metrics used by ITU-R Working Party 3J are based on mean and root-mean-square (RMS) relative errors:

$$\epsilon(i,j) = \frac{RR_E(P_j) - RR_O(P_j)}{RR_O(P_j)} \qquad (4a)$$

$$E = \frac{\sum_{i=1}^{N_{st}} \sum_{j=1}^{n_i} \alpha_i \varepsilon(i,i)}{\sum_{i=1}^{N_{st}} n_i \alpha_i} \qquad (4b)$$

$$RMS = \sqrt{\frac{\sum_{i=1}^{N_{st}} \sum_{j=1}^{n_i} \alpha_i \varepsilon^2(i,i)}{\sum_{i=1}^{N_{st}} n_i \alpha_i}} \qquad (4c)$$

where N_{st} is the number of sites, n_i is the number of time percentages, and α_i is the number of years of data at the ith site. The 3J metrics indicate both bias and spread. It inherently assumes that the relative error is independent of time percentage, which is unlikely to be true. Weighting the mean with the number of years probably put too much weight of sites with multiple years of data due to correlations between years. The RMS spread puts more emphasis on outliers than (3).

Minimizing (3), where RR_E and RR_O are the downscaled TRMM $R_{0.01\%}$ predictions and the DBSG3 values respectively, and the constraint that $\alpha \geq 0$, yields new parameters: $\alpha=0$ and $\beta=1.7143$. The constraint is required to maintain a monotonic transformation when fitting to just $R_{0.01\%}$, rather than the full distribution as in [14].

Fig. 9 compares $R_{0.01\%}$ derived from the optimised transformation with Rec837 predictions and average site DBSG3 values for all the DBSG3 sites in the tropics. Sites with 4 or more years of data are plotted with error bars. Fitting metrics are provided in Section V.
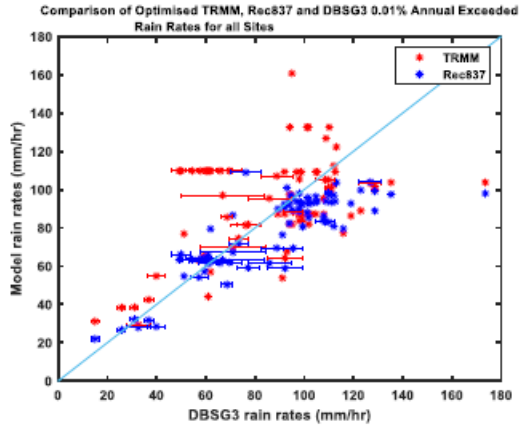
131

Fig. 9 Comparison of $R_{0.01\%}$ from optimised TRMM 1 km distributions, DBSG3 and Rec837.

Fig. 10. Comparison of optimized TRMM 1 km distributions, Rec837 and measured 0.01% exceeded rain rates for S&A sites

B. Fitting TRMM 1 km distributions to Alternative Site Data

TRMM distributions were fitted to the S&A data, and the constrained optimisation yields new transformation parameters $\alpha=0$ and $\beta=2.0046$. The optimised TRMM $R_{0.01\%}$ for S&A sites are presented in Table 2.

Fig. 10 compares $R_{0.01\%}$ derived from the optimally downscaled TRMM distributions and from Rec837, with average measured values for all the S&A sites that fall within the TRMM boundaries.
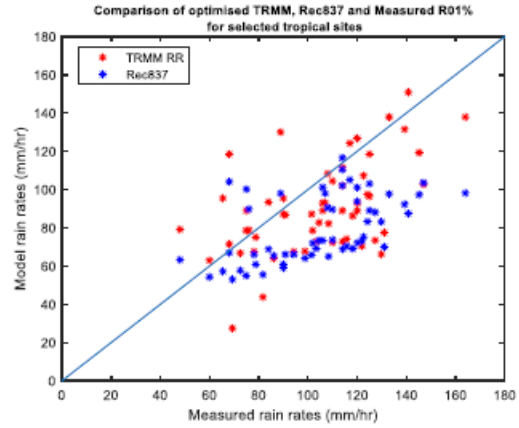
V. COMPARISON OF ANNUAL 0.01% EXCEEDED RAINRATES

Calculating $R_{0.01\%}$ using the methods a) and b) discussed in section IV yields estimates of DBSG3 measured data that are comparable in quality to those provided by Rec837. Figures 1 and 2 suggest a general tendency for Rec837 to underestimate and for the TRMM results to overestimate. In this section, the quality of TRMM and Rec837 predictions are quantified using a GoF metric defined to be the mean absolute difference (3) and WP3J metrics (4).

TABLE 2

COMPARISON OF S&A $R_{0.01\%}$ AND MODEL PREDICTIONS

				Method a)		Method b)			
SITE	LAT	LON	S&A R01%	TRMM	Rec837	TRMM	Rec837	Optimised TRMM fitted to S&A	Optimised TRMM fitted to DBSG3
BANDUNG	-6.91	107.61	120.0	110.1	104.3	110.4	101.0	148.3	126.8
AMRITSAR	31.63	74.87	48.00	56.43	51.99	53.90	62.05	92.57	79.16
THIRUVANANTHAPURAM	8.50	76.90	76.00	97.07	104.6	98.35	97.52	92.09	78.75
GANDAKI	13.50	79.20	68.00	67.62	69.12	77.10	78.28	83.62	71.51
KIANSAM	5.98	116.25	108.0	107.0	85.2	109.6	92.5	126.6	108.3
MIRI AIRPORT	4.31	113.98	117.0	121.5	109.3	114.2	118.4	145.2	124.2
DALAS	6.03	116.48	110.0	111.8	98.6	115.2	107.6	122.1	104.4
BINTULULU	3.16	113.03	114.0	128.9	115.4	125.7	119.2	130.4	111.5
STAPANG	2.38	112.13	114.0	124.6	108.7	131.7	126.2	119.3	102.1
NTU, SINGAPORE	1.34	103.68	106.0	109.6	100.9	111.7	106.7	104.1	89.01
BUKIT TIMAH	1.33	103.80	75.00	106.5	100.9	111.7	106.7	104.1	89.01
USM	5.35	100.30	68.00	108.5	106.7	111.0	104.6	138.6	118.5
SKUDAI	1.45	103.75	120.0	109.3	100.9	111.7	106.7	104.1	89.01
NGURU	12.87	10.45	69.30	46.69	55.97	51.40	55.09	32.11	27.46

BORNO	11.50	12.97	72.50	65.79	57.74	61.01	60.19	78.05	66.75
KATSINA	12.98	7.62	74.90	62.05	64.91	66.01	61.85	91.86	78.56
GUSAU	12.16	6.67	78.10	73.80	66.36	65.70	63.92	78.99	67.55
SOKOTO	13.00	5.24	78.80	56.31	61.17	52.56	56.57	87.78	75.07
DIKWA	12.04	13.91	81.70	54.24	58.61	49.80	55.93	51.20	43.79
MAIDUGURI	7.73	13.15	84.00	88.51	66.59	81.60	65.96	109.2	93.41
GOMBE	10.24	11.16	86.10	73.49	67.04	65.46	62.22	74.90	64.05
BAUCHI	10.67	10.08	90.80	76.68	65.87	73.79	69.33	101.4	86.73
ADAMAWA	9.32	12.43	94.20	76.16	64.73	70.13	65.26	78.98	67.54
KANO	12.00	8.59	98.80	71.39	63.35	66.95	66.51	79.19	67.72
KADUNA	10.15	8.13	101.5	77.94	66.16	77.71	66.52	101.9	87.17
MINNA	9.58	6.54	101.9	82.97	72.53	80.69	73.96	91.88	78.58
ILE-IFE	7.49	4.55	106.0	86.82	76.49	89.91	77.55	108.8	93.00
ILORIN	8.47	4.54	103.4	82.46	69.53	79.57	70.72	85.04	72.72
ABUJA	9.07	7.39	104.5	86.25	74.71	85.66	70.35	96.69	82.69
JOS	9.89	8.85	108.4	76.35	70.93	78.92	66.14	96.18	82.25
MAKURDI	7.73	8.53	110.0	83.59	81.73	83.63	78.33	84.60	72.35
OGHOMOSO	8.12	4.24	114.1	84.42	69.53	79.57	70.72	85.04	72.72
LOKOJA	7.80	6.70	115.7	77.37	81.32	82.26	75.44	86.69	74.14
SAKI	8.67	3.39	118.2	81.45	69.61	79.89	70.75	100.9	86.28
OSOGBO	7.68	4.45	120.1	85.19	76.49	89.91	77.55	108.8	93.00
ABEOKUTA	7.14	3.35	121.9	82.49	73.88	86.62	76.24	82.39	70.45
AKURE	7.25	5.20	122.6	87.15	77.88	87.48	76.31	125.5	107.3
LAGOS	6.52	3.37	124.2	96.21	81.51	95.77	86.42	114.0	97.50
ABIA	5.43	7.52	127.3	98.00	87.37	104.1	91.47	85.87	73.44
ENUGU	6.45	7.54	129.8	98.31	84.91	95.82	87.26	77.44	66.23
BENIN	9.30	2.31	131.0	72.33	69.72	78.79	70.89	90.59	77.47
CALABAR	4.97	8.34	139.3	110.2	102.6	110.9	100.6	153.8	131.5
PORT HARCOURT	4.81	7.04	140.8	99.15	91.57	106.0	93.66	176.4	150.9
WARRI	5.55	5.79	145.2	105.7	102.2	113.9	105.6	139.5	119.3
GWANJU	35.16	126.86	90.00	72.86	54.03	76.37	61.99	101.8	87.06
DAEGU	35.87	128.60	60.00	66.59	62.63	74.32	66.51	73.66	62.99
BUSAN	35.18	129.08	90.00	80.01	62.33	73.50	60.74	111.6	95.44
ULSAN	35.54	129.31	65.40	71.77	62.33	73.50	60.74	111.6	95.44
PENANG	5.27	100.29	125.0	102.5	106.7	111.0	104.6	138.6	118.5
JOHOR BAHRU	1.30	103.43	114.0	111.4	100.9	111.7	106.7	104.1	89.01
ALOR STAR	6.15	100.25	107.0	103.9	103.9	101.7	95.38	108.8	93.03
KUALA LUMPUR	3.04	101.36	133.0	107.9	94.98	113.3	105.6	161.2	137.9
KOTOTABANG	-0.20	100.32	88.88	118.9	117.6	120.1	108.7	152.0	130.0
BUKIT JALIL	3.08	101.42	164.0	107.0	94.98	113.3	105.6	161.2	137.9
TAIPING	4.85	100.74	147.0	117.9	113.7	112.3	103.2	120.1	102.7
TEMERLOH	3.45	102.42	125.0	107.6	92.35	105.8	96.50	112.8	96.49

TABLE 3

GoF FOR 0.01% ANNUAL EXCEEDED RAIN RATES			
	DBSG3		S&A
	With Ayura	Without Ayura	

3

Rec837 a)	15.36	15.64	27.05
Rec837 b)	12.55	12.04	26.70
TRMM a)	16.87	14.54	21.26
TRMM b)	17.58	13.05	21.66
Fit DBSG3	20.92	16.27	20.41
Fit S&A	25.70	21.96	20.24

Table 4

WP3J ERROR METRICS FOR TRMM Methods A and B											
	DBSG3						S&A				
	TRMM a)			TRMM b)			TRMM a)			TRMM b)		
%	0.1	0.01	0.001	0.1	0.01	0.001	0.1	0.01	0.001	0.1	0.01	0.001
E	0.12	0.20	0.70	0.21	0.28	0.85	-0.41	0.02	0.59	-0.41	0.02	0.67
RMS	0.49	0.42	0.90	0.67	0.54	1.0	0.43	0.24	0.65	0.43	0.24	0.67

Table 5

WP3J ERROR METRICS FOR Rec837						
	DBSG3			S_A		
%	0.1	0.01	0.001	0.1	0.01	0.001
E	0.04	0.002	0.32	-0.42	0.20	0.34
RMS	0.51	0.28	0.50	0.45	0.29	0.48

Table 3 compares the absolute error GoF for DBSG3 data with and without the Colombian Ayura Valley sites, and S&A data. Rec837 performs almost as well with and without Ayura data, indicating the fit to the Ayura sites is similar in quality to the fit to other sites. As Ayura Valley data are not representative of the rest of the 1° grid square, this suggests that Rec837 has been over-fitted to DBSG3 data and would not perform as well on other nearby sites. In contrast, both TRMM methods perform much better over sites excluding the Ayura Valley.

Rec837, using Rec837 input data, corresponds to Method a). Oddly, Method b) using primary data sources, performs better for the tropical DBSG3 sites. This may not be true if non-tropical sites were included in the analysis. There is a possibility that Method b) climate data from 2004 to 2012 are more representative for the more recently acquired site data than the long-term average used in Method a), due to climate change. However, there is insufficient data to conclude this.

When comparing to DBSG3 tropical data, the use of downscaled TRMM conditional probability distributions performs only slightly worse than Rec837 distributions i.e. by an average of about 1 mm/hr over all sites. This difference is probably insignificant given the spread and uncertainty in the data. This agreement is surprising given that the conditional probability distributions were derived by averaging over all of the tropics, and the downscaling transformation was based on temperate UK Nimrod data. When S&A comparison site data is used, the methods using TRMM conditional probability distributions perform significantly better than Rec837. This is further evidence that Rec837 has been over-fitted to DBSG3 data.

The third TRMM method considered did not use the conditional probability distributions, but instead used the observed distributions of 5 km spatially averaged rain rates, over 1-degree squares accumulated over 9 years, downscaled to 1 km distributions. Surprisingly, this did not fit the DBSG3 data as well as the Rec837 method based on sums of conditional probability distributions. One possibility for this is that the 2004 -2012 TRMM data are not representative of the climate experienced by site when the data was collected, some as long as 60 years ago. Another possibility is that the 1-degree 9-year accumulations of TRMM data yield 0.01%

exceeded rain rates with some uncertainty due to low sample numbers. The spatial averaging used to calculate the TRMM conditional probability distributions may have made the estimated $R_{0.01\%}$ more reliable. There is some evidence for this in the spatial variation of $R_{0.01\%}$ derived directly from TRMM data. This map, presented in [14], exhibits far more variation between adjacent 1-degree squares than the equivalent produced by Rec837. Some spatial averaging may improve this result.

Fitting the downscaling transformation to yield the best fit to DBSG3 site data yielded a significant improvement, but the predictions still did not perform as well as the methods based on conditional probability distributions. The improvement does suggest that the transformation based on Nimrod data can be improved upon when applied to tropical data. However, a reservation is that the Nimrod transformation was derived for the whole distribution but optimisation has only considered the 0.01% level.

DBSG3 provides only 81 sites to characterize the tropics and no sites in Africa. There is a concern that ITU-R Recommendations may be over-fitted to these data. The results from comparisons to S&A site data provide some weight to this. Downscaled TRMM data provides a much better fit to these sites than Rec837. TRMM with Nimrod downscaling does not perform as well as the optimised TRMM but it performs better than Rec837 with an average of 1.5 mm/hr closer to the S&A site data. Either downscaling transformation based on tropical data yields a significant improvement over Rec837 between 5 and 6 mm/hr averaged across sites.

Tables 4 and 5 compare the WP3J errors for the three probability levels: 0.1%, 0.01% and 0.001%, and the two databases DBSG3 (without Ayura) and S&A. Rec837 performs particularly well against the DBSG3 database, but less well against S&A, again suggesting some over-fitting. The TRMM methods exhibit greater RMS spread of values, but significantly lower bias than Rec837 on the S&A dataset.

VI. CONCLUSION

Rec837 relies on an input derived from rain gauges, which are sparsely distributed in the tropics. Furthermore, there is little

validation data from the Tropics, and none from Africa. These factors could reduce the accuracy of the method in countries that require the ITU-R model, as they often do not have historical rapid-response rain gauge data.

The DBSG3 data includes a group of sites in Ayura Valley Columbia that are unlikely to be representative of the region. Tests of GoF to DBSG3 are considered with and without these outlier sites. Rec837 fits the DBSG3 data similarly well, with or without outliers, while the TRMM methods perform much better when these sites are excluded. This implies that the evaluation of the performance of Rec837 model has been distorted by these data and so it may not accurately represent the climate in the region outside the valley.

The Rec837 method works similarly well when the conditional probability distributions are replaced by distributions derived from TRMM. This suggests that the method based on conditional probability distributions is robust.

Estimation of $R_{0.01\%}$ from downscaled observed TRMM distributions, performs significantly better than Rec837 when compared to S&A data, and only slightly worse when compared to DBSG3 data.

Rain rate distribution data underpins the design and regulation of microwave networks. A method to estimate these distributions in the tropics, based on rain rates measured from satellite, has been presented and validated. TRMM and future satellite missions should provide valuable data to improve the estimation of rain rate distributions globally. Particularly in the tropics, these data could yield significantly improved estimations without the investment of resources and time in setting up networks of high resolution rain gauges. The results suggest that the conditional distributions may benefit from the addition of latitude as a conditioning parameter. Using a method that moves from using TRMM in the tropics to Rec837 for the temperate region could be a solution to the current Rec837 limitations.

ACKNOWLEDGMENT

REFERENCES

[1] *Propagation Data and Prediction Methods Required for the Design of Terrestrial Line-of-Sight Systems*, Recommendation ITU-R p. 530–16, 2017.

[2] *Propagation Data and Prediction Methods Required for the Design of Earth-Space Telecommunication Systems*, Recommendation ITU-R p.618-13, 2017

[3] *Characteristics of precipitation for propagation modelling*, Recommendation ITU-R P.837-7, 2017

[4] L. Luini et al, "Rainfall Rate Prediction for Propagation Applications: Model Performance at Regional Level Over Ireland," IEEE Transactions on Antennas and Propagation, vol. 65, (11), pp. 6185-6189, 2017.

[5] L. Luini and C. Capsoni, "A Unified Model for the Prediction of Spatial and Temporal Rainfall Rate Statistics," IEEE Transactions on Antennas and Propagation, vol. 61, (10), pp. 5249-5254, 2013.

[6] K.S. Paulson, G.R. Rimven and T. Bellerby, "A Rain Model for the Tropics Based on TRMM Data Fitted to DBSG3," 12th European Conference on Antennas and Propagation (EuCAP 2018), DOI: 10.1049/cp.2018.1075, 2018

[7] K.S. Paulson, G.R. Rimven and T. Bellerby, "Comparing One-Minute Rain Rate Distributions from TRMM Satellite Data and Rec. ITU-R P.837-7 in the Tropics," USNC-URSI Radio Science Meeting (Joint with AP-S Symposium), DOI: 10.1109/USNC-URSI.2018.8602570, 2018.

[8] A. Becker, P. Finger, A. Meyer-Christoffer, K. Schamm, U. Schneider, M. Ziese, "A description of the global land-surface precipitation data products of the Global Precipitation Climatology Centre with sample applications including centennial analysis from 1901-present," Earth System Science Data, vol. 5, (1), pp. 71-99, 2013.

[9] U. Schneider, P. Finger, A. Meyer-Christoffer, E. Rustemeier, M. Ziese, A. Becker, "Evaluating the Hydrological Cycle over Land Using the Newly-Corrected Precipitation Climatology from the Global Precipitation Climatology Centre (GPCC)," Atmosphere, vol. 8, (3), pp. 52, 2017.

[10] F. J. Tapiador et al, "Global precipitation measurement: Methods, datasets and applications," Atmos. Res., vol. 104–105, pp. 70-97, 2, 2012.

[11] I. Strangeways, "Measuring precipitation with raingauges," in Precipitation: Theory, Measurement and Distribution, Anonymous Cambridge: Cambridge University Press, 2006, pp. 151-164.

[12] C. Ranatunga, "Introducing an Effect of Climate Change into Global Models of Rain Fade on Telecommunication Links," 2014.

[13] T. Islam, M.A. Rico-Ramirez, Dawei Han, P. K. Srivastava and A. M. Ishak, "Performance evaluation of the TRMM precipitation estimation using ground-based radars from the GPM validation network," Journal of Atmospheric and Solar-Terrestrial Physics, vol. 77, pp. 194-208, 2012. DOI: https://doi.org/10.1016/j.jastp.2012.01.001.

[14] G. Rimven, K. Paulson and T. Bellerby, "Estimating One-Minute Rain Rate Distributions in the Tropics From TRMM Satellite Data ," IEEE Journal of Selected Topics in Applied Earth Observations and Remote Sensing, vol. 11, (10), pp. 3660-3667, 2018.

[15] D. B. Wolff, D. A. Marks, E. Amitai, D. S. Silberstein, B. L. Fisher, A. Tokay, J. Wang and J. L. Pippitt, "Ground validation for the tropical rainfall measuring Mission (TRMM)", J. Atmos. Ocean. Technol., vol. 22, (4), pp. 365-380, 2005. DOI: 10.1175/JTECH1700.1.

[16] K. S. Paulson, "Evidence of trends in rain event size effecting trends in rain fade: Trends in Rain Event Size Effecting Fade," Radio Sci., vol. 51, (3), pp. 142-149, 2016.

[17] README Document for the Tropical Rainfall Measurement Mission (TRMM) Version 007, [Online]. Available: https://disc2.gesdisc.eosdis.nasa.gov/data/TRMM_L2/TRMM_2A25.7/doc/README.TRMM_V7.pdf. Accessed on: May 30, 2017.

[18] H. Sauvageot, F. Mesnard and R. S. Tenório, "The relation between the area-average rain rate and the rain cell size distribution parameters," J. Atmos. Sci., vol. 56, (1), pp. 57-70, 1999.

[19] N. H. H. Khamis, J. Din and T. A. Rahman, "Determination of rain cell size distribution for microwave link design in Malaysia," in 2004, DOI: 10.1109/RFM.2004.1411069.

[20] P. Kirstetter et al, "Comparison of TRMM 2A25 Products, Version 6 and Version 7, with NOAA/NSSL Ground Radar–Based National Mosaic QPE," J. Hydrometeorol., vol. 14, (2), pp. 661-669, 2013.

[21] P. Kirstetter et al, "Impact of sub-pixel rainfall variability on spaceborne precipitation estimation: evaluating the TRMM 2A25 product: Impact of Sub-Pixel Rainfall Variability on TRMM 2A25," Q. J. R. Meteorol. Soc., vol. 141, (688), pp. 953-966, 2015.

[22] U. Schneider, A. Becker, P. Finger, A. Meyer-Christoffer, B. Rudolf, M. Ziese, "GPCC Full Data Monthly Product Version 7.0 at 0.5°: Monthly Land-Surface Precipitation from Rain-Gauges built on GTS-based and Historic Data," 2015, DOI: 10.5676/DWD_GPCC/FD_M_V7_050.

[23] *Acquisition, Presentation and Analysis of Data in Studies of Radiowave Propagation*, Recommendation ITU-R P.311-17, 2017

[24] K. S. Paulson, C. Ranatunga and T. Bellerby, "Estimation of trends in distributions of one-minute rain rates over the UK," presented at EuCAP 2014, The Hague, The Netherlands, doi: 10.1109/EuCAP.2014.6901749.

[25] T. Tjelta and J. Mamen, "Climate trends and variability of rain rate derived from long-term measurements in Norway," Radio Sci., vol. 49, (9), pp. 788-797, 2014.

[26] R. Singh and R. Acharya, "Development of a New Global Model for Estimating One-Minute Rainfall Rate," IEEE Trans. Geosci. Remote Sens., pp. 1-7, 2018.

135

REFERENCES

Alam, M., Jan, M. A., Shu, L., He, X. & Chen, Y. (2018) Editorial: Current and future trends in wireless communications protocols and technologies. *Mobile Networks and Applications,* 23 (3), 377-381.

Barclay, L. (2003) *Propagation of radiowaves, 2nd edition* London, United Kingdom: Institution of Electrical Engineers.

Beard, K. V., Bringi, V. N. & Thurai, M. (2010) A new understanding of raindrop shape. *Atmospheric Research,* 97 (4), 396-415.

Beard, K. V. & Chuang, C. (1987) A new model for the equilibrium shape of raindrops. *Journal of the Atmospheric Sciences,* 44 (11), 1509-1524.

Becker, A., Finger, P., Meyer-Christoffer, A., Rudolf, B., Schamm, K., Schneider, U. & Ziese, M. (2013) A description of the global land-surface precipitation data products of the global precipitation climatology centre with sample applications including centennial analysis from 1901-present. *Earth System Science Data,* 5 (1), 71-99.

Berrisford, P., Dee, D., Poli, P., Brugge, R. & Fielding, K. (2011) *The ERA-Interim Archive (Version 2.0), ERA Report Series.* Available online: http://www.ecmwf.int/sites/default/files/elibrary/2011/8174-era-interim-archive-version-20.pdf [Accessed January/29 2017].

Blarzino, G., Castanet, L., Luini, L., Capsoni, C. & Martellucci, A. (2009) *Development of a new global rainfall rate model based on ERA40, TRMM, GPCC and GPCP products*.

Bowman, K. P. (2005) Comparison of TRMM precipitation retrievals with rain gauge data from ocean buoys. *Journal of Climate,* 18 (1), 178-190.

Bringi, V. N., Chandrasekar, V., Hubbert, J., Gorgucci, E., Randeu, W. L. & Schoenhuber, M. (2003) Raindrop size distribution in different climatic regimes from disdrometer and dual-polarized radar analysis. *Journal of the Atmospheric Sciences,* 60 (2), 354-365.

Chan, S. H., Halterman, R. R. & Long, D. G. (2004) Cross-validation of jason-1 and QuikSCAT wind speeds. IEEE.

Danby, H. (1933) *The mishnah* New York: Oxford University Press Inc.

Dee, D. P., Uppala, S. M., Simmons, A. J., Berrisford, P., Poli, P., Kobayashi, S., Andrae, U., Balmaseda, M. A., Balsamo, G., Bauer, P., Bechtold, P., Beljaars, A. C. M., van de Berg, L., Bidlot, J., Bormann, N., Delsol, C., Dragani, R., Fuentes, M., Geer, A. J., Haimberger, L., Healy, S. B., Hersbach, H., Hólm, E. V., Isaksen, L., Kållberg, P., Köhler, M., Matricardi, M., McNally, A. P., Monge‐Sanz, B. M., Morcrette, J.‐, Park, B.‐, Peubey, C., de Rosnay, P., Tavolato, C., Thépaut, J.‐ & Vitart, F. (2011) The ERA‐Interim reanalysis: Configuration and performance of the data assimilation system. *Quarterly Journal of the Royal Meteorological Society,* 137 (656), 553-597.

DeMoss, J. D. & Bowman, K. P. (2007) Changes in TRMM rainfall due the orbit boost estimated from buoy rain gauge data. *Journal of Atmospheric and Oceanic Technology,* 24 (9), 1598-1607.

Duan, Y., Wilson, A. M. & Barros, A. P. (2015) Scoping a field experiment: Error diagnostics of TRMM precipitation radar estimates in complex terrain as a basis for IPHEx2014. *Hydrology and Earth System Sciences,* 19 (3), 1501-1520.

Ebert, E. E., Janowiak, J. E. & Kidd, C. (2007) Comparison of near-real-time precipitation estimates from satellite observations and numerical models. *Bulletin of the American Meteorological Society,* 88 (1), 47-64.

ECMWF (2011) ***Data usage and quality control for ERA-40, ERA-Interim and the operational ECMWF data assimilation system****.* ECMWF. Available online: https://www.ecmwf.int/en/elibrary/12573-data-usage-and-quality-control-era-40-era-interim-and-operational-ecmwf-data [Accessed May,/28 2019].

Feidas, H., Kokolatos, G., Negri, A., Manyin, M., Chrysoulakis, N. & Kamarianakis, Y. (2009) Validation of an infrared-based satellite algorithm to estimate accumulated rainfall over the mediterranean basin. *Theoretical and Applied Climatology,* 95 (1), 91-109.

Fu, Y., Chen, F., Liu, G., Yang, Y., Yuan, R., Li, R., Liu, Q., Wang, Y., Zhong, L. & Sun, L. (2016) Recent trends of summer convective and stratiform precipitation in mid-eastern china. *Scientific Reports,* 6 33044.

Fulton, R. A., Breidenbach, J. P., Seo, D., Miller, D. A. & O'Bannon, T. (1998) The WSR-88D rainfall algorithm. *Weather and Forecasting,* 13 (2), 377-395.

Gao, J., Tang, G. & Hong, Y. (2017) Similarities and improvements of GPM dual-frequency precipitation radar (DPR) upon TRMM precipitation radar (PR) in global precipitation rate estimation, type classification and vertical profiling. *Remote Sensing,* 9 (11), 1142.

Gebregiorgis, A. S. & Hossain, F. (2015) How well can we estimate error variance of satellite precipitation data around the world? *Atmospheric Research,* 154 39-59.

Gorgucci, E., Baldini, L. & Chandrasekar, V. (2006) What is the shape of a raindrop? an answer from radar measurements. *Journal of the Atmospheric Sciences,* 63 (11), 3033-3044.

GPCC (2018) *Global Precipitation Climatology Centre.* Available online: https://climatedataguide.ucar.edu/climate-data/gpcc-global-precipitation-climatology-centre [Accessed July/25 2018].

Green, A. W. (1975) An approximation for the shapes of large raindrops. *Journal of Applied Meteorology (1962-1982),* 14 (8), 1578-1583.

Haddad, Z. S., Short, D. A., Durden, S. L., Im, E., Hensley, S., Grable, M. B. & Black, R. A. (1997) A new parametrization of the rain drop size distribution. *IEEE Transactions on Geoscience and Remote Sensing,* 35 (3), 532-539.

Harrison, D. L., Driscoll, S. J. & Kitchen, M. (2000) Improving precipitation estimates from weather radar using quality control and correction techniques. *Meteorological Applications,* 7 (2), 135-144.

Huffman, G. J., Adler, R. F., Bolvin, D. T., Gu, G., Nelkin, E. J., Bowman, K. P., Hong, Y., Stocker, E. F. & Wolff, D. B. (2007) The TRMM multisatellite precipitation analysis (TMPA): Quasi-global, multiyear, combined-sensor precipitation estimates at fine scales. *Journal of Hydrometeorology,* 8 (1), 38-55.

IDC (2018) *The Digitization of the World From Edge to Core.* Available online: https://www.seagate.com/files/www-content/our-story/trends/files/idc-seagate-dataage-whitepaper.pdf [Accessed July/14 2019].

Iguchi, T., Kozu, T., Meneghini, R., Awaka, J. & Okamoto, K. I. (2000) Rain-profiling algorithm for the TRMM precipitation radar. *Journal of Applied Meteorology,* 39 (12), 2038-2052.

Iguchi, T., Kozu, T., Meneghini, R. & Okamoto, K. (2000) A new hybrid surface reference method for the TRMM precipitation radar. IEEE.

Iguchi, T. (2011) Evolution of the rain profiling algorithm for the TRMM precipitation radar.

Islam, M. N. & Uyeda, H. (2007) Use of TRMM in determining the climatic characteristics of rainfall over bangladesh. *Remote Sensing of Environment,* 108 (3), 264-276.

Islam, T., Rico-Ramirez, M. A., Han, D., Srivastava, P. K. & Ishak, A. M. (2012) Performance evaluation of the TRMM precipitation estimation using ground-based radars from the GPM validation network. *Journal of Atmospheric and Solar-Terrestrial Physics,* 77 194-208.

Islam, T., Rico-Ramirez, M. A., Thurai, M. & Han, D. (2012) Characteristics of raindrop spectra as normalized gamma distribution from a Joss–Waldvogel disdrometer. *Atmospheric Research,* 108 57-73.

ITU, (2017), ***Report on the Implementation of the Strategic Plan and Activities of the Union 2014 - 2018.*** ITU Reoprt 2014 - 2018, ITU, Available online: https://www.itu.int/en/annual-report-2017/itu-r/Pages/default.aspx [Accessed: 11/02/2019].

ITU-R (2019) *International Telecommunication Union – Radiocommunication Sector .* Available online: https://www.itu.int/en/ITU-R/information/Pages/mission-statement.aspx [Accessed May/9 2019].

ITU-R (2018a) *"Propagation data and prediction methods required for the design of Earth-space telecommunication systems", Recommendation ITU-R p.618-13.* Available online: https://www.itu.int/rec/R-REC-P.618/en [Accessed December/15 2018].

ITU-R (2018b) *"Propagation data and prediction methods required for the design of terrestrial line-of-sight systems", Recommendation ITU-R p.530-17.* Available online: https://www.itu.int/rec/R-REC-P.530-17-201712-I/en [Accessed November/15 2018].

ITU-R (2018c) *''Acquisition, presentation and analysis of data in studies of radiowave propagation'', Recommendation ITU-R P.311-17.* Available online: https://www.itu.int/rec/R-REC-P.311-17-201712-I/en [Accessed February/3 2019].

ITU-R (2018d) ***Propagation data and prediction methods required for the design of Earth-space telecommunication systems.*** Available online: https://www.itu.int/rec/R-REC-P.618-13-201712-I/en [Accessed May/21 2019].

ITU-R (2017a) *"Mean Surface Temperature", Recommendation ITU-R P.1510-1.* Available online: https://www.itu.int/rec/R-REC-P.1510/en [Accessed January/15 2018].

ITU-R (2017b) *''Characteristics of precipitation for propagation modelling'', Recommendation ITU-R P.837-7.* Available online: https://www.itu.int/rec/R-REC-P.837-7-201706-I/en [Accessed November/15 2017].

ITU-R (2016) *"Prediction procedure for trhe evaluation of interference between stations on the surface of the Earth at frequencies above about 0.1GHz", Recommendation ITU-R p.452-16.* Available online: https://www.itu.int/rec/R-REC-P.452-16-201507-I/en [Accessed December/13 2016].

ITU-R (2015a) *"Rain height model for prediction methods", Recommendation ITU-R p.839-4.* Available online: https://www.itu.int/rec/R-REC-P.839-4-201309-I/en [Accessed December/17 2016].

ITU-R (2015b) *''Characteristcs of precipitation for propagation modelling'', Recommendation ITU-R p.837-6.* Available online: https://www.itu.int/rec/R-REC-P.837-6-201202-I/en [Accessed December/13 2016].

ITU-R (2008) *"Specific attenuation model for rain for use in prediction methods", Recommendation ITU-R p.838-3.* Available online: https://www.itu.int/rec/R-REC-P.838-3-200503-I/en [Accessed December/13 2018].

ITU-R Study Group 3. (2012) ITU-R Propagation Prediction Methods for Interference and Sharing Studies . 2012th edn. Geneva: .

ITU-R WP 3J (2017) *Working Party 3J Fascicle.* Available online: https://www.itu.int/oth/R0A0400006B/en [Accessed Jun/28 2019].

Joshi, M. K., Rai, A. & Pandey, A. C. (2012) Validation of TMPA and GPCP 1DD against the ground truth rain-gauge data for indian region: VALIDATION OF PRECIPITATION ESTIMATES FROM SATELLITES WITH RAIN-GAUGE. *International Journal of Climatology,* n/a.

Kestwal, M. C., Joshi, S. & Garia, L. S. (2014) Prediction of rain attenuation and impact of rain in wave propagation at microwave frequency for tropical region (uttarakhand, india). *International Journal of Microwave Science and Technology,* 2014 1-6.

Kidd, C. & Huffman, G. (2011) Global precipitation measurement. *Meteorological Applications,* 18 (3), 334-353.

Kummerow, C., Barnes, W., Kozu, T., Shiue, J. & Simpson, J. (1998) The tropical rainfall measuring mission (TRMM) sensor package. *Journal of Atmospheric and Oceanic Technology,* 15 (3), 809-817.

Laws, J. O. & Parsons, D. A. (1943) The relation of raindrop-size to intensity. *Eos, Transactions American Geophysical Union,* 24 (2), 452-460.

Lin, S. H. (1973) Statistical behavior of rain attenuation. *The Bell System Technical Journal,* 52 (4), 557-581.

Long S. CHIU Zhong LIU Jearanai VONGSAARD Stanley MORAIN Amy BUDGE Paul NEVILLE Chandra BALES (2006) Comparison of TRMM and water district rain rates over new mexico. *大气科学进展：英文版,* 23 (1), 1-13.

Luini, L., Emiliani, L., Boulanger, X., Riva, C. & Jeannin, N. (2017) Rainfall rate prediction for propagation applications: Model performance at regional level over ireland. *IEEE Transactions on Antennas and Propagation,* 65 (11), 6185-6189.

Marshall, J. S. & Palmer, W. M. (1948) **The distribution of raindrops with size**. *Journal of Meteorology,* 5 165-166.

Michaelides, S., Levizzani, V., Anagnostou, E., Bauer, P., Kasparis, T. & Lane, J. E. (2009) Precipitation: Measurement, remote sensing, climatology and modeling. *Atmospheric Research,* 94 (4), 512-533.

NASA (n.d.) *Explanation of Data Products.* Available online: https://pmm.nasa.gov/data-access/data-products [Accessed February/7 2017].

NASA (2012) *TRMM Composite Climatology Information.* Available online: https://disc.gsfc.nasa.gov/precipitation/documentation/climatology/trmm-composite-climatology [Accessed February/11 2017].

NASA Goddard Space Flight Center (2015) *README Document for the Tropical Rainfall Measurement Mission.* Goddard Earth Sciences Data and Information Services Center. Available online: https://disc2.gesdisc.eosdis.nasa.gov/data/TRMM_L2/TRMM_2A23.7/doc/TRMM_Readme_v3.pdf [Accessed February/7 2017].

Nelson, A. R. & Gokhale, N. R. (1972) Oscillation frequencies of freely suspended water drops. *Journal of Geophysical Research (1896-1977),* 77 (15), 2724-2727.

Okamoto, K., Komukai, J., Shige, S. & Manabe, T. (2010) Surface reference normalized radar cross section over land for the improvement of the TRMM PR algorithm. IEEE.

Paulson, K. S. (2017) Estimating 1 min rain rate distributions from numerical weather prediction. *Radio Science,* 52 (1), 176-184.

Paulson, K. S. (2016) Evidence of trends in rain event size effecting trends in rain fade: TRENDS IN RAIN EVENT SIZE EFFECTING FADE. *Radio Science,* 51 (3), 142-149.

Paulson, K. S., Ranatunga, C. & Bellerby, T. (2014a) Estimation of trends in distributions of one-minute rain rates over the UK. European Association on Antennas and Propagation.

Paulson, K. S., Ranatunga, C. & Bellerby, T. (2014b) Estimation of trends in distributions of one-minute rain rates over the UK. European Association on Antennas and Propagation.

Poaires Baptista, J. P. V. & Salonen, E. T. (1998) Review of rainfall rate modelling and mapping. *URSI Commission F Open Symposium on Climatic Parameters in Radiowave Propagation Prediction (CLIMPARA'98), .* Ottawa, Ontario, Canada1998.

Pruppacher, H. R. & Beard, K. V. (1970) A wind tunnel investigation of the internal circulation and shape of water drops falling at terminal velocity in air. *Quarterly Journal of the Royal Meteorological Society,* 96 (408), 247-256.

Pruppacher, H. R. & Pitter, R. L. (1971) A semi-empirical determination of the shape of cloud and rain drops. *Journal of the Atmospheric Sciences,* 28 (1), 86-94.

Ranatunga, C. (2014) *Introducing an effect of climate change into global models of rain fade on telecommunication links.* Unpublished PhD. University of Hull.

Rimven, G., Paulson, K. & Bellerby, T. A comparison of tropical One–Minute rain rate distributions derived from TRMM with rec. ITU-R P.837-7 *IEEE Transactions on Antennas and Propagation, .*

Salonen, E. T. & Poiares Baptista, J. P. V. (1997a) A new global rainfall rate model. London: IEE.

Salonen, E. T. & Poiares Baptista, J. P. V. (1997b) A new global rainfall rate model. London: IEE.

Sapiano, M. R. P. & Arkin, P. A. (2009) An intercomparison and validation of high-resolution satellite precipitation estimates with 3-hourly gauge data. *Journal of Hydrometeorology,* 10 (1), 149-166.

Sauvageot, H., Mesnard, F. & Tenório, R. S. (1999) The relation between the area-average rain rate and the rain cell size distribution parameters. *Journal of the Atmospheric Sciences,* 56 (1), 57-70.

Schneider, U., Finger, P., Meyer-Christoffer, A., Rustemeier, E., Ziese, M. & Becker, A. (2017) Evaluating the hydrological cycle over land using the newly-corrected precipitation climatology from the global precipitation climatology centre (GPCC). *Atmosphere,* 8 (3), 52.

Schneider, U., Becker, A., Finger, P., Meyer-Christoffer, A., Ziese, M. & Rudolf, B. (2014) GPCC's new land surface precipitation climatology based on quality-controlled in situ data and its role in quantifying the global water cycle. *Theoretical and Applied Climatology,* 115 (1), 15-40.

Singh, R. & Acharya, R. (2018) Development of a new global model for estimating one-minute rainfall rate. *IEEE Transactions on Geoscience and Remote Sensing,* 1-7.

Sorooshian, S., Aghakouchak, A., Arkin, P., Eylander, J., Foufoula-Georgiou, E., Harmon, R., Hendrickx, J. M. H., Imam, B., Kuligowski, R., Skahill, B. & Skofronick-Jackson, G. (2011) Advanced concepts on remote sensing of precipitation at multiple scales. *Bulletin of the American Meteorological Society,* 92 (10), 1353-1357.

Strangeways, I. (2006a) Early attempts to measure rainfall. In Anonymous *Precipitation: Theory, measurement and distribution.* Cambridge: Cambridge University Press, 139-140,141,143.

Strangeways, I. (2006b) Measuring precipitation with radar. In Anonymous *Precipitation: Theory, measurement and distribution.* Cambridge: Cambridge University Press, 190-191,192.

Strangeways, I. (2006c) Measuring precipitation with raingauges. In Anonymous *Precipitation: Theory, measurement and distribution.* Cambridge: Cambridge University Press, 151-152,154,155,157,159,160,161,162,163,164.

Strangeways, I. (2004) Improving precipitation measurement. *International Journal of Climatology,* 24 : 1443-1444,1445,1446,1447,1448,1449,1450,1451,1452,1453,1454,1455,1456,1457,1458,1459,1460.

T. Oguchi (1983) Electromagnetic wave propagation and scattering in rain and other hydrometeors. *Proceedings of the IEEE,* 71 (9), 1029-1078.

Tapiador, F. J., Turk, F. J., Petersen, W., Hou, A. Y., García-Ortega, E., Machado, L. A. T., Angelis, C. F., Salio, P., Kidd, C., Huffman, G. J. & de Castro, M. (2012) Global precipitation measurement: Methods, datasets and applications. *Atmospheric Research,* 104–105 70-97.

Thurai, M., Bringi, V. N., Manić, A. B., Šekeljić, N. J. & Notaroš, B. M. (2014) Investigating raindrop shapes, oscillation modes, and implications for radio wave propagation: INVESTIGATING RAIN DROP SHAPES. *Radio Science,* 49 (10), 921-932.

Tjelta, T. & Mamen, J. (2014) Climate trends and variability of rain rate derived from long‐term measurements in norway. *Radio Science,* 49 (9), 788-797.

Tokay, A. & Short, D. A. (1996) Evidence from tropical raindrop spectra of the origin of rain from stratiform versus convective clouds. *Journal of Applied Meteorology (1988-2005),* 35 (3), 355-371.

Ulbrich, C. W. (1983) Natural variations in the analytical form of the raindrop size distribution. *Journal of Climate and Applied Meteorology,* 22 (10), 1764-1775.

Ulbrich, C. W. & Atlas, D. (1984) Assessment of the contribution of differential polarization to improved rainfall measurements. *Radio Science,* 19 (1), 49-57.

Wang, J., Adler, R., Huffman, G. & Bolvin, D. (2014) An updated TRMM composite climatology of tropical rainfall and its validation. *Journal of Climate,* 27 (1), 273-284.

Willis, P. T. (1984) Functional fits to some observed drop size distributions and parameterization of rain. *Journal of the Atmospheric Sciences,* 41 (9), 1648-1661.

Yang, Z., Hsu, K., Sorooshian, S., Xu, X., Braithwaite, D. & Verbist, K. M. J. (2016) Bias adjustment of satellite‐based precipitation estimation using gauge observations: A case study in chile. *Journal of Geophysical Research: Atmospheres,* 121 (8), 3790-3806.